ON THE MECHANISM OF CAVITATION DAMAGE BY NON-HEMISPHERICAL CAVITIES COLLAPSING IN CONTACT WITH A SOLID BOUNDARY

Thesis by

Charl F. Naudé

In Partial Fulfillment of the Requirements
For the Degree of
Doctor of Philosophy

California Institute of Technology
Pasadena, California
1960

Acknowledgements

The writer wishes to express his sincere appreciation for the encouragement and generous assistance offered by his adviser, Professor A. T. Ellis, throughout the course of his studies.

Sincere thanks are also due to Professor P. A. Lagerstrom for his assistance in the theoretical work.

During the course of his studies the writer received financial support from

1. Research Bursary, from the South African Council for Scientific and Industrial Research (1956 - 1959).
2. Queen Victoria Stipendium from the University of Stellenbosch, South Africa (1957 - 1959).
3. Francis J. Cole Fellowship (1959 - 1960).

The experimental work was carried on with support from

1. National Science Foundation grant G-2586.
2. U. S. Navy Bureau of Ordinance contract NOrd 16200.
3. Office of Naval Research equipment loan NOnr 218100.

The writer feels deeply indebted to the following persons for various services rendered: C. Eastvedt, Miss E. Gibson, Mrs. B. Hawk, M. Slater, R. H. Taylor, and last, but not least, his wife.

Abstract

A perfect fluid perturbation theory, which neglects the effect of gravity, and which assumes that the pressure inside a cavitation bubble remains constant during the collapse process, is given for the case of a non-hemispherical, but axially symmetric cavity which collapses in contact with a solid boundary. The theory suggests the possibility that such cavities may deform to the extent that the cavity wall strikes the solid surface before minimum cavity volume is reached.

High speed motion pictures of cavities generated by spark methods are used to test the theory experimentally. It is found that the theory describes the change of shape of such cavities fairly well, and that the phenomenon of the cavity wall striking the solid boundary does indeed occur.

By studying the damaging effects of various cavities of this type on aluminum samples, it is shown that pressures resulting from the cavity wall striking the surface are much higher than pressures caused by compression of gases inside the cavity. It is furthermore found that the estimated impact velocities of the cavity walls on the solid boundary can account for water hammer pressures sufficiently large to have caused the observed damage.

O

Contents

Chapter | Page

Chapter I

Introduction

Cavitation is the occurrence of cavities containing substances in the gaseous phase in a region of liquid phase. The gaseous substances always include some vapor of the surrounding liquid, and may be composed completely of such vapor in special cases.

The equilibrium size of cavities of this nature is determined by the difference between the local pressure of the liquid and the pressure of the included gas, as well as by the surface tension of the liquid. If equilibrium is disturbed by a change of this pressure difference, the cavity will grow or collapse depending on whether the change was negative or positive. If one neglects the effect of surface tension it is seen that no equilibrium size exists when the pressure of the liquid is below its own vapor pressure. Cavities can thus be expected to form in regions where liquid pressures satisfy this requirement.*

In the collapse process of a cavity it is possible to obtain very high local pressures due to the convergent nature of the flow. Under certain conditions pressures may become high enough to damage most known solid materials. The process is known as cavitation damage.

The first experimental investigations of cavitation resulted from observations of severe pitting on propeller blades of English warships around 1915. The Propeller Subcommittee of the Institute of Naval

---

* The effect of surface tension and the presence of nuclei around which cavities may grow play a very important part in the formation of cavities (1) **.

** Numbers in parentheses refer to Bibliography.

Architects was commissioned to study the problem. The report (2)* published by them attributed the pitting to the localized repeated hammering that resulted from the collapse of small cavities directly on the blade surfaces. In an experiment performed to substantiate the statements of the report, pressures of the order of 300,000 p.s.i. were demonstrated to occur during the collapse process.

Attempts towards analytical solution of the problem were made as early as 1917 by Cook (2) and Rayleigh (3). Both achieved essentially the same results independently. Their efforts were based on an earlier work of Besant (4) who formulated the problem as follows:

> An infinite mass of homogeneous incompressible fluid acted upon by no forces is at rest, and a spherical portion of the fluid is suddenly annihilated; it is required to find the instantaneous alteration of the pressure at any point of the mass, and the time in which the cavity will be filled up, the pressure at an infinite distance being supposed to remain constant.

The main difficulty of their solution was that physically unacceptable infinite velocities and pressures occurred at the end of collapse.

In the years which followed much time and effort were devoted to experimental and theoretical studies of the cavitation problem. Schneider (5) gives a good summary of the literature up to 1949. It became apparent that experimental investigation of the detailed process of cavitation damage is extremely difficult because of the very high interface velocities, and the microscopic sizes of the cavities close to the collapse point. High speed motion picture cameras with higher framing rates and optical resolution than those available today would

---

* Numbers in parentheses refer to Bibliography.

be needed for a successful study.

Work in the theoretical field indicated that the collapse process of a spherical bubble required a much more sophisticated analysis than that used by Rayleigh and Cook. The compressibility of the liquid becomes important at the high collapse velocities, and viscous effects may become quite large close to the collapse point.

One of the most comprehensive theoretical surveys of the subject was done by Gilmore (6) at the California Institute of Technology. He included effects of compressibility, surface tension and viscosity. His analysis is based on the so-called Kirkwood-Bethe (7) assumption which certainly appears to be a plausible one. Gilmore's results indicate that the real fluid properties do not eliminate the infinite velocities at the end of collapse, as long as the pressure in the cavity is assumed to remain constant.

It appears that the only remaining physical effect which can remove the singularity in the mathematical solution is the compression of the gas in the cavity. If the cavity contains a gas which does not dissolve in the liquid, the gas will be compressed along a curve which must lie somewhere between the adiabatic and the isothermal curves. Such a compression does remove the infinite collapse velocity. The final pressure which is reached depends strongly on the amount of gas present, increasing as the amount of permanent gas is reduced. It seems logical to expect that the highest collapse pressure will be obtained when the cavity contains no gas other than the vapor of the surrounding liquid. In this case the behavior of the vapor under high rates of compression becomes of decisive importance, and since very little is known about this subject, the maximum pressure cannot be calculated.

As a conclusion one may state that there are still several aspects of the problem of the collapse of a spherical cavity in an infinite liquid which are not completely understood. Of these the behavior of the vapor during the collapse of a vaporous cavity appears to be the most important.

It was usually argued that once the collapse of a spherical cavity in an infinite liquid is solved, it would be a relatively simple matter to extend the results to the collapse of a hemispherical cavity on a solid plane bounding a semi-infinite liquid, and thus into the field of cavitation damage. If asymmetric perturbing effects like those of gravity, viscosity and adhesion were negligible, the solution would in fact be directly applicable.

A recent paper by Plesset and Mitchell (8) shows that the spherical shape of a collapsing cavity is unstable in the sense that a finite perturbation of the initial spherical shape will grow very large as the collapse point is approached. In the light of this result one may be led to think that the occurrence of a completely spherical collapse in practice would be the exception rather than the rule. One meaningful consequence is readily observed when one considers the small perturbing effect of viscosity when a hemispherical cavity collapses in contact with a boundary. It becomes apparent that it will be impossible to apply the theory of a spherical cavity in an infinite liquid.

In a study of the mechanism of cavitation damage it therefore appears of importance to examine the collapse process of cavities which do not remain hemispherical.

The object of the present study is to investigate the collapse process of, and the mechanism of damage by, cavities in contact with a solid boundary in the case where these cavities collapse non-hemispherically because of initial perturbations of the hemispherical shape. It is hoped that such a study may be the first step in understanding the mechanism of cavitation damage for cavities which collapse non-hemispherically as a result of other effects.

Chapter II

Theoretical Treatment of the Collapse of a Nearly Hemispherical Cavity on a Plane Boundary of a Semi-Infinite Liquid

1. The assumptions and the basic equations.

Experimental observations of hemispherical cavities in water, collapsing on a plane boundary, show that such cavities retain their hemispherical shape very well for a very large portion of the collapse process. Since viscous forces will have a definite tendency to distort the hemispherical shape, it will be assumed that viscous forces are small in the problem under consideration.

The effect of compressibility of the liquid will be omitted with the realization that the resulting equations will be a poor approximation when liquid velocities become comparable to the velocity of sound in the liquid.

The only external force acting on the flow in this problem is gravity. The effect of gravity will be neglected because of experimental evidence that hemispherical cavities on a boundary, with lifetimes as long as 1 millisecond, do not suffer visible distortion during the collapse. This experimental result was also obtained with cavities in water. External forces are therefore omitted from the equation of motion.

With these simplifications the equation of continuity becomes (9):

$$\nabla \cdot \vec{q} = 0 \qquad (2.1)$$

where $\vec{q}$ is the velocity vector. The momentum equation reduces to (9):

$$\frac{\partial \vec{q}}{\partial t} + \frac{1}{2}\nabla(q^2) = -\frac{1}{\rho}\nabla p + \vec{q} \times (\nabla \times \vec{q}) \tag{2.2}$$

where p is the pressure

ρ is the liquid density

t is the time.

It is further assumed that the flow is initially irrotational (i.e. $\nabla \times \vec{q}$ vanishes throughout the liquid). Helmholtz's theorem (10) then states that the flow will remain irrotational for the entire duration of the motion, because the only forces acting on the nonviscous, incompressible liquid are conservative pressure forces.

One may therefore write

$$\vec{q} = \nabla \Phi \tag{2.3}$$

where Φ is a scalar potential function of position and time. Equation 2.1 now becomes:

$$\nabla^2 \Phi = 0. \tag{2.4}$$

Equation 2.2 can be written

$$\nabla \left[\frac{\partial \Phi}{\partial t} + \frac{1}{2}(\nabla \Phi)^2 + \frac{p}{\rho} \right] = 0 \tag{2.5}$$

due to the interchangeability of partial derivatives. Integration of equation 2.5 gives:

$$\frac{\partial \Phi}{\partial t} + \frac{1}{2}(\nabla \Phi)^2 + \frac{p}{\rho} = C(t). \tag{2.6}$$

$C(t)$ is an integration constant which depends on time only. It can be evaluated at infinity because the velocity, $\nabla \Phi$, vanishes at infinity while the pressure assumes a constant value p_∞. Φ becomes independent of the space coordinates at infinity, and may be set equal to zero.

Thus equation (2.5) becomes

$$\frac{\partial \Phi}{\partial t} + \frac{1}{2}(\nabla \Phi)^2 = \frac{p_\infty - p}{\rho}. \tag{2.7}$$

It will now be assumed that the pressure inside the cavity is a constant, and that surface tension is negligible. These assumptions are known to become bad when the cavity reaches small sizes near the end of collapse. With these assumptions equation 2.7 yields the following condition on Φ at the bubble wall:

$$\frac{\partial \Phi}{\partial t} + \frac{1}{2}(\nabla \Phi)^2 = \frac{p_\infty - p_c}{\rho} \tag{2.8}$$

where p_c is the constant cavity pressure.

Because the shape of the cavity boundary is unknown a further condition is required to determine Φ uniquely throughout the liquid. The Kinematical condition (10) will be used for this purpose. This condition states that if a free surface can be represented by the equation

$$f(\text{position}, t) = 0 \tag{2.9}$$

then

$$\frac{Df}{Dt} = \frac{\partial f}{\partial t} + \vec{q} \cdot \nabla f = 0. \tag{2.10}$$

The problem is thus reduced to solving equation 2.4 with the following boundary conditions.

i) Φ vanishes at infinity.

ii) The derivative of Φ in a direction normal to the plane boundary of the liquid half-space vanishes on this boundary.

iii) Conditions 2.8 and 2.10 are satisfied on the cavity wall, the shape and motion of which are known initially.

2. The coordinate system and the mathematical formulation of the problem.

Only cavities which are symmetric around a line normal to the solid plane boundary will be considered. This line will then be chosen as the $\theta = 0$ line of a spherical coordinate system, as indicated in figure 1.

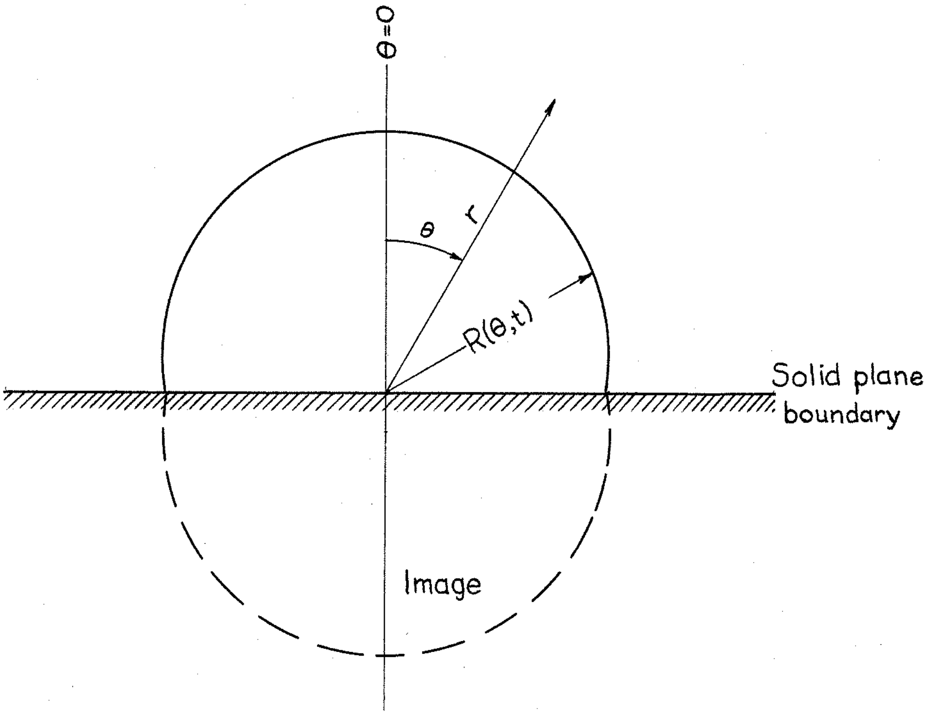

Figure 2.1

The condition that the normal derivative of Φ vanishes on the solid plane boundary is satisfied by means of a reflection in the plane $\theta = \pi/2$. Such a reflection removes the solid boundary as far as the mathematics is concerned, and equation 2.4 is now valid everywhere except in the region occupied by the cavity. The only requirement is that the flow be symmetric around the plane $\theta = \pi/2$.

The solution of equation 2.4 which vanishes at infinity and which satisfies the condition of symmetry around the plane $\theta = \pi/2$ is:

$$\Phi(r, \theta, t) = \sum_{n=0}^{\infty} \phi_{2n}(t) \frac{1}{r^{2n+1}} P_{2n}(\cos\theta) \qquad (2.11)$$

where ϕ_{2n} are the time dependent coefficients in the series, and $P_{2n}(\cos\theta)$ are Legendre Polynomials.

The only boundary conditions that still have to be satisfied are those expressed by equations 2.8 and 2.10. Writing these in the spherical coordinate system one obtains for equation 2.8

$$\left[\frac{\partial\Phi}{\partial t} + \frac{1}{2}\left(\frac{\partial\Phi}{\partial r}\right)^2 + \frac{1}{2r^2}\left(\frac{\partial\Phi}{\partial\theta}\right)^2\right]_{r=R} = \frac{p_\infty - p_c}{\rho}. \qquad (2.12)$$

Equation 2.9 for the bubble wall becomes

$$R(\theta, t) - r = 0. \qquad (2.13)$$

Thus equation 2.10 takes the form

$$\left[\frac{\partial\Phi}{\partial r} - \frac{1}{r^2}\frac{\partial\Phi}{\partial\theta}\frac{\partial R}{\partial\theta}\right]_{r=R} = \frac{\partial R}{\partial t}. \qquad (2.14)$$

The form of Φ as given by equation 2.11, and the boundary conditions 2.12 and 2.14 leads one to express $R(\theta, t)$ in the following way

$$R(\theta, t) = \sum_{n=0}^{\infty} R_{2n}(t) P_{2n}(\cos\theta) \qquad (2.15)$$

where the R_{2n} are time dependent coefficients in the Legendre series expansion of $R(\theta, t)$.

In view of the nonlinearity of the boundary conditions it is hoped to obtain a perturbation solution for a cavity whose shape does not deviate much from the hemispherical. The initial conditions are therefore specified in the form

$$R(\theta, 0) = R_o(0) P_o(\cos\theta) + \epsilon \sum_{r=1}^{\infty} R'_{2n}(0) P_{2n}(\cos\theta) \qquad (2.16)$$

$$\frac{dR}{dt}(\theta, 0) = \epsilon \sum_{n=1}^{\infty} \frac{dR'_{2n}}{dt}(0)\, P_{2n}(\cos\theta)\,. \qquad (2.17)$$

The quantities $R_o(0)$, $\epsilon R'_{2n}(0)$ and $\frac{\epsilon\, dR'_{2n}}{dt}(0)$ are given. It is supposed that $\frac{dR_o}{dt}$ vanishes initially.

A solution of the following form is sought:

$$R(\theta, t) = R_o(t) P_o(\cos\theta) + \epsilon \sum_{n=1}^{\infty} R'_{2n}(t) P_{2n}(\cos\theta) \qquad (2.18)$$

$$\Phi(r, \theta, t) = \frac{1}{r} \phi_o(t) P_o(\cos\theta) + \epsilon \sum_{n=1}^{\infty} \phi'_{2n}(t) \frac{1}{r^{2n+1}} P_{2n}(\cos\theta). \qquad (2.19)$$

The quantity ϵ is introduced only for mathematical convenience. Equations 2.11, 2.15, 2.18 and 2.19 show that

$$\sum_{n=1}^{\infty} \phi_{2n}(t) \frac{P_{2n}(\cos\theta)}{r^{2n+1}} = \epsilon \sum_{n=1}^{\infty} \phi'_{2n}(t) \frac{P_{2n}(\cos\theta)}{r^{2n+1}} \qquad (2.20)$$

and

$$\sum_{n=1}^{\infty} R_{2n}(t) P_{2n}(\cos\theta) = \epsilon \sum_{n=1}^{\infty} R'_{2n}(t) P_{2n}(\cos\theta). \qquad (2.21)$$

ϵ is to be chosen such that the sums on the right hand side of equations

2.20 and 2.21 are of the same magnitude as ϕ_o/r and R_o respectively.

3. The Solutions.

The procedure for solution is now to substitute expressions 2.18 and 2.19 into the boundary conditions 2.12 and 2.14, neglecting terms of order ϵ^2. Due to the orthogonality of the Legendre polynomials the terms multiplied by P_{2n} on the left must equal the terms multiplied by P_{2n} on the right of the resulting equations. In this way the differential equations that must be satisfied by $\phi_o(t)$, $R_o(t)$, $\phi_{2n}(t)$ and $R_{2n}(t)$ are obtained. These equations are then solved with the initial conditions 2.16 and 2.17.

Substituting equations 2.18 and 2.19 into equation 2.12 one obtains

$$\frac{1}{R_o}\frac{d\phi_o}{dt}\left[1-\frac{\epsilon}{R_o}\sum_{n=1}^{\infty} R'_{2n}P_{2n}(\cos\theta)\right] + \epsilon\sum_{n=1}^{\infty}\frac{d\phi'_{2n}}{dt}\,\frac{P_{2n}(\cos\theta)}{R_o^{2n+1}}$$

$$+\frac{1}{2}\left(\frac{\phi_o^2}{R_o^4}\right)\left[1-\frac{4\epsilon}{R_o}\sum_{n=1}^{\infty}R'_{2n}P_{2n}(\cos\theta)\right]+\frac{\epsilon}{R_o^2}\sum_{n=1}^{\infty}\frac{(2n+1)}{R_o^{2n+2}}\,\phi'_{2n}P_{2n}$$

$$=\frac{p_\infty - p_c}{\rho}+O(\epsilon^2). \qquad (2.22)$$

It will be noted that the relation

$$(1+\xi)^{-k} = 1 - k\xi + \frac{k(k+1)}{2!}\xi^2 - \dots \qquad (2.23)$$

was used in the above substitution. Substituting equations 2.18 and 2.19 into equation 2.14 and using relation 2.23 one gets

$$\frac{-\phi_o}{R_o^2}\left[1 - \frac{2\epsilon}{R_o}\sum_{n=1}^{\infty} R'_{2n}P_{2n}\right] - \epsilon\sum_{n=1}^{\infty}\frac{(2n+1)}{R_o^{2n+2}}\phi'_{2n}P_{2n}$$

$$= \frac{dR_o}{dt} + \epsilon\sum_{n=1}^{\infty}\frac{dR'_{2n}}{dt}P_{2n} + O(\epsilon^2). \qquad (2.24)$$

The $P_o(\cos\theta)$ terms of equations 2.22 and 2.24 give respectively

$$\frac{1}{R_o}\frac{d\phi_o}{dt} + \frac{1}{2}\frac{\phi_o^2}{R_o^4} = \frac{p_\infty - p_c}{\rho} + O(\epsilon^2) \qquad (2.25)$$

$$\frac{dR_o}{dt} = -\frac{\phi_o}{R_o^2} + O(\epsilon^2). \qquad (2.26)$$

The $P_{2n}(\cos\theta)$ terms of equations 2.22 and 2.24 can be combined in the following general equations

$$-\frac{1}{R_o^2}\frac{d\phi_o}{dt}R'_{2n} + \frac{1}{R_o^{2n+1}}\frac{d\phi'_{2n}}{dt} - \frac{2\phi_o^2}{R_o^5} + (2n+1)\frac{\phi_o\phi'_{2n}}{R_o^{2n+4}} = 0 + O(\epsilon)$$

$$n = 1, 2, \ldots \qquad (2.27)$$

$$\frac{\phi_o}{R_o^3}R'_{2n} - (2n+1)\frac{\phi'_{2n}}{R_o^{2n+2}} = \frac{dR'_{2n}}{dt} + O(\epsilon), \qquad n = 1, 2, \ldots . \qquad (2.28)$$

The time t is now eliminated from the equations 2.27 and 2.28 with the use of the following relationship, which follows from equation 2.26

$$\frac{d\xi}{dt} = \frac{d\xi}{dR_o}\cdot\frac{dR_o}{dt} = -\frac{\phi_o}{R_o^2}\frac{d\xi}{dR_o} + O(\epsilon^2). \qquad (2.29)$$

Elimination yields

$$\frac{d\phi_o}{dR_o}R'_{2n} - \frac{1}{R_o^{2n-1}}\frac{d\phi'_{2n}}{dR_o} - 2\frac{\phi_o}{R_o}R'_{2n} + (2n+1)\frac{\phi'_{2n}}{R_o^{2n}} = 0 + O(\epsilon) \qquad (2.30)$$

$$n = 1, 2, \ldots$$

$$\phi_o \frac{dR'_{2n}}{dR_o} = -\frac{2\phi_o}{R_o} R'_{2n} + (2n+1)\frac{\phi'_{2n}}{R_o^{2n}} + O(\epsilon) \qquad n = 1, 2, \ldots . \qquad (2.31)$$

Equations 2.30 and 2.31 can be written

$$\frac{d}{dR_o}\left(\frac{\phi'_{2n}}{R_o^{2n+1}}\right) = R'_{2n} \frac{d}{dR_o}\left(\frac{\phi_o}{R_o^2}\right) + O(\epsilon) \qquad n = 1, 2, \ldots \qquad (2.32)$$

$$(2n+1)\frac{\phi'_{2n}}{R_o^{2n+2}} = \frac{\phi_o}{R_o^4}\frac{d}{dR_o}\left(R_o^2 R'_{2n}\right) + O(\epsilon) \qquad n = 1, 2, \ldots . \qquad (2.33)$$

ϕ_{2n} is now eliminated between equations 2.32 and 2.33 giving

$$R'_{2n}\frac{d}{dR_o}\left(\frac{\phi_o}{R_o^2}\right) = \frac{1}{2n+1}\frac{d}{dR_o}\left[\frac{\phi_o}{R_o^3}\frac{d}{dR_o}\left(R_o^2 R'_{2n}\right)\right] + O(\epsilon) \qquad (2.34)$$

$$n = 1, 2, \ldots .$$

Equation 2.34 reduces to

$$R_o^2 \frac{d^2R'_{2n}}{dR_o^2} + \left(1 + \frac{R_o}{\phi_o}\frac{d\phi_o}{dR_o}\right) R_o \frac{dR'_{2n}}{dR_o} + (2n-1)\left(2 - \frac{R_o}{\phi_o}\frac{d\phi_o}{dR_o}\right) R'_{2n}$$

$$= 0 + O(\epsilon) \qquad n = 1, 2, \ldots . \qquad (2.35)$$

Before equation 2.35 can be further simplified it is necessary to obtain the solution for ϕ_o from equations 2.25 and 2.26. Using relation 2.29 to eliminate time from equation 2.25 one obtains

$$-\phi_o \frac{d\phi_o}{dR_o} + \frac{1}{2}\frac{\phi_o^2}{R_o} = R_o^3 \frac{(p_\infty - p_c)}{\rho} + O(\epsilon^2)$$

which can be written

$$-\frac{d}{dR_o}\left[\frac{1}{R_o}\phi_o^2\right] = 2R_o^2 \frac{(p_\infty - p_c)}{\rho} + O(\epsilon^2) . \qquad (2.36)$$

Noting that ϕ_o must vanish initially in order for $\frac{dR_o}{dt}$ to vanish, equation 2.36 can be integrated to give:

$$\phi_o^2 = \frac{2}{3} R_o \left[\frac{p_\infty - p_c}{\rho}\right] (R_o^3(0) - R_o^3) + O(\epsilon^2)$$

or

$$\phi_o = \sqrt{\frac{2}{3} \left(\frac{p_\infty - p_c}{\rho}\right) R_o \,(R_o^3(0) - R_o^3)} + O(\epsilon^2) \qquad (2.37)$$

where the positive sign is used for a collapsing cavity. Substituting the value of ϕ_o in equation 2.26 one obtains R_o as a function of time

$$\int_0^t dt = t = -\frac{1}{\sqrt{\frac{2}{3}\frac{p_\infty - p_c}{\rho}}} \int_{R_o(0)}^{R_o} \frac{dR_o}{\sqrt{\frac{R_o^3(0)}{R_o^3} - 1}} + O(\epsilon^2)$$

$$= \frac{R_o(0)}{\sqrt{\frac{2}{3}\frac{p_\infty - p_c}{\rho}}} \int_{\frac{R_o}{R_o(0)}}^{1} \frac{d\xi}{\sqrt{\frac{1}{\xi^3} - 1}} + O(\epsilon^2). \qquad (2.38)$$

The functions $\phi_o(R_o)$ and $R_o(t)$ thus obtained correspond to the Rayleigh solution.

The time for complete collapse is given by (11)

$$T = \frac{R_o(0)}{\sqrt{\frac{2}{3}\frac{p_\infty - p_c}{\rho}}} \int_0^1 \frac{d\xi}{\sqrt{\frac{1}{\xi^3} - 1}} + O(\epsilon^2) = .915 \frac{R_o(0)}{\sqrt{\frac{p_\infty - p_c}{\rho}}} + O(\epsilon^2). \qquad (2.39)$$

A graphical representation of $R_o/R_o(0)$ as a function of t/T is given in figure 2.2.

Substituting the value of ϕ_o given by equation 2.37 into equation

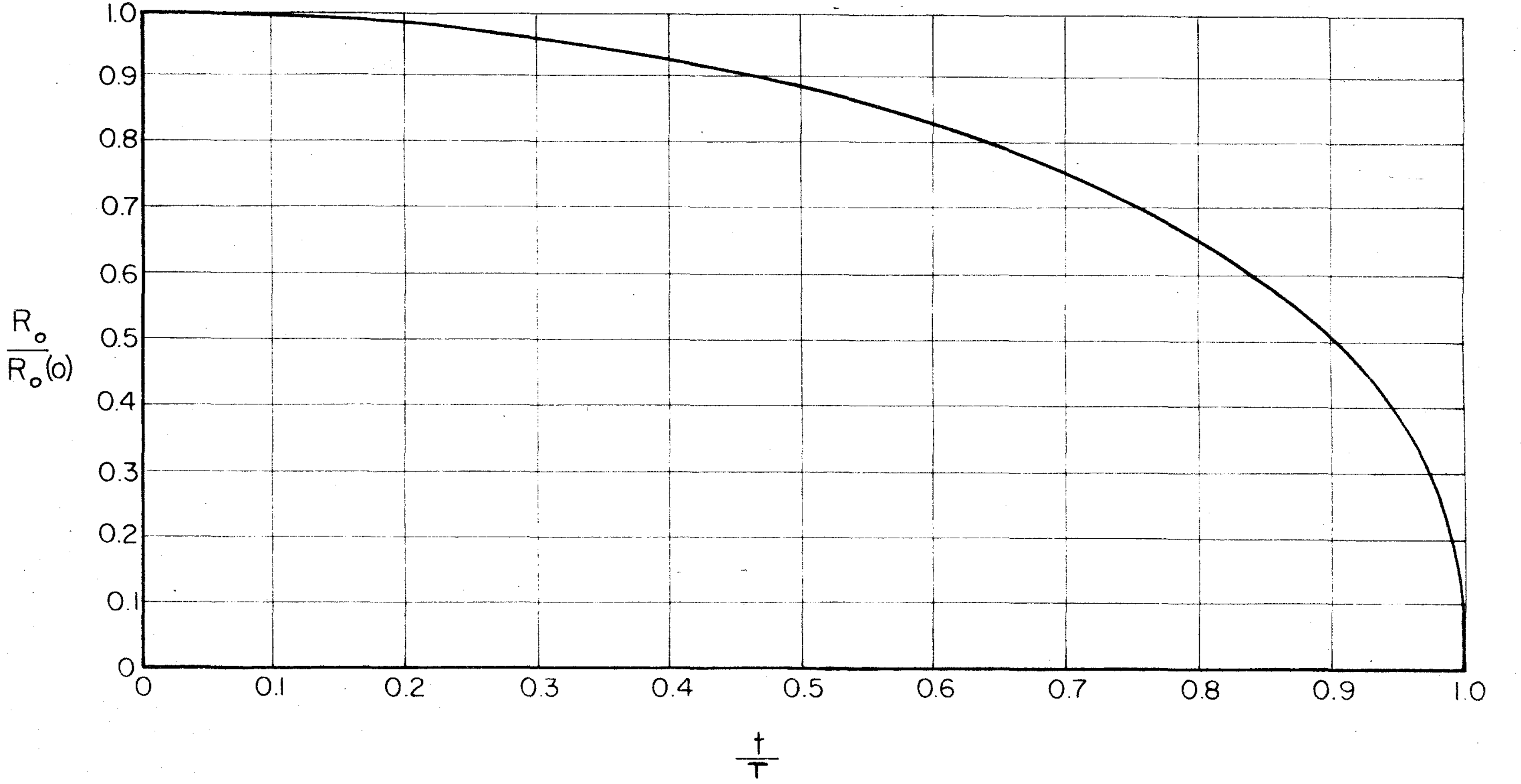

Fig. 2.2. $R_o/R_o(0)$ as a function of t/T

2.35 one obtains the differential equation which must be satisfied by the R'_{2n}, with $n = 1, 2, 3, \ldots$.

$$(R_o^3(0) - R_o^3)\, R_o^2 \frac{d^2R'_{2n}}{dR_o^2} + (\tfrac{3}{2}R_o^3(0) - 3R_o^3)\, R_o \frac{dR'_2}{dR_o} + \frac{3(2n-1)}{2} R_o^3(0)\, R'_{2n}$$

$$= 0 + O(\epsilon) \;. \qquad (2.40)$$

With the substitutions $R_o^3(0)/R_o^3 = x$, and $R'_{2n}/R'_{2n}(0) = \frac{R_{2n}}{R_{2n}(0)} = y_{2n}$ equation 2.40 becomes:

$$(1-x)x\frac{d^2y_{2n}}{dx^2} + (\tfrac{1}{3} - \tfrac{5}{6}x)\, \frac{dy_{2n}}{dx} - \tfrac{1}{6}\,(2n-1)\, y_{2n} = 0 + O(\epsilon). \qquad (2.41)$$

The hypergeometric differential equation can be written in the form (12)

$$(1-z)z\, \frac{d^2u}{dz^2} + \quad c - (a+b+1)z\; \frac{du}{dz} - abu = 0. \qquad (2.42)$$

It is seen that equation 2.41 is of hypergeometric form with

$$c = \tfrac{1}{3} \qquad (2.43)$$

$$a(n) = \tfrac{1}{12}\,(-1 + i\,(48n - 25)^{1/2}) \qquad (2.44)$$

$$b(n) = \tfrac{1}{12}\,(-1 - i(48n - 25)^{1/2}). \qquad (2.45)$$

The general solutions of equation 2.41 can thus be written (12)

$$y_{2n} = A'_{2n}\, y_{2n_1} + B'_{2n}\, y_{2n_2}$$

$$= A'_{2n}\, x^{-a}\; F(a, a+1-c; a+b+1-c; 1-\tfrac{1}{x})$$

$$+ B'_{2n}\, x^{b-c}\, (1-x)^{c-a-b}\; F(c-b; 1-b; c+1-a-b; 1-\tfrac{1}{x})$$

or

$$y_{2n} = A_{2n} x^{-a} F(a, a+\tfrac{2}{3}; \tfrac{1}{2}; 1-\tfrac{1}{x})$$

$$+ B_{2n} x^{-a} (1-\tfrac{1}{x})^{1/2} F(-b+\tfrac{1}{3}; -b+1; \tfrac{3}{2}; 1-\tfrac{1}{x})$$

$$= A_{2n} y_{2n_1} + B_{2n} y_{2n_2} \tag{2.46}$$

where a and b are specified by relations 2.44 and 2.45 and

$$F(\alpha, \beta; \gamma; z) = \sum_{m=0}^{\infty} \frac{(\alpha)_m (\beta)_m}{(\gamma)_m} z^m \tag{2.47}$$

with

$$(\alpha)_m = \Gamma(\alpha+m)/\Gamma(\alpha). \tag{2.48}$$

The hypergeometric functions in equation 2.46 are complex, and so is x^{-a}. One can see that the products must be real for a limited range by using alternative expressions for these products. Such expressions are given by (12)

$$x^{-a} F(a, a+1-c; a+b+1-c; 1-\tfrac{1}{x}) = F(a, b; a+b+1-c; 1-x)$$

$$\text{for } 1 \leq x \leq 2. \tag{2.49}$$

Because a and b as given by equations 2.44 and 2.45 are complex conjugates the right hand side of equation 2.49 is purely real, so that the left hand side must be purely real.

Similarly

$$x^{b-c} F(c-b, 1-b; c+1-a-b; 1-\tfrac{1}{x}) = F(c-a, c-b; c+1-a-b; 1-x)$$

$$1 \leq x \leq 2. \tag{2.50}$$

The right hand side of equation 2.50 is again purely real, and since with a, b and c specified by equations 2.44, 2.45 and 2.43 x^{b-c} is the same as $x^{-a} x^{-1/2}$, y_{2n_2} is real.

Since the derivatives of a hypergeometric function can be written in the form (12)

$$\frac{d^n}{dz^n} F(\alpha, \beta; \gamma; z) = \frac{(\alpha)_n (\beta)_n}{(\gamma)_n} F(\alpha+n, \beta+n; \gamma+n; z) \tag{2.51}$$

it is seen from equations 2.49 and 2.50 that the imaginary parts of all the derivatives of y_{2n_1} and y_{2n_2} vanish in the range $1 \leq x \leq 2$. Furthermore it is noted that y_{2n} as given by equation 2.46, and all its derivatives as calculated by equation 2.51 are analytic except at the points $x = 0, 1, \infty$. One may therefore conclude that y_{2n} is real throughout the range of variation of x.

The solutions obtained here correspond exactly to the solutions given by Plesset and Mitchell (8) in their work on the stability of the spherical shape of a collapsing cavity. This result could have been anticipated immediately after it was shown that the only effect of the boundary is to eliminate odd Legendre polynomials from the expansion

$$R(\theta, t) = R_o(t) + \sum_{n=0}^{\infty} R_n(t) P_n(\cos\theta).$$

The method of solution was nonetheless demonstrated here in order to clarify the work which follows in chapter III.

In figures 2.3 and 2.4, y_{2n_1} and y_{2n_2} are presented as functions of $R_o/R_o(0)$ for n between 1 and 6. The values of y_{2n_1}

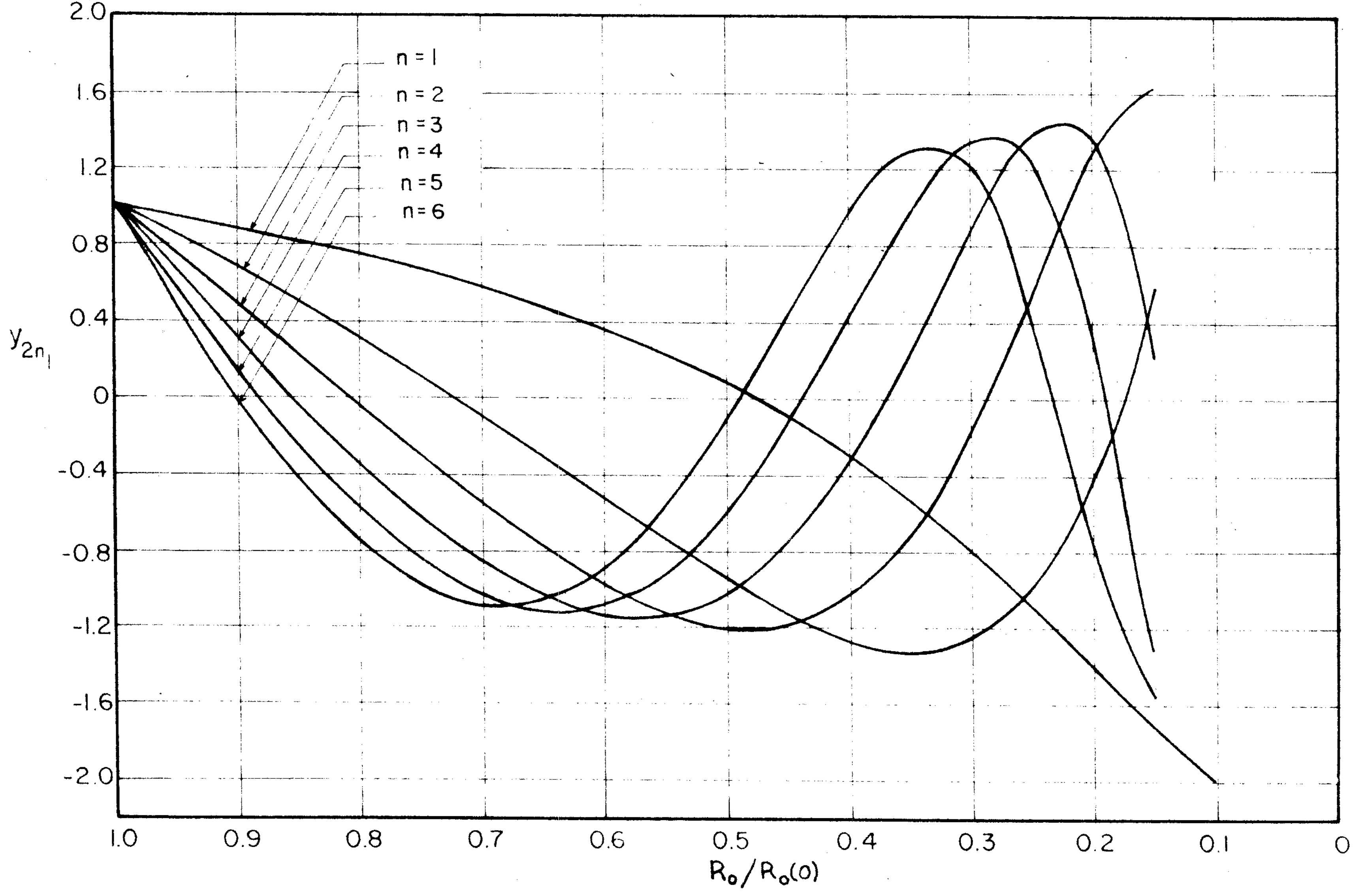

Fig. 2.3. y_{2n_1} as a function of $R_o/R_o(0)$.

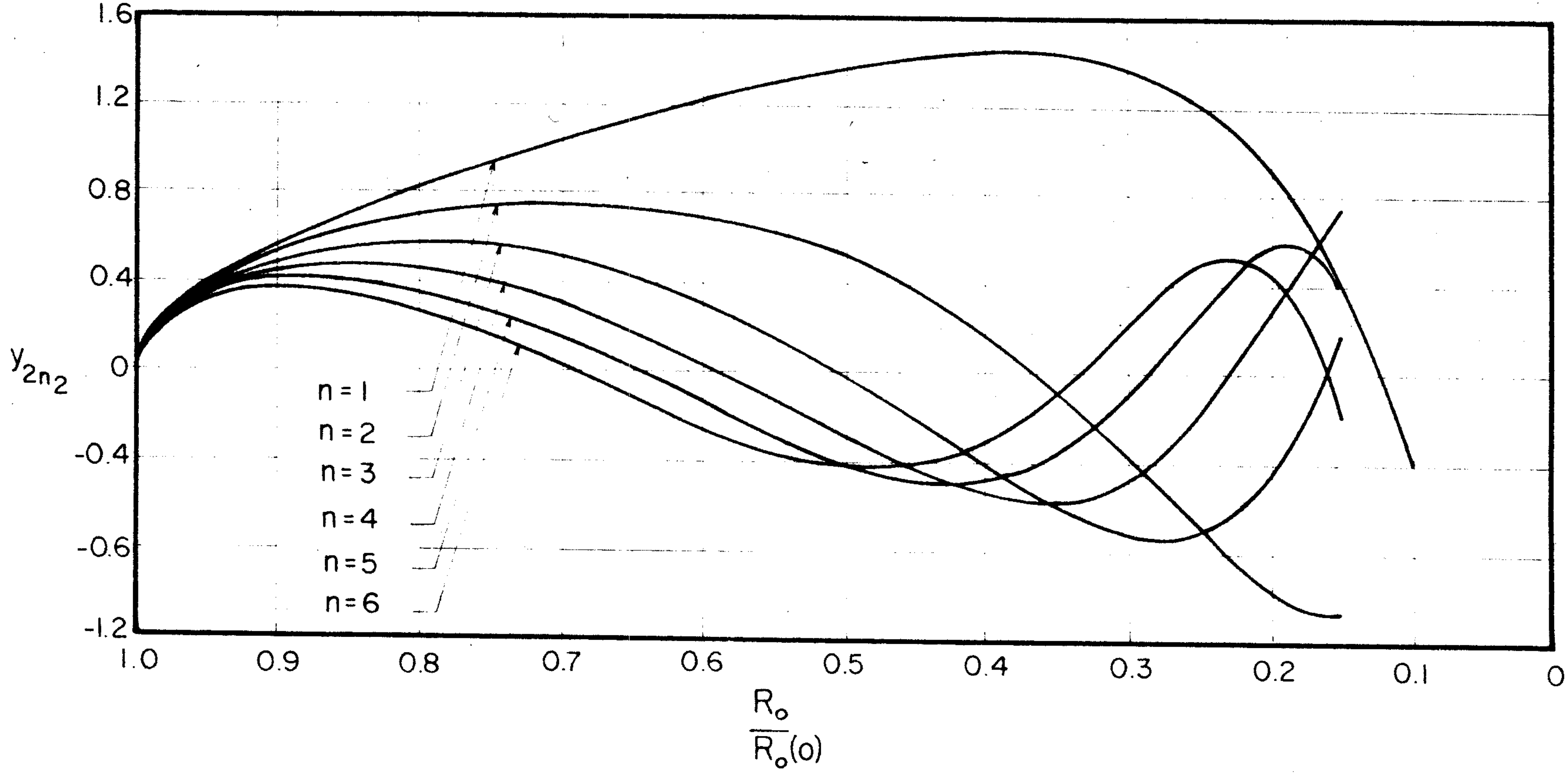

Fig. 2.4. y_{2n_2} as a function of $R_o/R_o(0)$.

and y_{2n_2} were calculated by means of an electronic computer. The accuracy in the range where the functions are shown was estimated to be within 1%. Close to the point $R_o/R_o(0) = 0$ the hypergeometric series of equation 2.46 converges extremely slowly. It was however expected that the theory would become invalid in this range, due to the effects of compressibility, surface tension and viscosity which were neglected. For this reason the functions y_{2n_1} and y_{2n_2} for n between 2 and 6 were not computed for $R_o/R_o(0)$ less than 0.15. The functions y_{22} and y_{21} were computed for $R_o/R_o(0)$ larger than 0.1.

The constants A_{2n} and B_{2n} still have to be evaluated in terms of the initial conditions. Consider y_{2n} as given by equation 2.46 at $x = 1$. This gives

$$A_{2n} = 1. \tag{2.52}$$

Consider also $\frac{dy_{2n}}{d(t/T)}$ at $x = 1$

$$\frac{dy_{2n}}{d(t/T)} = T\,\frac{dy_{2n}}{dt} = -T\,\frac{\phi_o}{R_o^2}\,\frac{dx}{dR_o}\,(y_{2n})$$

$$= 3T\sqrt{\frac{2}{3}}\sqrt{\frac{p_\infty - p_c}{\rho}} \cdot \frac{1}{R_o(0)}\,x^{4/3}\sqrt{x-1}\,\frac{dy_{2n}}{dx}. \tag{2.53}$$

Substituting the value of T as given by equation 2.39 into equation 2.53 one obtains

$$\frac{dy_{2n}}{d(t/T)} = 3(.915)\sqrt{\frac{2}{3}}\,x^{11/6}\sqrt{1-\frac{1}{x}}\,\frac{dy_{2n}}{dx}$$

$$\frac{dy_{2n}}{d(t/T)}(0) = \frac{3}{2}\sqrt{\frac{2}{3}}\,(.915)\,B_{2n}$$

$$B_{2n} = .892 \frac{dy_{2n}}{d(t/T)}(0). \tag{2.54}$$

It is observed in figures 2.3 and 2.4 that the R_{2n} oscillate with increasing amplitude and increasing frequency as R_o approaches zero. The perturbation theory is expected to become invalid when $\epsilon \sum_{n=1}^{\infty} R'_{2n}(t) P_{2n}(\cos\theta)$ becomes comparable to R_o.

If the requirement that the perturbation remains small is ignored for the present, one notices that the theory becomes invalid by a completely different mechanism when $\epsilon \sum_{n=1}^{\infty} R'_{2n}(t) P_{2n}(\cos\theta)$ becomes equal and opposite to R_o for any value of θ. Physically this means that the bubble becomes deformed to the extent that opposite sides of it strike one another. The effect is demonstrated in figure 2.5.

Nothing conclusive can be said about this type of collapse at the present stage because of the large perturbation quantities that are involved. The experimental study described in Chapters IV, V and VI will cast more light on the subject.

The solutions given here were obtained by treating the sums $\epsilon \sum_{n=1}^{\infty} R'_{2n}(t) P_{2n}(\cos\theta)$ and $\epsilon \sum_{n=1}^{\infty} \phi'_{2n}(t) \frac{P_{2n}(\cos\theta)}{r^{2n+1}}$ as perturbation quantities. Terms of order ϵ^2 were assumed to have a negligible effect on these sums. It should be realized that if the terms corresponding to a given n in these sums were very small, they may be seriously affected by terms of order ϵ^2. The effect of such small individual terms are however negligible as far as the values of the perturbation quantities are concerned, provided ϵ is very small.

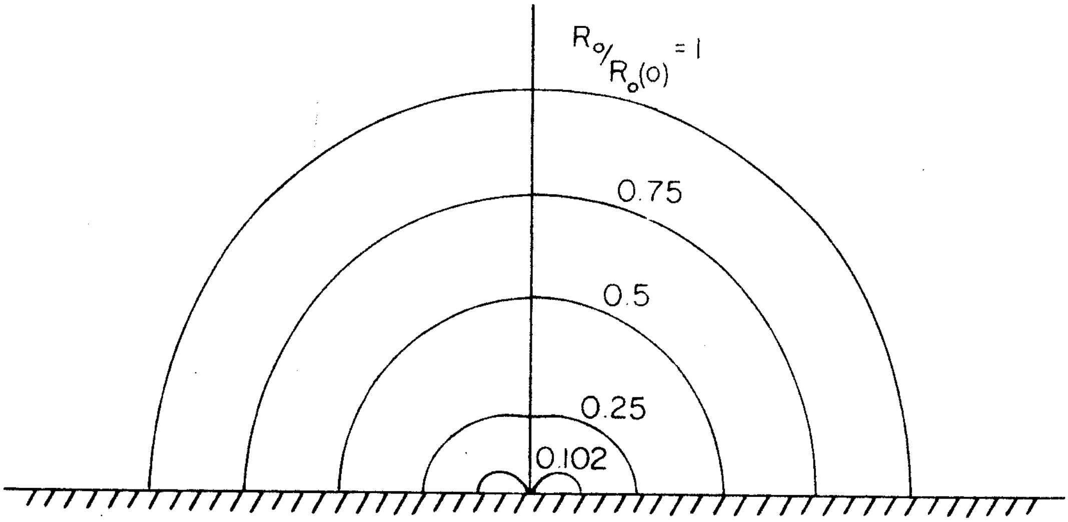

a) $$R(\theta, 0) = R_o(0) + 0.05\, R_o(0)\, P_2(\cos\theta)$$

$$\frac{dR}{dt}(\theta, 0) = 0.$$

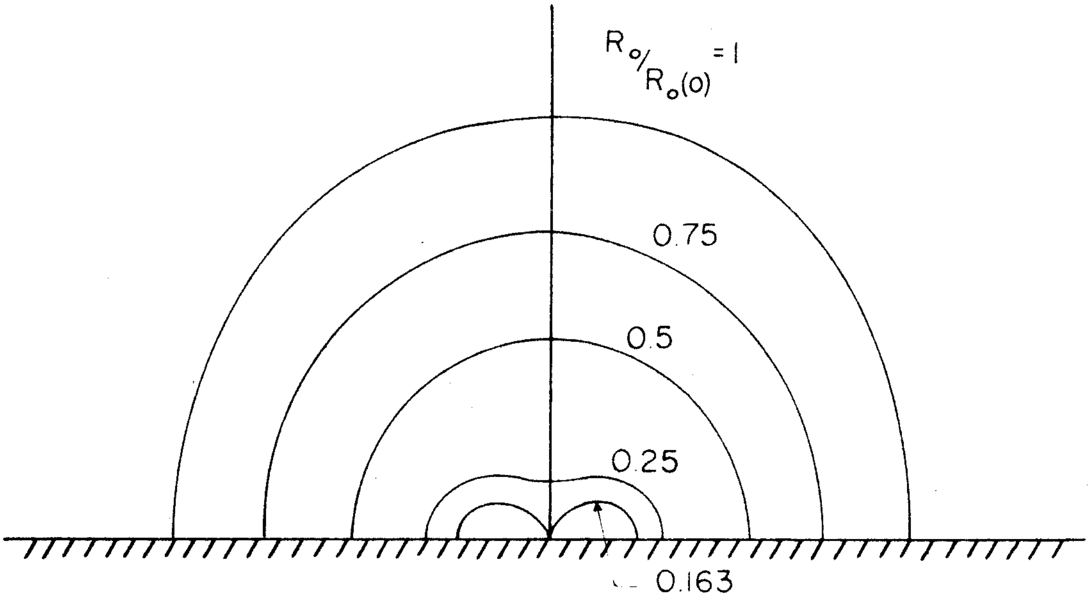

b) $$R(\theta, 0) = R_o(0) + 0.1\, R_o(0)\, P_2(\cos\theta)$$

$$\frac{dR}{dt}(\theta, 0) = 0.$$

Fig. 2.5. Theoretical cavity shapes during the collapse process shown at different values of $R_o/R_o(0)$.

For larger values of ϵ effects of the type discussed above may become important. Chapter III deals with a special case which falls in this category.

Chapter III

An Extension of the Theory for Large Perturbations

The results of Chapter II indicate that experimental investigations of the problem will have to be performed before any conclusions can be reached. The experimental results will consist of high speed motion pictures of collapsing cavities, which will have to be analysed to find the values of the Legendre components of the bubble shape. Since the optical resolution of high speed photographs is limited, one is forced to use fairly large perturbations of the hemispherical shape in order to obtain accurate results. With this purpose in mind the results of Chapter II will be extended to cover larger perturbations.

Before one plunges into the theoretical work it is useful to consider some experimental results in order to obtain an idea of the order of magnitude of quantities that are involved. The experimental result which will be used here is that if the shape of a normal cavity collapsing in contact with a wall is expressed as

$$R(\theta, t) = R_0(t) P_0(\cos\theta) + R_2(t) P_2(\cos\theta) + R_4(t) P_4(\cos\theta) + \dots \quad (3.1)$$

where the coordinate system is chosen as in figure 2.1, then $R_0 > R_2 > R_4 > R_6$. R_6 is usually so small that it becomes comparable to errors in the measurements.

The analysis proceeds in exactly the same way as that of Chapter II, the main difference being that the most important terms of order ϵ^2 are saved.

In order to keep track of the relative sizes of quantities, the initial conditions are now specified as follows:

$$R(\theta, 0) = R_o(0) P_o(\cos\theta) + \epsilon \Big[R'_2(0) P_2(\cos\theta) + \alpha R''_4(0) P_4(\cos\theta) + \beta R''_6(0) P_6(\cos\theta) + \cdots \Big] \qquad (3.2)$$

$$\frac{dR}{dt}(\theta, 0) = \epsilon \left[\frac{dR'_2}{dt}(0) P_2(\cos\theta) + \alpha \frac{dR''_4}{dt}(0) P_4(\cos\theta) + \beta \frac{dR''_6}{dt}(0) P_6(\cos\theta) + \cdots \right]. \qquad (3.3)$$

A solution of the following form is sought

$$R(\theta, t) = R_o(t) P_o(\cos\theta) + \epsilon \Big[R'_2(t) P_2(\cos\theta) + \alpha R''_4(t) P_4(\cos\theta) + \beta R''_6(t) P_6(\cos\theta) + \cdots \Big] \qquad (3.4)$$

$$\Phi(r, \theta, t) = \frac{\phi_o(t)}{r} P_o(\cos\theta) + \epsilon \left[\frac{\phi'_2(t)}{r^3} P_2(\cos\theta) + \alpha \frac{\phi''_4(t)}{r^5} P_4(\cos\theta) + \beta \frac{\phi''_6(t)}{r^7} P_6(\cos\theta) + \cdots \right]. \qquad (3.5)$$

Referring to equations 2.11, 2.15, 2.18 and 2.19 it is seen that

$$\begin{aligned} \epsilon R'_2 &= R_2 \\ \epsilon \phi'_2 &= \phi_2 \\ \epsilon \alpha R''_4 &= \epsilon R'_4 = R_4 \\ \epsilon \alpha \phi''_4 &= \epsilon \phi'_4 = \phi_4 \\ \epsilon \beta R''_6 &= \epsilon R'_6 = R_6 \\ \epsilon \beta \phi''_6 &= \epsilon \phi'_6 = \phi_6 \end{aligned} \qquad (3.6)$$

The values of ϵ, α and β are to be chosen such that the quantities R'_2, R''_4 and R''_6 are of the same magnitude as R_o, while ϕ'_2/r^3, ϕ''_4/r^5 and ϕ''_6/r^7 are comparable to ϕ_o/r.

Substituting expressions 3.4 and 3.5 into equation 2.12 and saving terms of order ϵ, $\epsilon\alpha$, $\epsilon\beta$, ϵ^2 and $\epsilon^2\alpha$ one obtains

$$\begin{aligned}
&\frac{1}{R_o}\frac{d\phi_o}{dt}\Big[1-\epsilon\frac{R'_2P_2}{R_o}-\epsilon\alpha\frac{R''_4P_4}{R_o}-\epsilon\beta\frac{R''_6P_6}{R_o}+\epsilon^2\frac{R'^2_2}{R_o^2}\left(\frac{18}{35}P_4+\frac{2}{7}P_2+\frac{1}{5}\right)\\
&\quad+2\epsilon^2\alpha\frac{R'_2R''_4}{R_o^2}\left(\frac{5}{11}P_6+\frac{20}{77}P_4+\frac{2}{7}P_2\right)\Big]+\frac{1}{R_o^3}\frac{d\phi'_2}{dt}\Big[\epsilon P_2-3\epsilon^2\frac{R'_2}{R_o}\Big(\frac{18}{35}P_4\\
&\quad+\frac{2}{7}P_2+\frac{1}{5}\Big)-3\epsilon^2\alpha\frac{R'_4}{R_o}\left(\frac{5}{11}P_6+\frac{20}{77}P_4+\frac{2}{7}P_2\right)\Big]+\frac{1}{R_o^5}\frac{d\phi''_4}{dt}\Big[\epsilon\alpha P_4\\
&\quad-5\epsilon^2\alpha\frac{R'_2}{R_o}\left(\frac{5}{11}P_6+\frac{20}{77}P_4+\frac{2}{7}P_2\right)\Big]+\frac{1}{R_o^7}\frac{d\phi''_6}{dt}\Big[\epsilon\beta P_6\Big]+\frac{1}{2}\frac{\phi_o^2}{R_o^4}\Big[1\\
&\quad-4\epsilon\frac{R'_2}{R_o}P_2-4\epsilon\alpha\frac{R''_4}{R_o}P_4-4\epsilon\beta\frac{R''_6}{R_o}P_6+10\epsilon^2\frac{R'^2_2}{R_o^2}\left(\frac{18}{35}P_4+\frac{2}{7}P_2+\frac{1}{5}\right)\\
&\quad+20\epsilon^2\alpha\frac{R'_2R''_4}{R_o^2}\left(\frac{5}{11}P_6+\frac{20}{77}P_4+\frac{2}{7}P_2\right)\Big]+\frac{\phi_o}{R_o^2}\Big[3\epsilon\frac{\phi'_2}{R_o^4}P_2\\
&\quad-18\epsilon^2\frac{\phi'_2R'_2}{R_o^5}\left(\frac{18}{35}P_4+\frac{2}{7}P_2+\frac{1}{5}\right)-18\epsilon^2\alpha\frac{\phi'_2R''_4}{R_o^5}\left(\frac{5}{11}P_6+\frac{20}{77}P_4+\frac{2}{7}P_2\right)\\
&\quad+5\epsilon\alpha\frac{\phi''_4}{R_o^6}P_4-40\epsilon^2\alpha\frac{\phi''_4R'_2}{R_o^7}\left(\frac{5}{11}P_6+\frac{20}{77}P_4+\frac{2}{7}P_2\right)+7\epsilon\beta\frac{\phi''_6}{R_o^3}P_6\Big]
\end{aligned}$$

$$+\frac{\phi_2'^2}{R_o^8}\Big[\frac{9}{2}\epsilon^2\left(\frac{18}{35}P_4+\frac{2}{7}P_2+\frac{1}{5}\right)+\frac{1}{2}\epsilon^2\left(-\frac{72}{35}P_4+\frac{6}{7}P_2+\frac{6}{5}\right)\Big]$$

$$+\frac{\phi_2'\phi_4''}{R_o^{10}}\Big[15\epsilon^2\alpha\left(\frac{5}{11}P_6+\frac{20}{77}P_4+\frac{2}{7}P_2\right)+\epsilon^2\alpha\left(-\frac{40}{11}P_6+\frac{60}{77}P_4+\frac{20}{7}P_2\right)\Big]$$

$$=\frac{p_\infty-p_c}{\rho}+O(\epsilon^2\beta). \qquad (3.7)$$

Substituting expressions 3.4 and 3.5 into 2.14 one obtains

$$\frac{\phi_o}{R_o^2}\Big[1-2\epsilon\frac{R_2'}{R_o}P_2-2\epsilon\alpha\frac{R_4''}{R_o}P_4-2\epsilon\beta\frac{R_6''}{R_o}P_6+3\epsilon^2\frac{R_2'^2}{R_o^2}\left(\frac{18}{35}P_4+\frac{2}{7}P_2+\frac{1}{5}\right)$$

$$+6\epsilon^2\alpha\frac{R_2'R_4''}{R_o^2}\left(\frac{5}{11}P_6+\frac{20}{77}P_4+\frac{2}{7}P_2\right)\Big]+\frac{\phi_2'}{R_o^4}\Big[3\epsilon P_2$$

$$-12\epsilon^2\frac{R_2'}{R_o}\left(\frac{18}{35}P_4+\frac{2}{7}P_2+\frac{1}{5}\right)-12\epsilon^2\alpha\frac{R_4''}{R_o}\left(\frac{5}{11}P_6+\frac{20}{77}P_4+\frac{2}{7}P_2\right)\Big]$$

$$+\frac{\phi_4''}{R_o^6}\Big[5\epsilon\alpha P_4-30\epsilon^2\alpha\frac{R_2'}{R_o}\left(\frac{5}{11}P_6+\frac{20}{77}P_4+\frac{2}{7}P_2\right)\Big]+\frac{\phi_6''}{R_o^8}\Big[7\beta\epsilon P_6\Big]$$

$$+\frac{\phi_2'}{R_o^4}\Big[\epsilon^2\frac{R_2'}{R_o}\left(-\frac{72}{35}P_4+\frac{6}{7}P_2+\frac{6}{5}\right)+\epsilon^2\alpha\frac{R_4''}{R_o}\left(-\frac{40}{11}P_6+\frac{60}{77}P_4+\frac{20}{7}P_2\right)\Big]$$

$$+\frac{\phi_4''}{R_o^6}\Big[\epsilon^2\alpha\frac{R_2'}{R_o}\left(-\frac{40}{11}P_6+\frac{60}{77}P_4+\frac{20}{7}P_2\right)\Big]+\frac{dR_o}{dt}+\epsilon\frac{dR_2'}{dt}P_2$$

$$+\epsilon\alpha\frac{dR_4''}{dt}P_4+\epsilon\beta\frac{dR_6''}{dt}P_6=0+O(\epsilon^2\beta). \qquad (3.8)$$

It will be noted that equation 2.23 and the following identities have been used repeatedly in the derivation of equations 3.7 and 3.8.

$$
\begin{aligned}
P_2^2 &= \frac{18}{35}P_4 + \frac{2}{7}P_2 + \frac{1}{5} \\
P_2P_4 &= \frac{5}{11}P_6 + \frac{20}{77}P_4 + \frac{2}{7}P_2 \\
\left(\frac{dP_2}{d\theta}\right)^2 &= -\frac{72}{35}P_4 + \frac{6}{7}P_2 + \frac{6}{5} \\
\frac{dP_2}{d\theta}\frac{dP_4}{d\theta} &= -\frac{40}{11}P_6 + \frac{60}{77}P_4 + \frac{20}{7}P_2 .
\end{aligned}
\qquad (3.9)
$$

Collecting the P_o terms of equations 3.7 and 3.8 one obtains

$$
\left[\frac{1}{R_o}\frac{d\phi_o}{dt} + \frac{1}{2}\frac{\phi_o^2}{R_o^4} - \frac{p_\infty - p_c}{\rho}\right] + \epsilon^2\left[\frac{1}{5R_o}\frac{d\phi_o}{dt}\frac{R_2'^2}{R_o^2} - \frac{3}{5R_o^3}\frac{d\phi_2'}{dt}\frac{R_2'}{R_o} - \frac{18}{5}\frac{\phi_o\phi_2'}{R_o^6}\frac{R_2'}{R_o} + \frac{3}{2}\frac{\phi_2'^2}{R_o^2} + \frac{\phi_o^2R_2'^2}{R_o^6}\right] = 0 + O(\epsilon^2\beta) \qquad (3.10)
$$

$$
\left[\frac{\phi_o}{R_o^2} + \frac{dR_o}{dt}\right] + \epsilon^2\left[\frac{3}{5}\frac{\phi_o}{R_o^2}\frac{R_2'^2}{R_o^2} - \frac{6}{5}\frac{\phi_2'}{R_o^4}\frac{R_2'}{R_o}\right] = 0 + O(\epsilon^2\beta). \qquad (3.11)
$$

The P_2 terms of equations 3.7 and 3.8 give

$$
\epsilon\left[-\frac{1}{R_o^2}\frac{d\phi_o}{dt}R_2' + \frac{1}{R_o^3}\frac{d\phi_2'}{dt} - 2\frac{\phi_o^2}{R_o^5}R_2' + 3\frac{\phi_o\phi_2'}{R_o^6}\right] + \epsilon^2\left[\frac{2}{7R_o^3}\frac{d\phi_o}{dt}R_2'^2 - \frac{6}{7R_o^4}\frac{d\phi_2'}{dt}R_2' + \frac{10}{7}\frac{\phi_o^2}{R_o^6}R_2'^2 - \frac{36}{7}\frac{\phi_o\phi_2'}{R_o^7}R_2' + \frac{12}{7}\frac{\phi_2'^2}{R_o^8}\right]
$$

$$\begin{aligned}
&+\epsilon^2\alpha\left[\frac{4}{7R_o^3}\frac{d\phi_o}{dt}R_2'R_4'' - \frac{6}{7R_o^4}\frac{d\phi_2'}{dt}R_4'' - \frac{10}{7R_o^5}\frac{d\phi_4''}{dt}R_2' + \frac{20}{7}\frac{\phi_o^2}{R_o^6}R_2'R_4''\right.\\
&\left.-\frac{36}{7}\frac{\phi_o}{R_o^7}\phi_2'R_4'' - \frac{80}{7}\frac{\phi_o}{R_o^9}\phi_4''R_2' + \frac{50}{7}\frac{\phi_2'\phi_4''}{R_o^{10}}\right] = 0 + O(\epsilon^2\beta)
\end{aligned} \tag{3.12}$$

$$\begin{aligned}
&\epsilon\left[-2\frac{\phi_o}{R_o^3}R_2' + 3\frac{\phi_2'}{R_o^4} + \frac{dR_2'}{dt}\right] + \epsilon^2\left[\frac{6}{7}\frac{\phi_o}{R_o^4}R_2'^2 - \frac{18}{7}\frac{\phi_2'}{R_o^5}R_2'\right]\\
&+\epsilon^2\alpha\left[\frac{12}{7}\frac{\phi_o}{R_o^4}R_2'R_4'' - \frac{4}{7}\frac{\phi_2'}{R_o^5}R_4'' - \frac{40}{7}\frac{\phi_4''}{R_o^7}R_2'\right] = 0 + O(\epsilon^2\beta).
\end{aligned} \tag{3.13}$$

The P_4 terms of equations 3.7 and 3.8 give

$$\begin{aligned}
&\epsilon\alpha\left[-\frac{1}{R_o^2}\frac{d\phi_o}{dt}R_4'' + \frac{1}{R_o^5}\frac{d\phi_4''}{dt} - 2\frac{\phi_o^2}{R_o^5}R_4'' + 5\frac{\phi_o}{R_o^8}\phi_4''\right] + \epsilon^2\left[\frac{18}{35}\frac{1}{R_o^3}\frac{d\phi_o}{dt}R_2'^2\right.\\
&\left.-\frac{54}{35}\frac{1}{R_o^4}\frac{d\phi_2'}{dt}R_2' + \frac{90}{35}\frac{\phi_o^2}{R_o^6}R_2'^2 - \frac{324}{35}\frac{\phi_o}{R_o^7}\phi_2'R_2' + \frac{45}{35}\frac{\phi_2'^2}{R_o^8}\right]\\
&+\epsilon^2\alpha\left[\frac{40}{77}\frac{1}{R_o^3}\frac{d\phi_o}{dt}R_2'R_4'' - \frac{60}{77}\frac{1}{R_o^4}\frac{d\phi_2'}{dt}R_4'' - \frac{100}{77}\frac{1}{R_o^6}\frac{d\phi_4''}{dt}R_2'\right.\\
&\left.+\frac{200}{77}\frac{\phi_o^2}{R_o^6}R_2'R_4'' - \frac{360}{77}\frac{\phi_o}{R_o^7}\phi_2'R_4'' - \frac{800}{77}\frac{\phi_o}{R_o^9}\phi_4''R_2' + \frac{360}{77}\frac{\phi_2'\phi_4''}{R_o^{10}}\right]\\
&= 0 + O(\epsilon^2\beta)
\end{aligned} \tag{3.14}$$

$$\epsilon\alpha\left[-2\frac{\phi_o}{R_o^3}R_4''+5\frac{\phi_4''}{R_o^6}+\frac{dR_4''}{dt}\right]+\epsilon^2\left[\frac{54}{35}\frac{\phi_o}{R_o^4}R_2'^2-\frac{288}{35}\frac{\phi_2'}{R_o^5}R_2'\right]$$

$$+\epsilon^2\alpha\left[\frac{120}{77}\frac{\phi_o}{R_o^4}R_2'R_4''-\frac{180}{77}\frac{\phi_2'}{R_o^5}R_4''-\frac{540}{77}\frac{\phi_4''}{R_o^7}R_2'\right]=0+O(\epsilon^2\beta).$$

(3.15)

The P_6 terms of equations 3.7 and 3.8 give

$$\epsilon\beta\left[-\frac{1}{R_o^2}\frac{d\phi_o}{dt}R_6''+\frac{1}{R_o^7}\frac{d\phi_6''}{dt}-2\frac{\phi_o^2}{R_o^5}R_6''+7\frac{\phi_o}{R_o^{10}}\phi_6''\right]+\epsilon^2\alpha\left[\frac{10}{11}\frac{1}{R_o^3}\frac{d\phi_o}{dt}R_2'R_4''\right.$$

$$-\frac{15}{11}\frac{1}{R_o^4}\frac{d\phi_2'}{dt}R_4''-\frac{25}{11}\frac{1}{R_o^6}\frac{d\phi_4''}{dt}R_2'+\frac{50}{11}\frac{\phi_o^2}{R_o^6}R_2'R_4''-\frac{90}{11}\frac{\phi_o}{R_o^7}\phi_2'R_4''$$

$$\left.-\frac{200}{11}\frac{\phi_o}{R_o^9}\phi_4''R_2'+\frac{35}{11}\frac{\phi_2'\phi_4''}{R_o^{10}}\right]=0+O(\epsilon^2\beta) \qquad (3.16)$$

$$\epsilon\beta\left[-2\frac{\phi_o}{R_o^3}R_6''+7\frac{\phi_6''}{R_o^8}+\frac{dR_6''}{dt}\right]+\epsilon^2\alpha\left[\frac{30}{11}\frac{\phi_o}{R_o^4}R_2'R_4''-\frac{100}{11}\frac{\phi_2'}{R_o^5}R_4''\right.$$

$$\left.-\frac{190}{11}\frac{\phi_4''}{R_o^7}R_2'\right]=0+O(\epsilon^2\beta). \qquad (3.17)$$

Studying the equations 3.10 to 3.17 one notices that R_o and ϕ_o will not be badly affected by large perturbations, because the largest perturbing terms in equations 3.10 and 3.11 are of order ϵ^2. The error caused by neglecting the terms of order ϵ^2 from equations 3.12 and 3.13 will be much larger, but will not be intolerable unless ϵ becomes very big. This is no longer true in equations 3.14 and 3.15 because terms of order ϵ^2 may be almost as big as the terms of order $\epsilon\alpha$. One must therefore include the ϵ^2 terms, while the $\epsilon^2\alpha$ terms may still be neglected. Similarly terms of order $\epsilon^2\alpha$ may become comparable to the $\epsilon\beta$ terms in equations 3.16 and 3.17 and must also be included.

Fortunately no non-linearities are introduced in the equations 3.14, 3.15, 3.16 and 3.17 by including these higher order terms, for by the time equations 3.14 and 3.15 are solved for R''_4 and ϕ''_4, R'_2 and ϕ'_2 are already known functions of R_o. Similarly R'_2, ϕ'_2, R''_4, ϕ''_4 are known when equations 3.16 and 3.17 are solved for ϕ''_6 and R''_6.

With the use of equation 3.11, equations 3.14 and 3.15 can be written in the following form:

$$\frac{d}{dR_o}\left(\frac{\phi''_4}{R_o^5}\right) = R''_4 \frac{d}{dR_o}\left(\frac{\phi_o}{R_o^2}\right) + \frac{18}{175}\left(\frac{\epsilon}{\alpha}\right)\left(\frac{R_o^2}{\phi_o}\right)\Bigg[-5\,\frac{\phi_o}{R_o^5}\,\frac{d\phi_o}{dR_o}\,R_2'^2 + 15\,\frac{\phi_o}{R_o^6}\,\frac{d\phi'_2}{dR_o}\,R'_2$$
$$+ 25\,\frac{\phi_o^2}{R_o^6}\,R_2'^2 - 90\,\frac{\phi_o\phi'_2}{R_o^7}\,R'_2 + \frac{25}{2}\,\frac{\phi_2'^2}{R_o^8}\Bigg] + O(\epsilon) \qquad (3.18)$$

$$\frac{\phi''_4}{R_o^5} = \frac{1}{5}\,\frac{\phi_o}{R_o^3}\,\frac{d}{dR_o}\left(R_o^2 R''_4\right) - \frac{18}{175}\left(\frac{\epsilon}{\alpha}\right)\left[3\,\frac{\phi_o}{R_o^4}\,R_2'^2 - 16\,\frac{\phi'_2}{R_o^5}\,R'_2\right] + O(\epsilon). \qquad (3.19)$$

Eliminating ϕ_4 between equations 3.18 and 3.19 one obtains

$$\frac{d}{dR_o}\left[\frac{\phi_o}{R_o^3}\,\frac{d}{dR_o}\left(R_o^2 R''_4\right)\right] - 5\,R''_4\,\frac{d}{dR_o}\left(\frac{\phi_o}{R_o^2}\right) = \frac{18}{35}\left(\frac{\epsilon}{\alpha}\right)\Bigg[-\frac{2}{R_o^3}\,\frac{d\phi_o}{dR_o}\,R_2'^2$$

$$- \frac{1}{R_o^4}\frac{d\phi_2'}{dR_o}R_2' + 16\frac{\phi_o}{R_o^4}R_2'^2 - 26\frac{\phi_2'}{R_o^5}R_2' + \frac{25}{2}\frac{\phi_2'^2}{\phi_o R_o^6} + 6\frac{\phi_o R_2'}{R_o^3}\frac{dR_2'}{dR_o}$$

$$- 16\frac{\phi_2'}{R_o^4}\frac{dR_2'}{dR_o}\Bigg] + O(\epsilon). \qquad (3.20)$$

Using equations 3.12 and 3.13 to eliminate ϕ_2 from equation 3.20 gives

$$\frac{d}{dR_o}\left[\frac{\phi_o}{R_o^3}\frac{d}{dR_o}(R_o^2 R_4'')\right] - 5R_4''\frac{d}{dR_o}\left(\frac{\phi_o}{R_o^2}\right) = \frac{1}{35}\left(\frac{\epsilon}{\alpha}\right)\Bigg[-\frac{54}{R_o^3}\frac{d\phi_o}{dR_o}R_2'^2$$

$$+ 76\frac{\phi_o}{R_o^4}R_2'^2 - 158\frac{\phi_o}{R_o^3}R_2'\frac{dR_2'}{dR_o} - 71\frac{\phi_o}{R_o^2}\left(\frac{dR_2'}{dR_o}\right)^2\Bigg] + O(\epsilon). \qquad (3.21)$$

Substituting the value of ϕ_o as given by equation 2.37, putting

$$x = \frac{R_o^3(0)}{R_o^3}; \qquad y_2 = \frac{R_2}{R_2(0)}; \qquad y_4 = \frac{R_4}{R_4(0)}$$

and using equation 3.6, the final form of the R_4 equation is obtained

$$(1 - x)x\frac{d^2y_4}{dx^2} + \left(\frac{1}{3} - \frac{5}{6}x\right)\frac{dy_4}{dx} - \frac{1}{2}y_4$$

$$= -\frac{1}{315}\left[\frac{R_2^2(0)}{R_o(0)\,R_4(0)}\right]\left[x^{-2/3}\right]\Bigg[(49x+32)y_2^2 + 474(x-1)xy_2\frac{dy_2}{dx}$$

$$- 639\,(x-1)x^2\left(\frac{dy_2}{dx}\right)^2\Bigg]. \qquad (3.22)$$

The differential equation thus remains the same as equation 2.41, except for the fact that a forcing function has been added.

When ϕ_6'' is eliminated between equations 3.16 and 3.17 one obtains

$$\frac{d}{dR_o}\left[\frac{\phi_o}{R_o^3}\frac{d}{dR_o}(R_o^2R_6'')\right] = 7R_6''\frac{d}{dR_o}\left(\frac{\phi_o}{R_o^2}\right) + \frac{5}{11}\left(\frac{\epsilon\alpha}{\beta}\right)\left[-\frac{8}{R_o^3}\frac{d\phi_o}{dR_o}R_2'R_4''\right.$$

$$+\frac{1}{R_o^4}\frac{d\phi_2'}{dR_o}R_4'' - \frac{3}{R_o^6}\frac{d\phi_4''}{dR_o}R_2' + 52\frac{\phi_o}{R_o^4}R_2'R_4'' - 46\frac{\phi_2'}{R_o^5}R_4'' - 52\frac{\phi_4''}{R_o^7}R_2'$$

$$+ 49\frac{\phi_2'\phi_4''}{R_o^8\phi_o} + 6\frac{\phi_o}{R_o^8}R_2'\frac{dR_4''}{dR_o} + 6\frac{\phi_o}{R_o^3}R_4''\frac{dR_2'}{dR_o} - 20\frac{\phi_2'}{R_o^4}\frac{dR_4''}{dR_o}$$

$$\left.- 38\frac{\phi_4''}{R_o^6}\frac{dR_2'}{dR_o}\right] + O(\epsilon). \qquad (3.23)$$

Eliminating ϕ_2 and ϕ_4 from equation 3.23 with the help of equations 3.12, 3.13, 3.14 and 3.15 one arrives at

$$\frac{d}{dR_o}\left[\frac{\phi_o}{R_o^3}\frac{d}{dR_o}(R_o^2R_6'')\right] = 7R_6''\frac{d}{dR_o}\left(\frac{\phi_o}{R_o^2}\right) + \frac{1}{33}\left(\frac{\epsilon\alpha}{\beta}\right)\left[-\frac{150}{R_o^3}\frac{d\phi_o}{dR_o}R_2'R_4''\right.$$

$$+ 204\frac{\phi_o}{R_o^4}R_2'R_4'' - 255\frac{\phi_o}{R_o^3}R_4''\frac{dR_2'}{dR_o} - 213\frac{\phi_o}{R_o^3}R_2'\frac{dR_4''}{dR_o}$$

$$\left.- 165\frac{\phi_o}{R_o^2}\frac{dR_2'}{dR_o}\frac{dR_4''}{dR_o}\right] - \frac{1}{385}\left(\frac{\epsilon^2}{\beta}\right)\left[\frac{540}{R_o^4}\frac{d\phi_o}{dR_o}R_2'^3 + 3148\frac{\phi_o}{R_o^5}R_2'^3\right.$$

$$\left.+ 5776\frac{\phi_o}{R_o^4}R_2'^2\frac{dR_2'}{dR_o} + 2155\frac{\phi_o}{R_o^3}R_2'\left(\frac{dR_2'}{dR_o}\right)^2\right] + O(\epsilon). \qquad (3.24)$$

Substituting again for ϕ_o from equation 2.37, putting

$$x = \frac{R_o^3(0)}{R_o^3}; \quad y_2 = \frac{R_2}{R_2(0)}; \quad y_4 = \frac{R_4}{R_4(0)} \quad \text{and} \quad y_6 = \frac{R_6}{R_6(0)}$$

and using equations 3.6, the final form of the R_6 equation is obtained

$$(1-x)\,x\,\frac{d^2y_6}{dx^2} + \left(\frac{1}{3} - \frac{5}{6}x\right)\frac{dy_6}{dx} - \frac{5}{6}y_6$$

$$= -\frac{1}{297}\left[\frac{R_2(0)\,R_4(0)}{R_o(0)\,R_6(0)}\right](x^{-2/3})\left[(129x+96)\,y_2\,y_4 + 765(x-1)x\,\frac{dy_2}{dx}\,y_4\right.$$

$$\left. + 639(x-1)xy_2\,\frac{dy_4}{dx} - 1485(x-1)x^2\,\frac{dy_2}{dx}\,\frac{dy_4}{dx}\right]$$

$$+ \frac{1}{3465}\left[\frac{R_2^3(0)}{R_o^2(0)\,R_6(0)}\right](x^{-1/3})\left[(3418x-4228)y_2^3\right.$$

$$\left. - 17328(x-1)xy_2^2\,\frac{dy_2}{dx} + 19395(x-1)x^2y_2\left(\frac{dy_2}{dx}\right)^2\right]. \qquad (3.25)$$

Again the equation is the same as equation 2.41 with $n = 3$, with the exception that a forcing function has been added.

Equations 3.22 and 3.25 can both be written in the form

$$(1-x)\,x\,\frac{d^2y_{2n}}{dx^2} + \left(\frac{1}{3} - \frac{5}{6}x\right)\frac{dy_{2n}}{dx} - \frac{1}{6}(2n-1)y_{2n} = F_{2n}(x). \qquad (3.26)$$

Since the solutions to the homogeneous equation are known, the complete solution can be formed by variation of parameters (13). The solutions to the homogeneous equation 2.41 as given by equation 2.46 already satisfy the initial conditions of equations 3.2 and 3.3 provided A_{2n} and B_{2n} are chosen according to equations 2.52 and 2.54. The complete solution will therefore satisfy the initial conditions if the particular solution of the nonhomogeneous equation 3.26, y_{2nP}, satisfies the homogeneous initial conditions

$$y_{2nP}(1) = 0 \tag{3.27}$$

$$\frac{dy_{2nP}}{dx}(1) \text{ is finite.} \tag{3.28}$$

Equation 3.28 gives rise to a homogeneous initial condition because $\frac{dx}{dt}$ vanishes initially

Let u_{2n} be a solution of the homogeneous differential equation and assume that a particular solution of equation 3.26 can be written in the form

$$y_{2nP} = u_{2n}\, U_{2n}(x). \tag{3.29}$$

Substituting equation 3.29 in equation 3.26 one obtains

$$\frac{d^2U_{2n}}{dx^2} + \frac{dU_{2n}}{dx}\left[\frac{2}{u_{2n}}\frac{du_{2n}}{dx} + \frac{(\frac{1}{3} - \frac{5}{6}x)}{(1-x)x}\right] = \frac{F_{2n}}{(1-x)x\,u_{2n}}. \tag{3.30}$$

Equation 3.30 is linear and of first order in $\frac{dU_{2n}}{dx}$, so that one may always find an integrating factor. Then $\frac{dU_{2n}}{dx}$ can be written

$$\frac{dU_{2n}}{dx} = -\frac{1}{u_{2n}^2(x-1)^{1/2}x^{1/3}} \int_1^x \frac{u_{2n}F_{2n}(x)}{(x-1)^{1/2}x^{2/3}}\,dx. \tag{3.31}$$

The lower limit has been chosen such that $\frac{dy_{2nP}}{dx}(1)$ is finite if either of y_{2n_1} or y_{2n_2} are used for u_{2n}. y_{2n_1} and y_{2n_2} are the solutions to the homogeneous equation as given by equation 2.46.

Integrating equation 3.31 and choosing the lower limit such that $y_{2nP}(1) = 0$ for $u_{2n} = y_{2n_1}$ or y_{2n_2}, one obtains

$$U_{2n}(x) = -\int_1^x \left[\frac{1}{u_{2n}^2 (x-1)^{1/2} x^{1/3}} \int_1^x \frac{u_{2n} F_{2n}}{(x-1)^{1/2} x^{2/3}} dx \right] dx. \quad (3.32)$$

The particular solution of equation 3.26 now follows from equations 3.29 and 3.32

$$y_{2nP} = -u_{2n} \int_1^x \left[\frac{1}{u_{2n}^2 (x-1)^{1/2} x^{1/3}} \int_1^x \frac{u_{2n} F_{2n}}{(x-1)^{1/2} x^{2/3}} dx \right] dx. \quad (3.33)$$

The general solution of equation 3.26 is then of the form

$$y_{2n} = A_{2n} y_{2n_1} + B_{2n} y_{2n_2} + y_{2nP}. \quad (3.34)$$

The integrals of equation 3.33 will now be examined in order to obtain an understanding of the meaning of the singular points in the integrands.

The singularities at $x = 1$ are considered first. Let

$$g_{2n}(x) = \frac{1}{(x-1)^{1/2} x^{1/3}} \int_1^x \frac{u_{2n} F_{2n}}{(x-1)^{1/2} x^{2/3}} dx. \quad (3.35)$$

If $u_{2n} = y_{2n_1}$, $g_{2n}(x)$ has no singular points for $1 \leq x < \infty$. In the neighborhood of $x = 1$, $g(x)$ can be expanded to give

$$g_{2n_1}(x) = 2 F_{2n}(1) + O(x-1). \quad (3.36)$$

If $u_{2n} = y_{2n_2}$, $g_{2n}(x)$ may be expanded to give

$$g_{2n_2}(x) = (x-1)^{1/2} F_{2n}(1) + O(x-1)^{3/2} \tag{3.37}$$

in the neighborhood of $x = 1$.

Using either of the equations 3.36 or 3.37, the following expansion for y_{2nP} is obtained in the neighborhood of $x = 1$

$$y_{2nP} = -2 F_{2n}(1) \cdot (x-1) + O(x-1)^2.$$

The point $x = 1$ thus presents no difficulty.

The other singular points which must be considered are the zeros of u_{2n} which do not coincide with the point $x = 1$. Both y_{2n_1} and y_{2n_2} have a finite number of zeros for $1 < x < \infty$. These zeros are simple, as can be seen from equation 2.41; for if $\frac{dy_{2n}}{dx}$ vanishes at a zero of y_{2n}, $\frac{d^2y_{2n}}{dx^2}$ and all the higher derivatives of y_{2n} must must also vanish. Then y_{2n} is identically zero, and this case may be excluded. The functions $g_{2n}(x)$ as given by equation 3.35 are well behaved for $1 < x < \infty$, and

$$y_{2nP} = -u_{2n} \int_1^x \frac{g(x)}{u_{2n}^2(x)}\, dx. \tag{3.38}$$

Let $u_{2n}(x)$ have its i^{th} zero at $x = \mu_i$. Then one may write

$$u_{2n}(x) = (x-\mu_i)\, h(x) \tag{3.39}$$

where $h(x) \neq 0$ for $\mu_{i-1} < x < \mu_{i+1}$. One may also write

$$\frac{g(x)}{h^2(x)} = \ell(x) = \ell(\mu_i) + (x-\mu_i)\frac{d\ell}{dx}(\mu_i) + (x-\mu_i)^2\, m(x) \tag{3.40}$$

where $m(x)$ contains no singularities for $\mu_{i-1} < x < \mu_{i+1}$. It can be shown that $\frac{d\ell}{dx}(\mu_i)$ vanishes*, viz:

$$\frac{d\ell}{dx}(\mu_i) = \frac{g(\mu_i)}{h^2(\mu_i)}\left[\frac{1}{g(\mu_i)}\frac{dg}{dx}(\mu_i) - \frac{2}{h(\mu_i)}\frac{dh}{dx}(\mu_i)\right]$$

$$\frac{1}{g(\mu_i)}\frac{dg}{dx}(\mu_i) = \frac{\frac{1}{3}-\frac{5}{6}\mu_i}{\mu_i(\mu_i-1)} = \frac{1}{\frac{du_{2n}}{dx}(\mu_i)} \cdot \frac{d^2u_{2n}}{dx^2}(\mu_i)$$

$$= \frac{1}{\frac{du_{2n}}{dx}(\mu_i)} \cdot \frac{d^2u_{2n}}{dx^2}(\mu_i) \qquad \text{from equation 2.41}$$

$$= \frac{2}{h(\mu_i)}\frac{dh}{dx}(\mu_i) \qquad \text{from equation 3.39}$$

$$\therefore \quad \frac{d\ell}{dx}(\mu_i) = 0. \tag{3.41}$$

Equation 3.40 can now be written

$$\frac{g(x)}{h^2(x)} = \ell(x) = \ell(\mu_i) + (x-\mu_i)^2\, m(x). \tag{3.42}$$

In the interval $\mu_{i-1} < \gamma < x < \mu_{i+1}$, the integral of equation 3.35 then becomes

$$\int_1^x \frac{g(x)}{u_{2n}^2(x)}\,dx = \int_1^\gamma \frac{g(x)}{u_{2n}^2(x)}\,dx + \int_\gamma^x \left[\frac{\ell(\mu_i)}{(x-\mu_i)^2} + m(x)\right] dx$$

$$= -\frac{\ell(\mu_i)}{(x-\mu_i)} + M(x) + C(\gamma) \tag{3.43}$$

---

* This is a general property of the integrals which arise from the variation of parameters method. A proof is given in appendix 1.

where $M(x) = \int m(x)\,dx$

$C(\gamma)$ is a constant which depends on γ.

One may now write

$$y_{2nP} = h(x)\,\frac{g(\mu_i)}{h^2(\mu_i)} - h(x)\,(x-\mu_i)\,M(x) - h(x)\,(x-\mu_i)\,C(\gamma)$$

in the interval $\mu_{i-1} < \gamma < x < \mu_{i+1}$, and

$$\lim_{x \to \mu_i} y_{2nP} = \frac{g(\mu_i)}{h(\mu_i)}\ . \qquad (3.43)$$

The singularities at all the zeros of u_{2n} are thus seen to be removable, and the resulting functions y_{2nP} are well behaved for $1 \leq x < \infty$.

The functions F_{2n} which appear in equation 3.26 contain non-linear terms in the y_{2n}, and since the analytical expressions for the y_{2n} consist of slowly converging power series, it appears the integrals are most easily evaluated numerically. A convenient method for numerical integration close to a singular point at $x = \mu_i$ is as follows:

$$\int_1^x \frac{g(x)}{u_{2n}^2(x)}\,dx = \int_1^\gamma \frac{g(x)}{u_{2n}^2(x)}\,dx + \int_\gamma^x \left[\frac{g(x)}{u_{2n}^2(x)} - \frac{g(\mu_i)}{\left[\frac{du_{2n}}{dx}(\mu_i)\right]^2 (x-\mu_i)^2}\right] dx$$

$$+ \int_\gamma^x \frac{g(\mu_i)}{\left[\frac{du_{2n}}{dx}(\mu_i)\right]^2 (x-\mu_i)^2}\,dx \qquad (3.44)$$

where γ is chosen in such a way that $\frac{g(x)}{u_{2n}^2(x)}$ has no singular points for $\gamma \leq x < \mu_i$. The second integral on the right hand side of equation 3.44 is now evaluated numerically, and is well behaved at $x = \mu_i$, while the third integral can be evaluated analytically.

A particular integral for equation 3.22 will now be calculated. In order to make the results generally applicable, y_2 is written in the form (cf. equation 2.46)

$$y_2 = A_2 y_{2_1} + B_2 y_{2_2} \tag{3.45}$$

where $A_2 = 1$ from equation 2.52, and B_2 is given by equation 2.54 with $n = 1$. The right hand side of equation 3.22 can then be written

$$F_4 = -\frac{1}{315}\left[\frac{R_2^2(0)}{R_o(0)\,R_4(0)}\right](x)^{-2/3}\Bigg[\Big[(49x+32)y_{2_1}^2 + 474(x-1)xy_{2_1}\frac{dy_{2_1}}{dx}$$

$$-639\,(x-1)x^2\left(\frac{dy_{2_1}}{dx}\right)^2\Big] + B_2\Big[2(49x+32)y_{2_1}\,y_{2_2}$$

$$+474(x-1)x\left(y_{2_1}\frac{dy_{2_2}}{dx} + y_{2_2}\frac{dy_{2_1}}{dx}\right) - 2(639)(x-1)x^2\,\frac{dy_{2_1}}{dx}\,\frac{dy_{2_2}}{dx}\Big]$$

$$+B_2^2\Big[(49x+32)y_{2_2}^2 + 474(x-1)xy_{2_2}\frac{dy_{2_2}}{dx} - 639(x-1)x^2\left(\frac{dy_{2_2}}{dx}\right)^2\Big]\Bigg]$$

$$= \frac{R_2^2(0)}{R_o(0)\,R_4(0)}\left[f_{4_1} + B_2 f_{4_2} + B_3 f_{4_3}\right]. \tag{3.46}$$

To obtain y_{4P} one must evaluate three integrals of the type

$$y_{4pi} = -y_{4_2}\int_1^x\left[\frac{1}{y_{4_2}^2(x-1)^{1/2}x^{1/3}}\int_1^x\frac{y_{4_2}f_{4i}}{(x-1)^{1/2}x^{2/3}}\,dx\right]dx \tag{3.47}$$

where y_{4_2} as given by equation 2.46 with $n = 2$ is used for the solution to the homogeneous equation, u_4.

The integrations of equation 3.47 can all be accomplished readily by the method of equation 3.44. y_{4p1}, y_{4p2} and y_{4p3} are shown in figures 3.1, 3.2 and 3.3 as functions of $R_o/R_o(0)$.

y_{4P} then becomes

$$y_{4P} = \frac{R_2^2(0)}{R_o(0)\,R_4(0)} \left[y_{4p1} + B_2\, y_{4p2} + B_2^2\, y_{4p3} \right] \qquad (3.48)$$

and the general solution of equation 3.22 is

$$y_4 = A_4\, y_{4_1} + B_4\, y_{4_2} + y_{4P} \qquad (3.49)$$

where y_{4_1} and y_{4_2} are given by equation 2.46 with $n = 2$, and A_4 and B_4 follow from equations 2.52 and 2.54.

A particular integral for equation 3.25 can be calculated in the same way. This will however not be done here, because the R_6 term is usually quite unimportant.

The following procedure is thus used to calculate the approximate behavior of cavities which satisfy the conditions expressed by equation 3.1:

$\frac{R_o}{R_o(0)}$ is calculated from equation 2.38.

$\frac{R_2}{R_2(0)}$ is calculated from equation 2.46 with $n = 1$.

A_2 and B_2 are obtained from equations 2.52 and 2.54.

$\frac{R_4}{R_4(0)}$ is calculated from equation 3.48

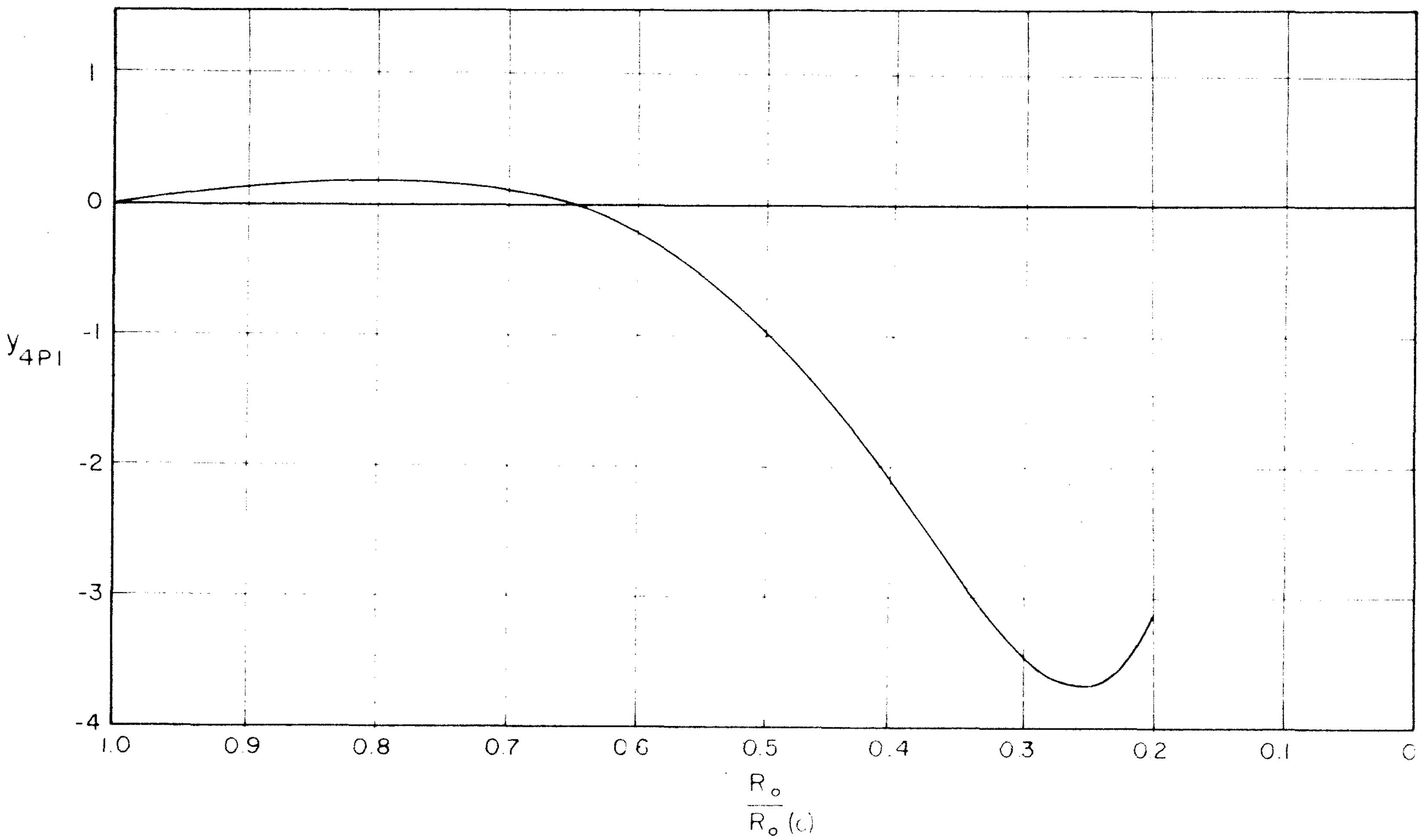

Fig. 3.1. y_{4p1} as a function of $R_o/R_o(0)$.

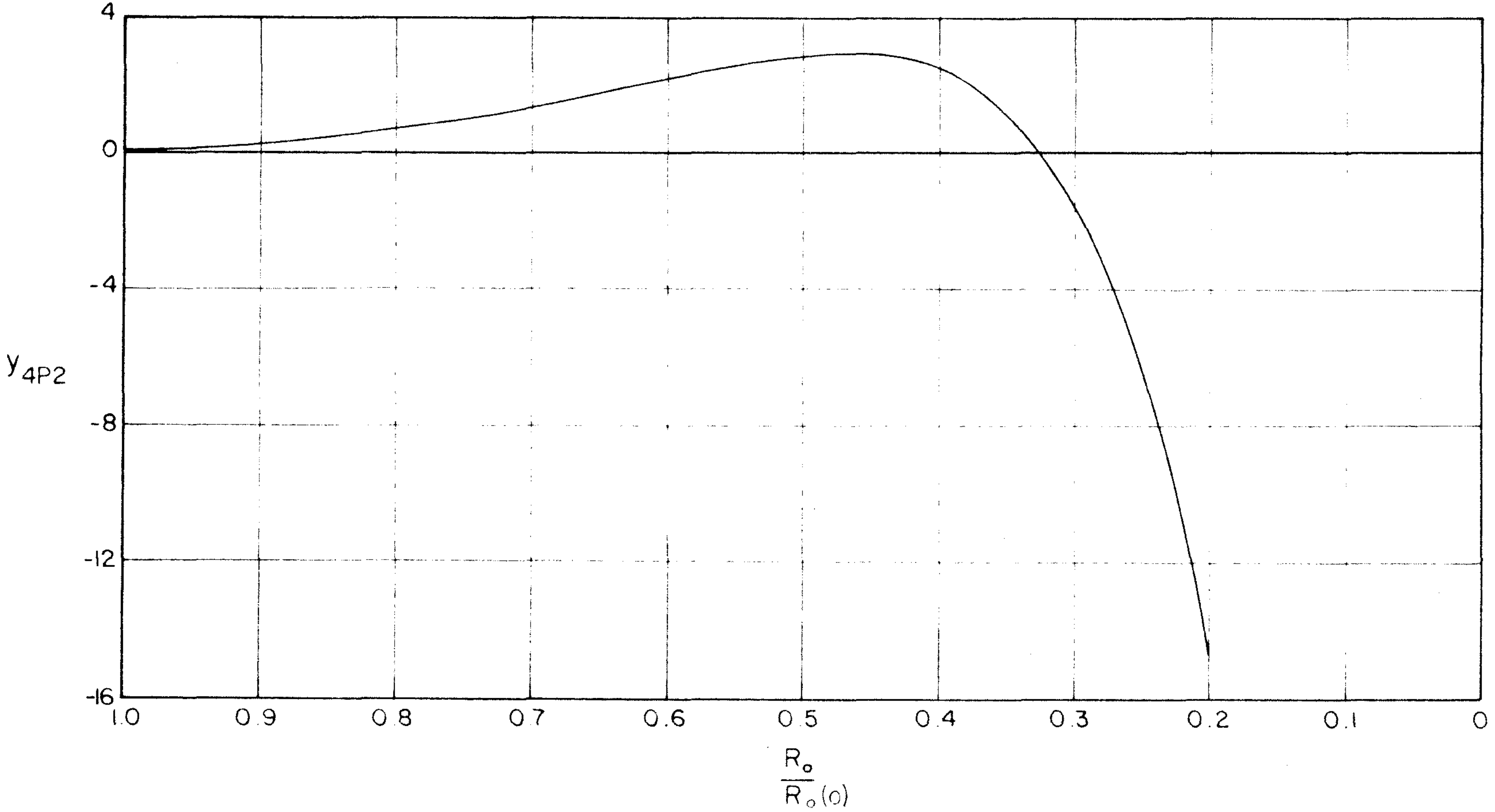

Fig. 3.2. y_{4p2} as a function of $R_o/R_o(0)$.

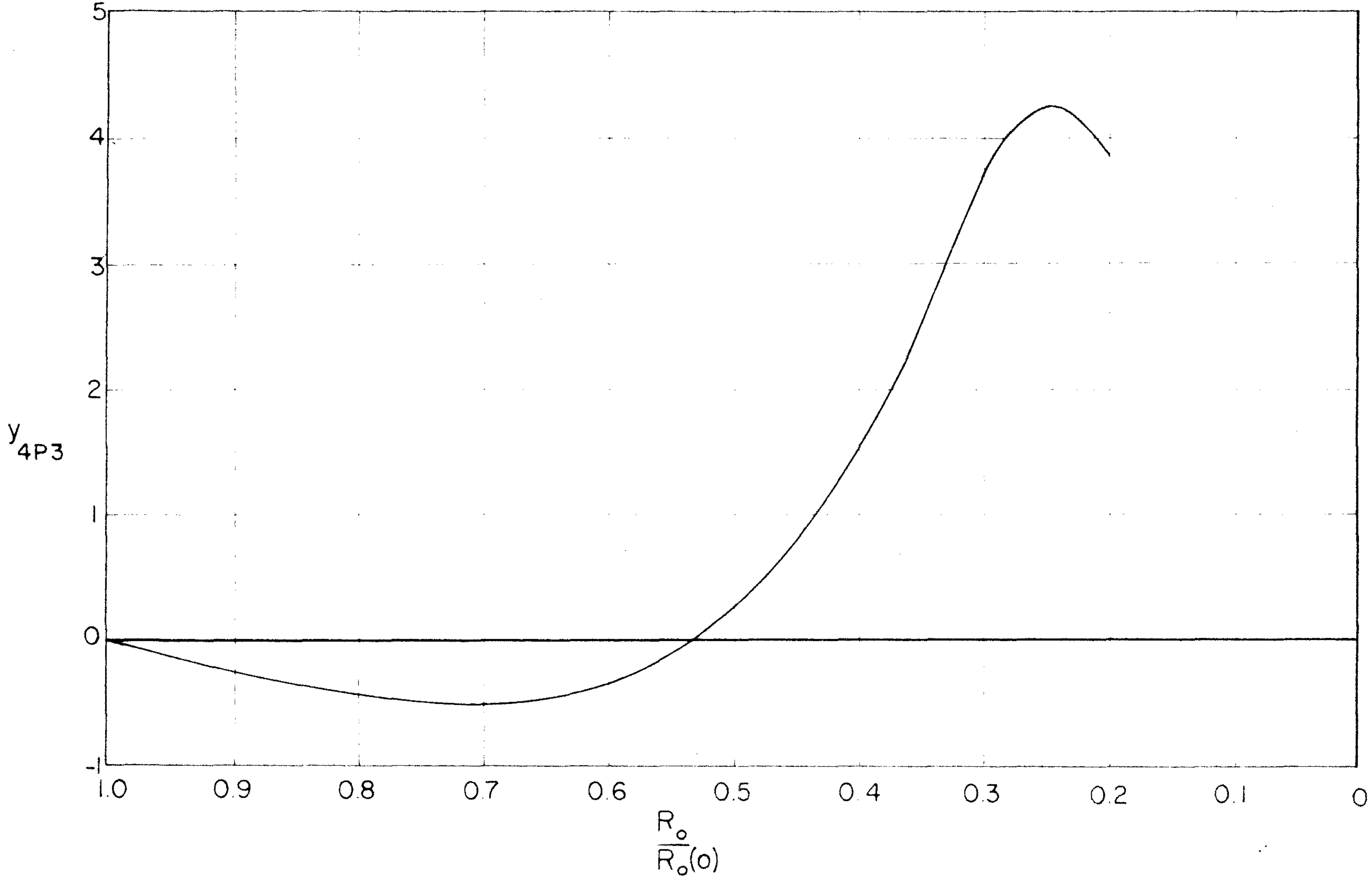

Fig. 3.3. y_{4p3} as a function of $R_o/R_o(0)$.

A_4 and B_4 are again found by means of equations 2.52 and 2.54.

As a concluding remark it may be emphasized again that the theoretical treatment presented here was based on the assumption that real fluid properties do not affect the problem appreciably. The validity of such an assumption is questionable, and too much importance should not be attached to the results without examining effects of the real fluid properties more carefully. Another weakness of the theoretical work is that the range of convergence of a perturbation solution of the type discussed here could not be shown theoretically.

These objections were not regarded as serious in cases of present interest, because it was possible to obtain experimental results which would expose any large errors in the theory.

Chapter IV

The Experimental Equipment and Procedure

1. The high speed camera

In an experimental study of the behavior of a collapsing cavity the high speed motion picture camera plays an essential role. The Ellis Kerr cell camera, which was developed specifically for a study of cavitation, is admirably suited for this purpose because of the relatively long history that can be covered at framing rates and exposure times that compare favorably with any other commercially available cameras. The camera used in this study can, for example, cover a history of 660 microseconds at 1,600,000 pictures per second, and with an exposure time of .05 μs per frame. By reducing the framing rate, longer processes can be studied, the only limitation being the duration of the light which is used to illuminate the subject. A brief discussion of the Ellis camera is included here. For more details the reader is referred to a publication by Ellis (14).

The Kerr cell shutter, which forms the basis of the Ellis camera is shown schematically in figure 4.1. The behavior of such a shutter when a voltage is applied to the electrodes is given by the equation (15)

$$I = I_o \sin^2 \pi B \ell E^2 \qquad (4.1)$$

where I = transmitted intensity

I_o = a constant fraction of the incident intensity

B = Kerr constant of the liquid in the cell

E = electric field in the Kerr cell

ℓ = length of the electrodes.

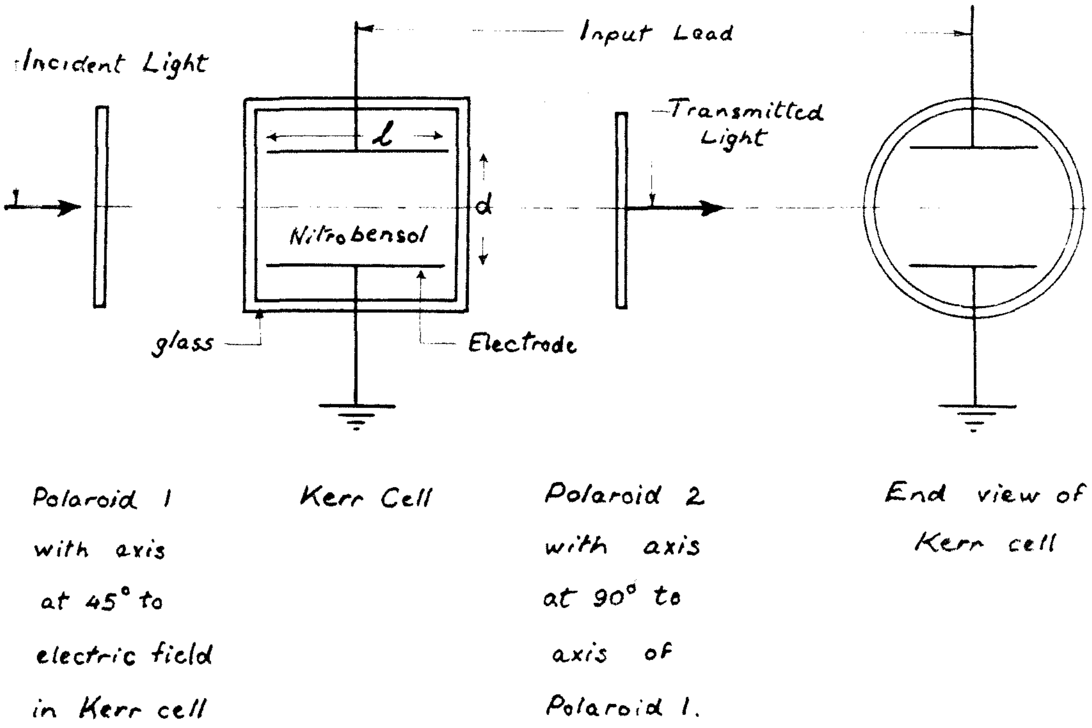

Fig. 4.1. The Kerr cell shutter of the Ellis camera.

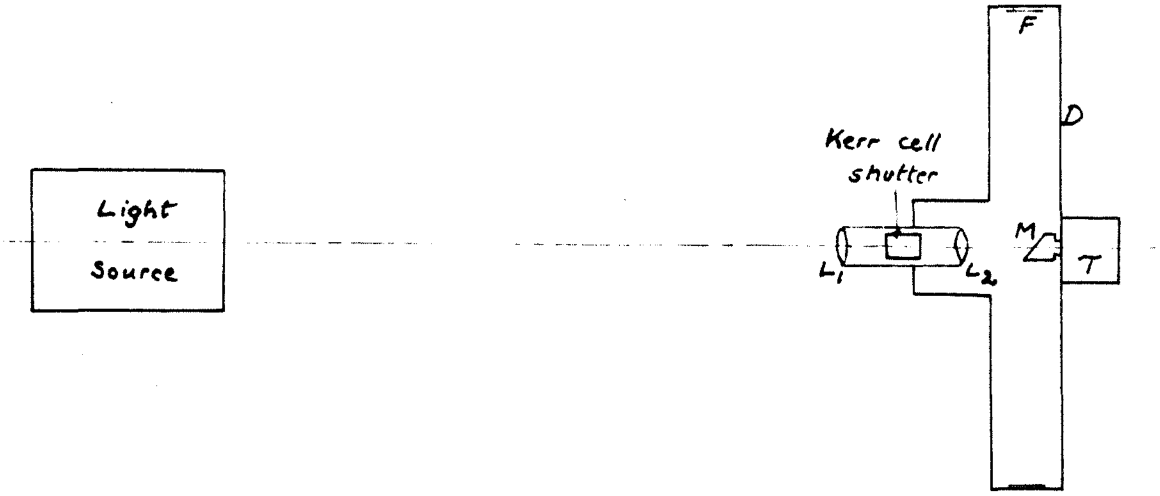

Fig. 4.2. Schematic diagram of the Ellis camera.

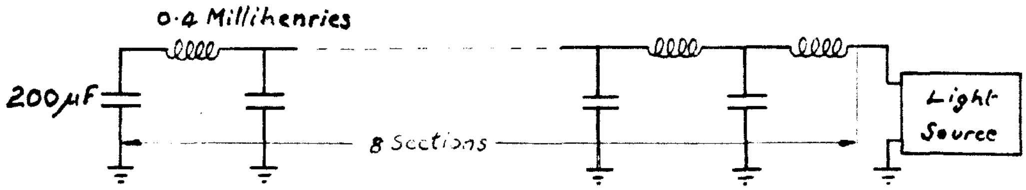

Fig. 4.3. The circuit used for the light source of the Ellis camera.

The theoretical treatment that leads to equation 4.1 is given by Kingsbury (16).

Maximum transmission takes place when the electric field is given by

$$E = \left(\frac{2n+1}{2B\ell}\right)^{1/2} \qquad \text{with } n = 0, 1, 2, \ldots . \qquad (4.2)$$

Using an average value of B for Nitrobenzol, which can be computed from the table given by Beams (15), the smallest voltage for maximum transmission is given by

$$V_M = 33.6 \frac{d}{\sqrt{\ell}} \text{ kilovolts} \qquad (4.3)$$

where d is the distance between the electrodes, and ℓ and d are in centimeters.

In the Ellis camera pulses of amplitude V_M, with variable frequency and width, are applied to the Kerr cell to operate it as a high speed shutter.

The rest of the camera is shown schematically in figure 4.2. In view of the dependence of the Kerr cell pulse voltage on the distance between the electrodes as expressed by equation 4.3 it is desirable to keep d a minimum. For this reason two lenses are used. The first lens L_1 forms an image between the Kerr cell electrodes, and the second lens L_2 focuses this image on the film F through the mirror M which is rotated by air turbine T. The film lies on the inside of the cylindrical drum D. The voltage pulses on the Kerr cell in this manner produce consecutive frames on the film.

The light source consists of a Xenon filled quartz helix (General Electric FT 623) through which a bank of condensers is discharged. In order to obtain a flash of light of reasonable duration the condenser bank is connected as shown in figure 4.3. With the circuit parameters given in figure 4.3 the light intensity stays approximately constant over a period of one millisecond. About thirty microseconds is required to reach full intensity after triggering. After the one millisecond period at full intensity, the intensity drops off fairly rapidly.

2. The method of producing cavities

The second basic requirement for an experimental study of the behavior of a collapsing cavity is that it must be possible to create such a cavity under controlled laboratory conditions at a predetermined time and position. Because the optical resolution of the high speed camera is limited, it is desirable to make the cavity as large as possible, the limitation being that the cavity lifetime should not exceed the duration of the light flash which illuminates the cavity. It should furthermore be taken into account that the effect of gravity was neglected in the theoretical work of chapters II and III, so that a check on the theory will only be obtained if bubble lifetimes are short enough to make this influence negligible.

Assuming that the cavity lifetime is about twice the collapse time T as given by equation 2.36, cavities in water as large as half an inch in diameter can be studied during the available period of illumination, provided the pressure difference, $(p_\infty - p_c)$, is approximately one atmosphere.

The only proven method of generating a cavity which satisfies the requirements mentioned above is that of discharging a spark in the liquid. Although a great deal of controversy still exists about whether spark bubbles are good imitations of actual cavitation bubbles, the spark method was used in this work because no alternative could be found. It was argued that if differences between the two types of cavities did not become evident from comparing the $P_o(\cos\theta)$ component of experimental cavities with the curve of figure 2.2, the spark cavities would be a sufficiently good imitation for the purpose of the study contemplated here. This argument can be justified from Gilmore's (7) results which show that the Rayleigh theory falls very close to the theory which includes effects of compressibility for a cavity collapsing under a constant pressure difference, provided the cavity wall does not exceed velocities of the order of 1/10 of the velocity of sound in the liquid.

The tank in which the spark bubbles were produced is shown in figure 4.4. The distance of the spark gap above the bottom plate is adjustable. Two types of spark gaps were used to determine the effect of the wires on the flow. These are demonstrated in figures 4.6a and b. After it became evident that the two different gap geometries were not causing any visible differences in the cavity shape, the gap of figure 4.6a was used throughout. This gap was chosen because it was better suited to the methods of obtaining pressure measurements on the boundary which are discussed in the next section. Figure 4.5 shows a single flash picture of a cavity in an advanced stage of collapse. The spark gap, and also the spark which produced the cavity are clearly visible.

The electronic circuit which was used to produce the spark is shown in figure 4.7. It was found that the bias of the 2050 thyratron

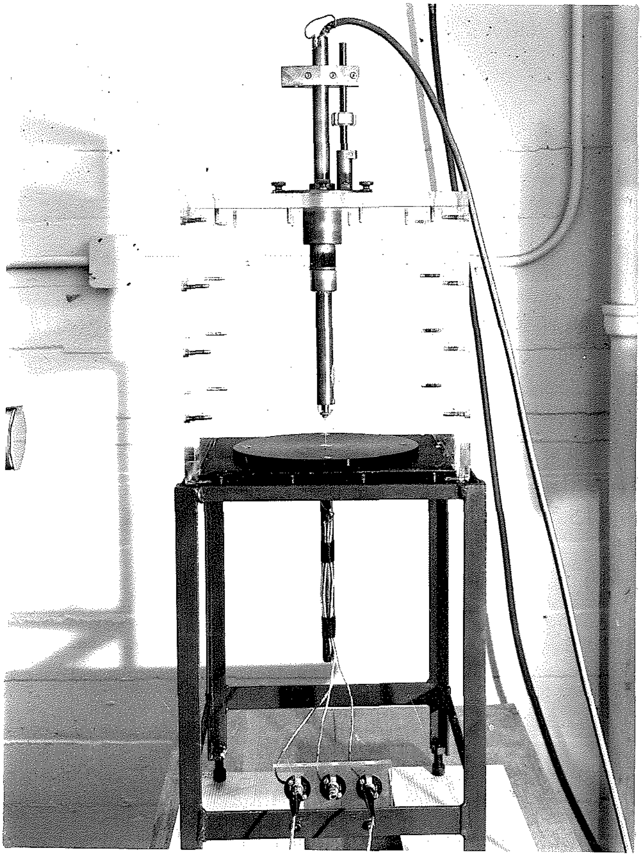

Fig. 4.4. The tank in which cavities were generated.

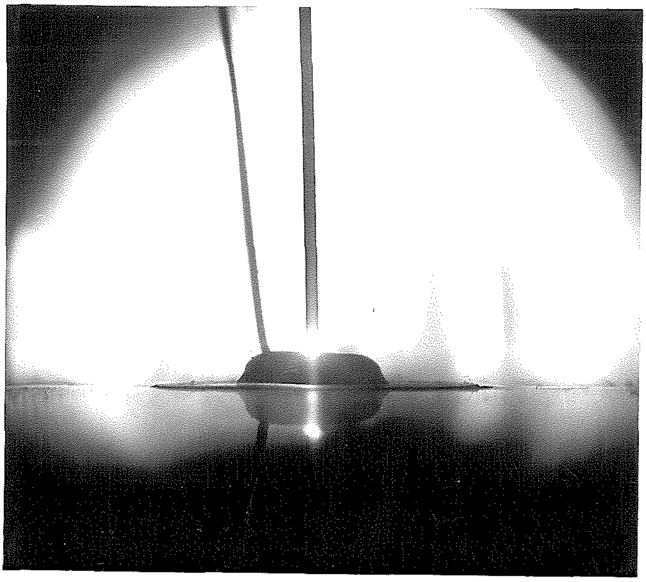

Fig. 4.5. A single flash photograph of a collapsing spark bubble.

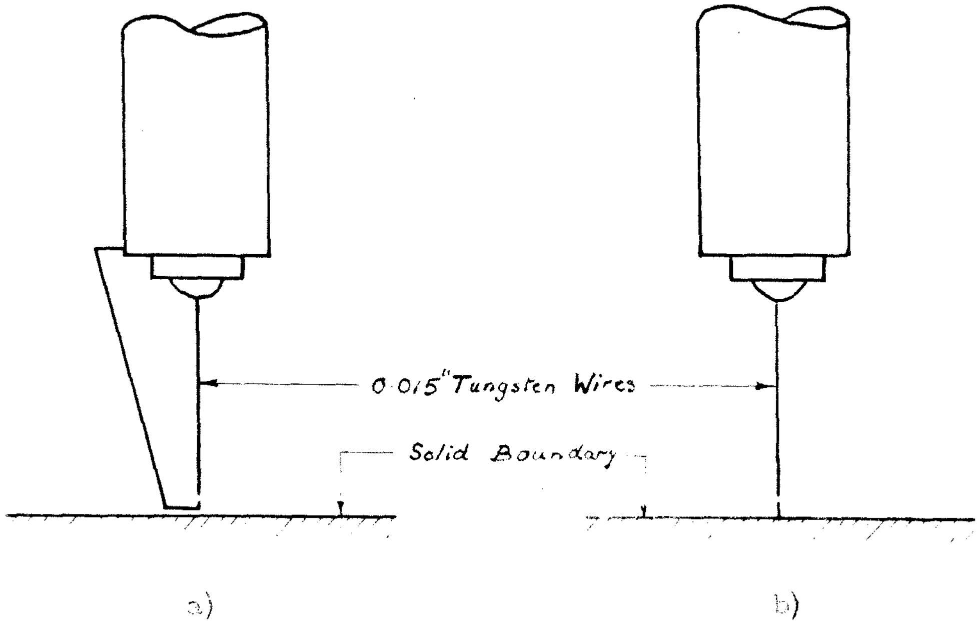

Fig. 4.6. The two types of spark gaps used for generating spark bubbles.

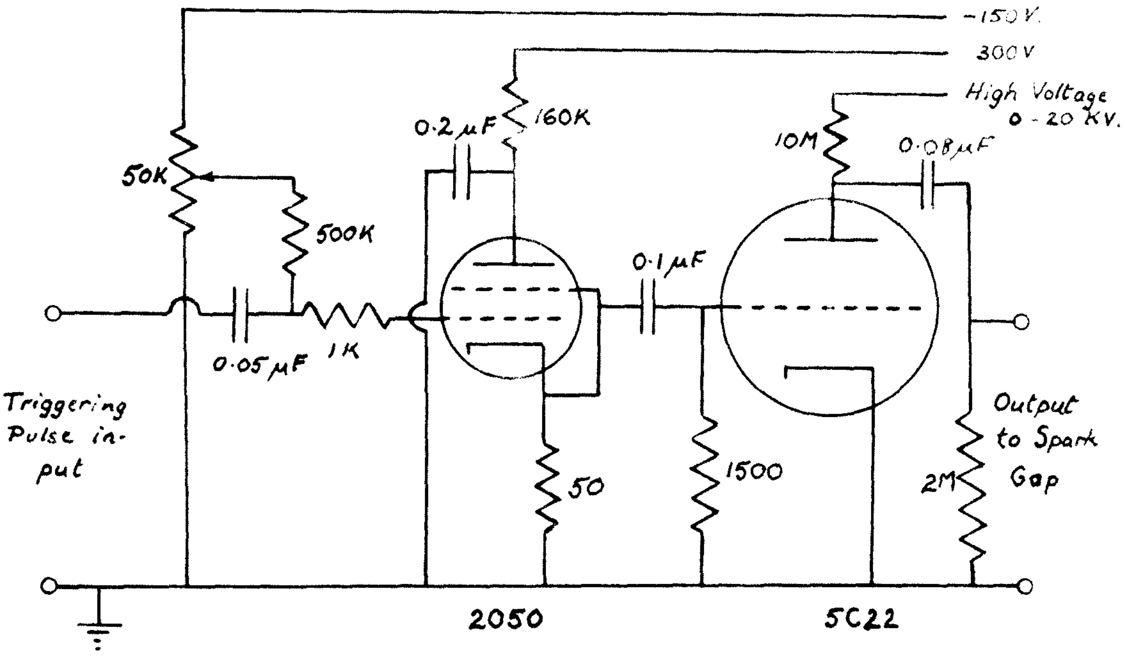

Fig. 4.7. The electronic circuit used to produce the sparks.

could be adjusted to give dependable triggering of the circuit with input pulses of 25V, and 1 μs duration.

3. Techniques used in an attempt to measure pressures on the boundary

A rather obvious fact is demonstrated in figure 4.5, namely that it is impossible to tell from high speed photographs alone whether the cavity actually folds in as is indicated in figure 2.5. Since this type of collapse is one of the most interesting features of the theoretical treatment, provision had to be made to obtain additional data. Several methods of measuring pressures on the boundary were tried in an effort to satisfy this requirement. These methods are discussed briefly below.

i) Quartz Crystal Pickup

The quartz crystal pickup which was constructed is shown in figure 4.8. The crystal Q is glued onto the end of an aluminum bar which is made up of the tubes C_1, C_2 and C_3 and the rod C_4. All these elements are electrically insulated from one another, and thus form the connections to four different areas on the back of the crystal. The insulation of C_1, C_2, C_3 and C_4 was achieved by anodizing them before they were glued together. The aluminum plate P forms the connection to the front of the crystal. Troubles from reflections were minimized by the lead bar L which was glued to the other end of the unit. Electrical connections to C_2, C_3 and C_4 are obtained with wires through size 80 holes drilled down the center of 0-80 nylon screws S_2, S_3 and S_4. An 0-80 brass screw S_1 forms the connection to C_1. The unit was inserted through a 1/2" hole in the bottom of the tank, and was suspended by friction of the O-ring seal. The

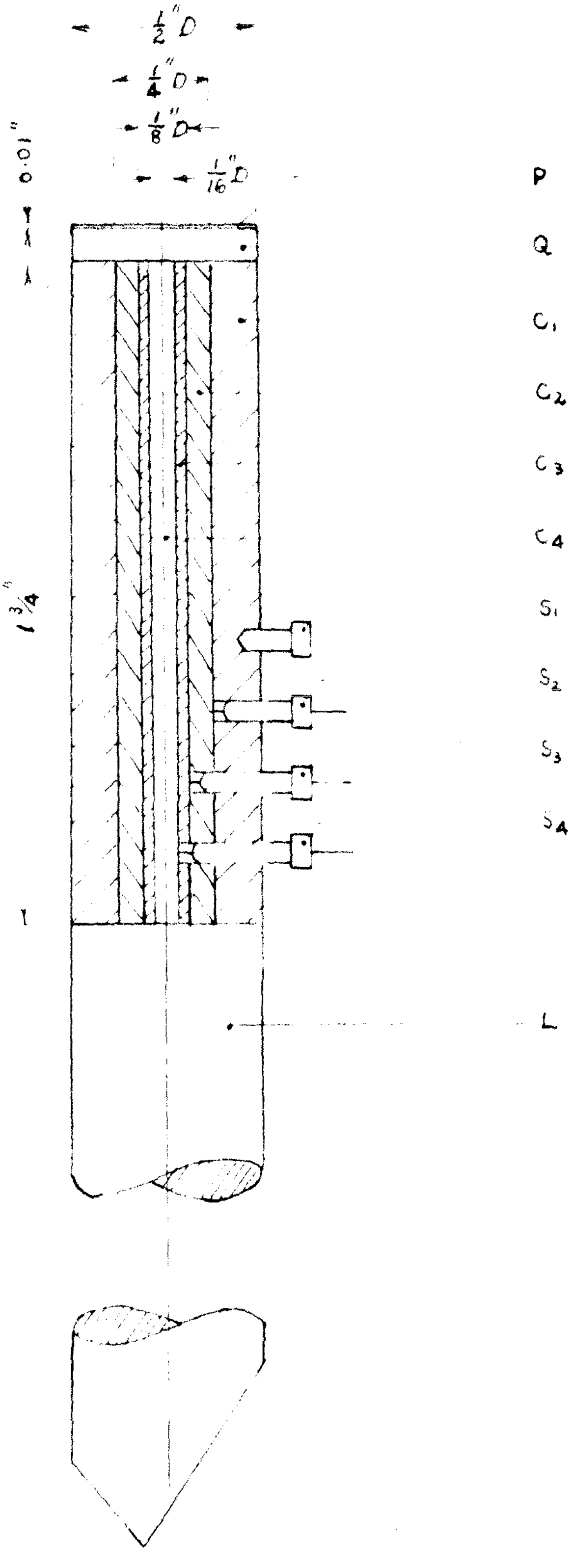

Fig. 4. 8. The quartz crystal pickup.

lower end of the unit is visible in figure 4.4.

Figure 4.9 shows the output obtained from C_2 and C_4 with C_1, C_3 and P grounded, when a 1/16" ball bearing is dropped on the center of the crystal. The curves are photographed from the screen of a Tektronix Type 551 Dual Beam oscilloscope. A 25 Megacycle X-cut quartz crystal was used to obtain these curves.

In view of the results shown in figure 4.9 it was hoped that a bubble which collapses as shown in figure 2.5 would produce a pulse on C_4 before a pulse on C_2 would be observed.

ii) Photoelastic Material

Figure 4.10 shows the photoelastic pickup which was used to indicate pressures on the boundary. The photoelastic material was placed between two half-inch thick Lucite plates, so that a fairly wide flat surface was obtained for the cavity to collapse on.

Two types of photoelastic materials were used, namely CR 39 and Hysol 8705.

iii) Damaging of Materials

The damaging of material samples inserted in the boundary provided a useful tool in obtaining rough estimates of the pressure distributions on the boundary. High purity aluminum samples of 1/2" diameter and approximately 3/8" long were sanded smooth on one end with number 600 metallurgical emery paper. These samples were then carefully annealed, and chemically polished with Alcoa R5 bright dip.

The samples were glued on the end of a 1/2" diameter aluminum

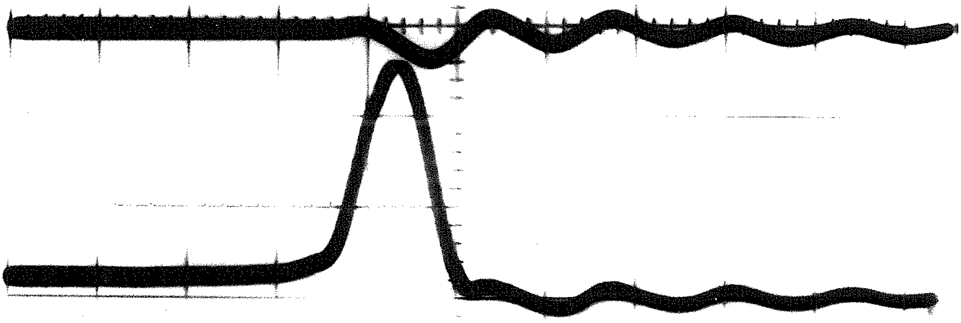

Fig. 4.9. The response of the quartz crystal pickup when a 1/16" ball bearing is dropped through 2" on the center of the crystal. The upper trace was connected to C_2 and the lower trace to C_4.

Horizontal scale 1 division = 10 μs.
Vertical scale 1 division = .005 V.

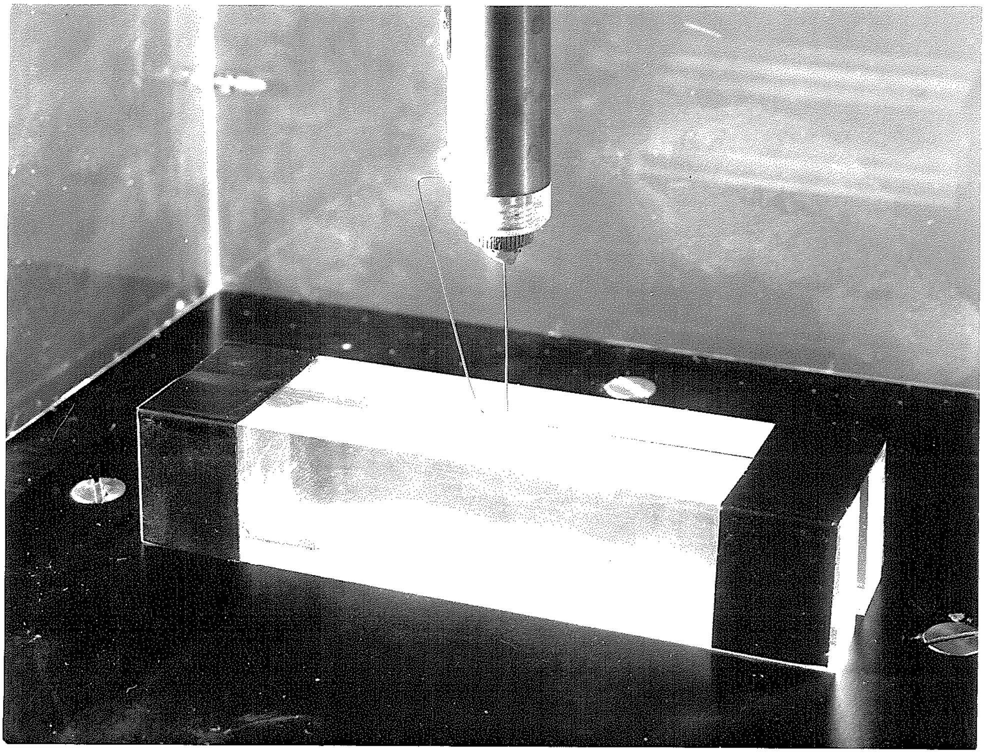

Fig. 4.10. The photoelastic pressure indicator.

rod, and inserted in the bottom of the tank through the same hole as was used with the quartz crystal pickup.

4. Procedure

Bubble pictures were obtained by triggering the camera and the spark with a single 25 V pulse of 1 μs duration. This pulse was made by feeding a single sawtooth wave form from a Tektronix Type 162 wave form generator into a Tektronix Type 163 pulse generator.

When the quartz crystal pickup was used it became necessary to trigger the oscilloscope shortly before the collapse pulse was expected. This was done with a 50 V pulse of about 1 μs duration generated by a Tektronix Type 161 pulse generator into which the same sawtooth was fed. Both pulse generators can be adjusted to trigger at any fraction of the maximum sawtooth voltage, and the duration of the sawtooth waveform can be varied. A delay could therefore be obtained between the pulse which triggered the camera and the pulse which triggered the scope.

The relative timing between the motion pictures and the scope records was easily observed, because stray fields from the Kerr cell pulses caused pulses on the scope. A reference point was obtained by adjusting the camera so that the Kerr cell pulses stopped shortly after the collapse pulse was observed, so that the last Kerr cell pulse on the scope corresponded in time to the last picture on the film.

For the photoelastic pictures it was necessary to place another polaroid between the tank and the light source with its axis parallel to that of the first polaroid of the shutter. Quarter wave plates were placed on both sides of the tank, and between the two polaroids mentioned above. Since all the data are in this case contained in the motion pictures the oscilloscope and its triggering equipment were not needed.

High speed motion pictures of the cavities which caused the damage of the aluminum samples were taken in the same way, but of course without the polaroid and quarter wave plates.

The equipment used is shown in figure 4.11. The rack on the far right contains the condenser bank for the light source, and the power supply used to charge it. The rack next to it contains the electronic equipment which produces the Kerr cell pulses. The light source is contained in the black cylinder, and is aimed at the camera through the tank in which the bubbles were made.

The small rack on the left contains the electronics needed for generating the spark, and the unit sitting on top of it contains the Tektronix Type 162 waveform generator, the Type 163 pulse generator, and the Type 161 pulse generator. The Type 551 Tektronix Dual Beam oscilloscope stands between the spark equipment and the bubble tank.

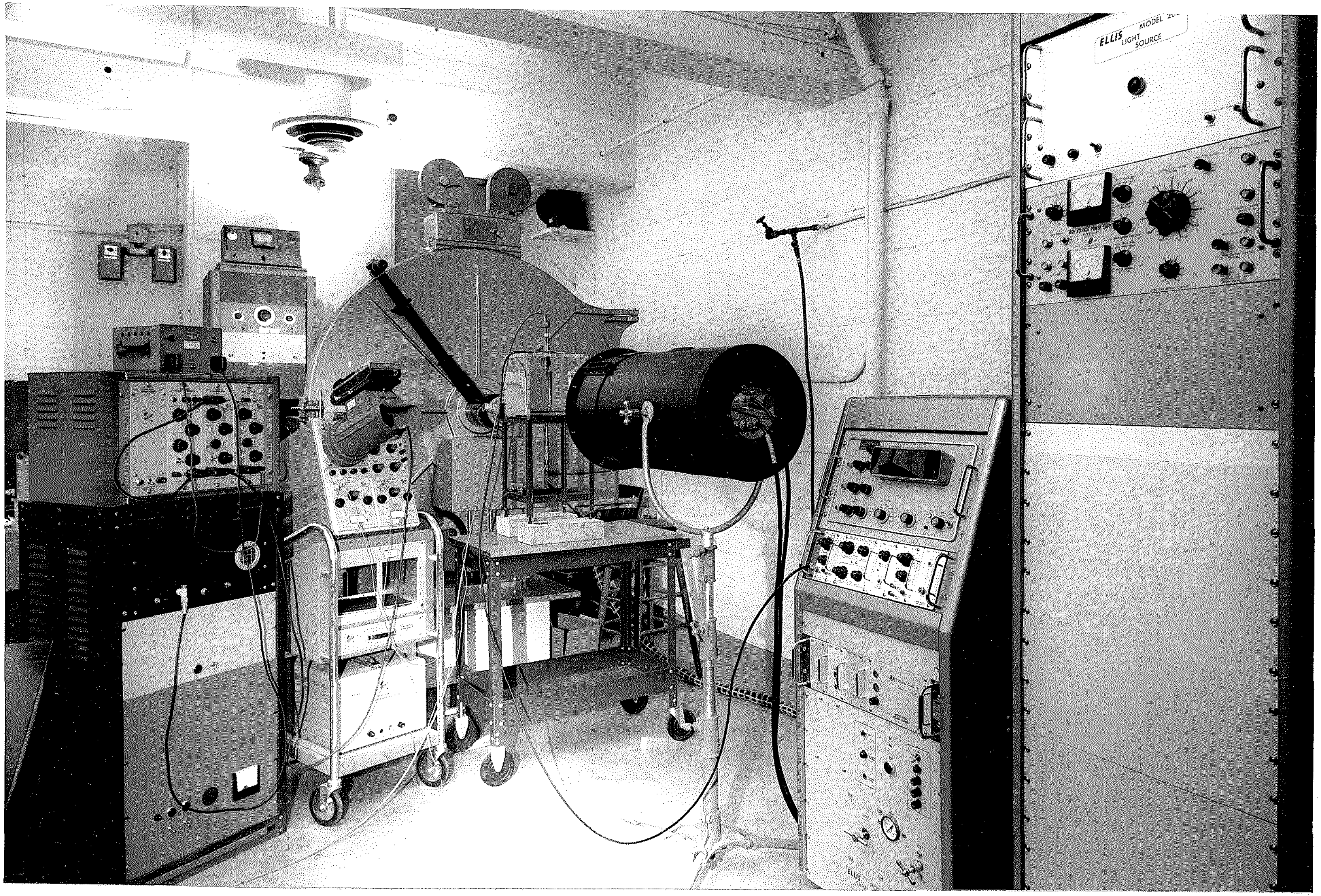

Fig. 4.11. The experimental equipment.

Chapter V

The Experimental Results Compared with the Theory

A large number of motion picture records of cavities collapsing in contact with a solid boundary were obtained by the methods discussed in chapter IV. In an attempt to demonstrate a representative sample of the results, the cavities of figures 5.1 through 5.7 were chosen. The pictures of figures 5.1 and 5.2 were obtained with CR-39 as a pressure indicator, and are different inasmuch as the cavity in figure 5.1 contains a larger initial perturbation of the hemispherical shape than the one of figure 5.2. The cavities of figures 5.3 and 5.4 were obtained with Hysol 8705 and the quartz crystal unit as the respective pressure indicators. The oscilloscope record accompanying figure 5.4 is shown in figure 5.8. Figures 5.5, 5.6 and 5.7 show the most important cavities which were used in the damage studies.

In all these reproductions frames below one another in the vertical columns are consecutive in the motion picture record. A vertical column follows the one immediately to its left. The following notation will be used in the discussion of the pictures:

Frame i, j = the j^{th} frame of the i^{th} column.

The cavities of figures 5.1, 5.2 and 5.3, which collapsed on photoelastic boundaries, all exhibit an important common characteristic, namely that they all become deformed to the extent that the cavity wall strikes the solid surface before the cavity reaches its minimum volume. The photoelastic materials show this effect in the form of a small disturbance close to the origin of the spherical coordinate

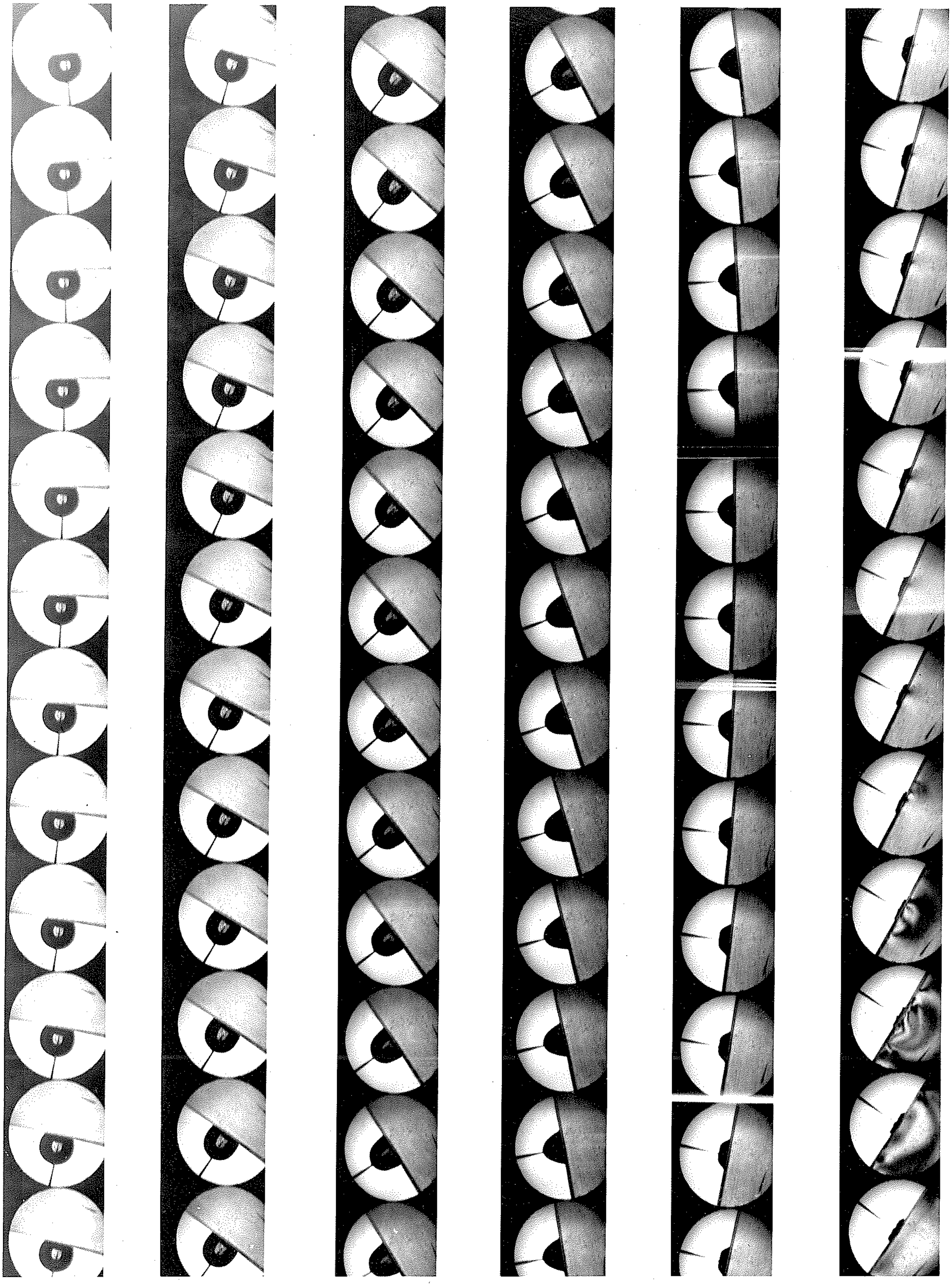

Fig. 5.1. A cavity collapsing on the CR-39 photoelastic boundary. Time between frames is 10 microseconds.

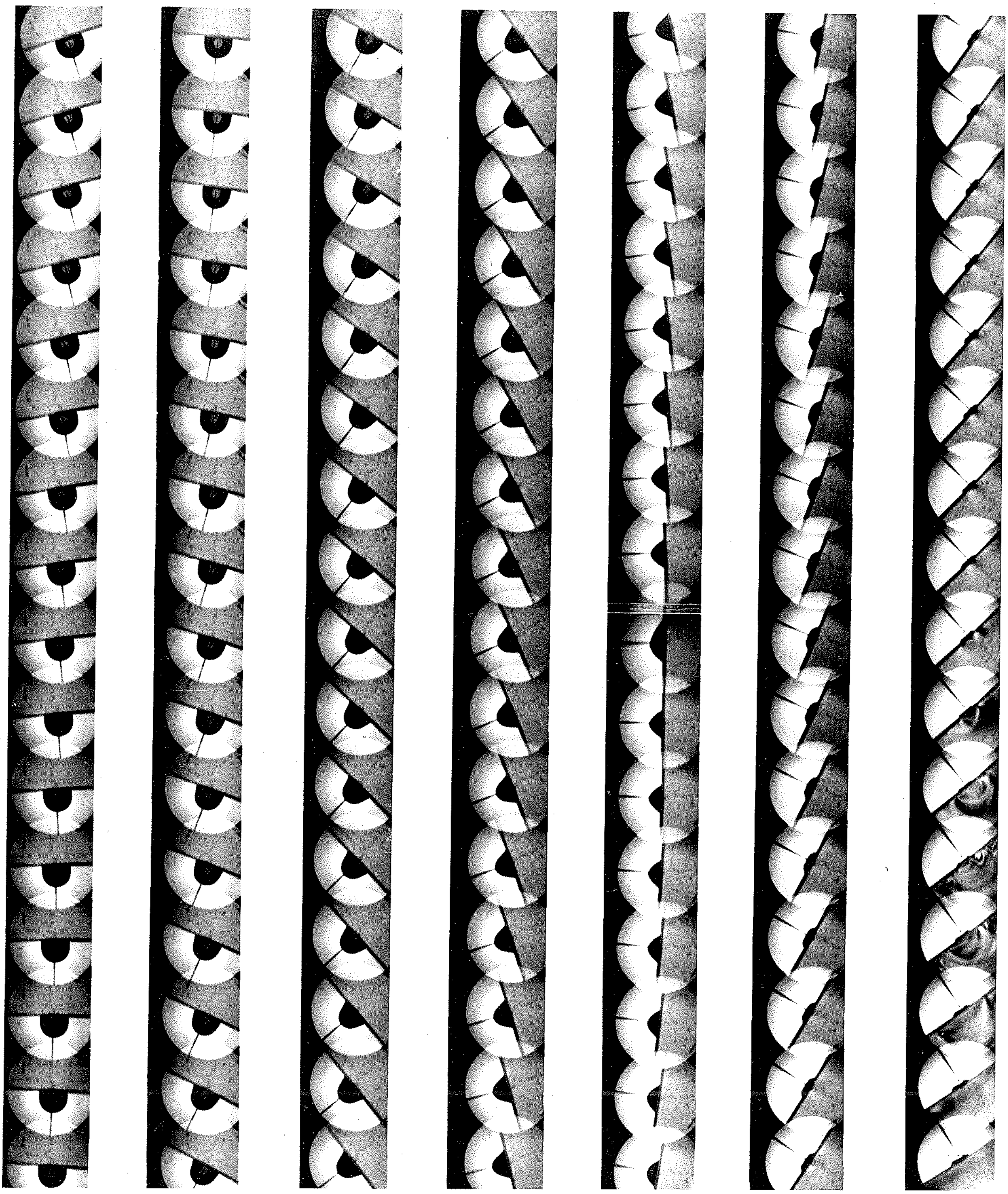

Fig. 5.2. A second cavity collapsing on the CR-39 photoelastic boundary. Time between frames is 5 microseconds.

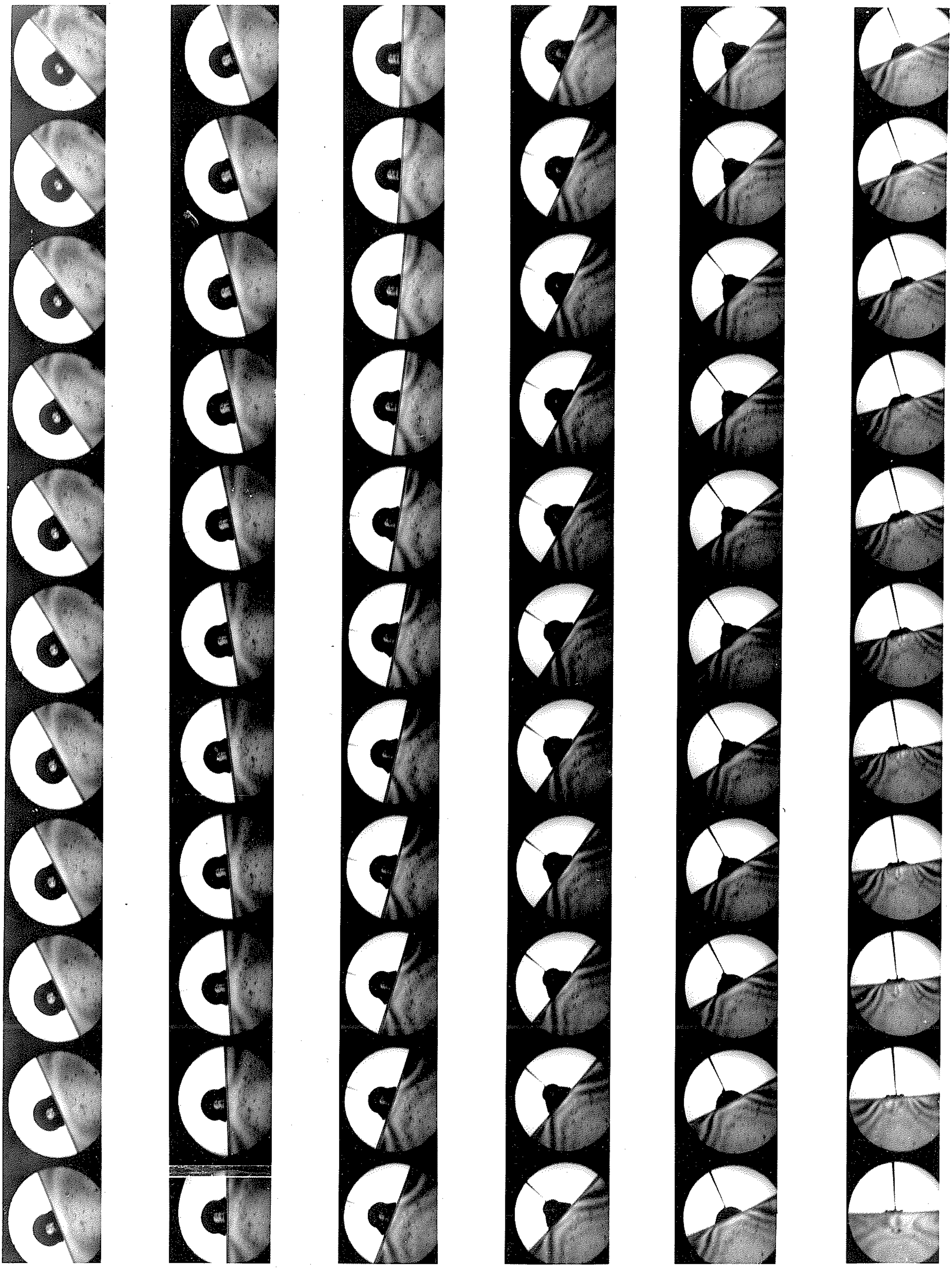

Fig. 5.3. A cavity collapsing on the Hysol 8705 photoelastic boundary. Time between frames is 10 microseconds.

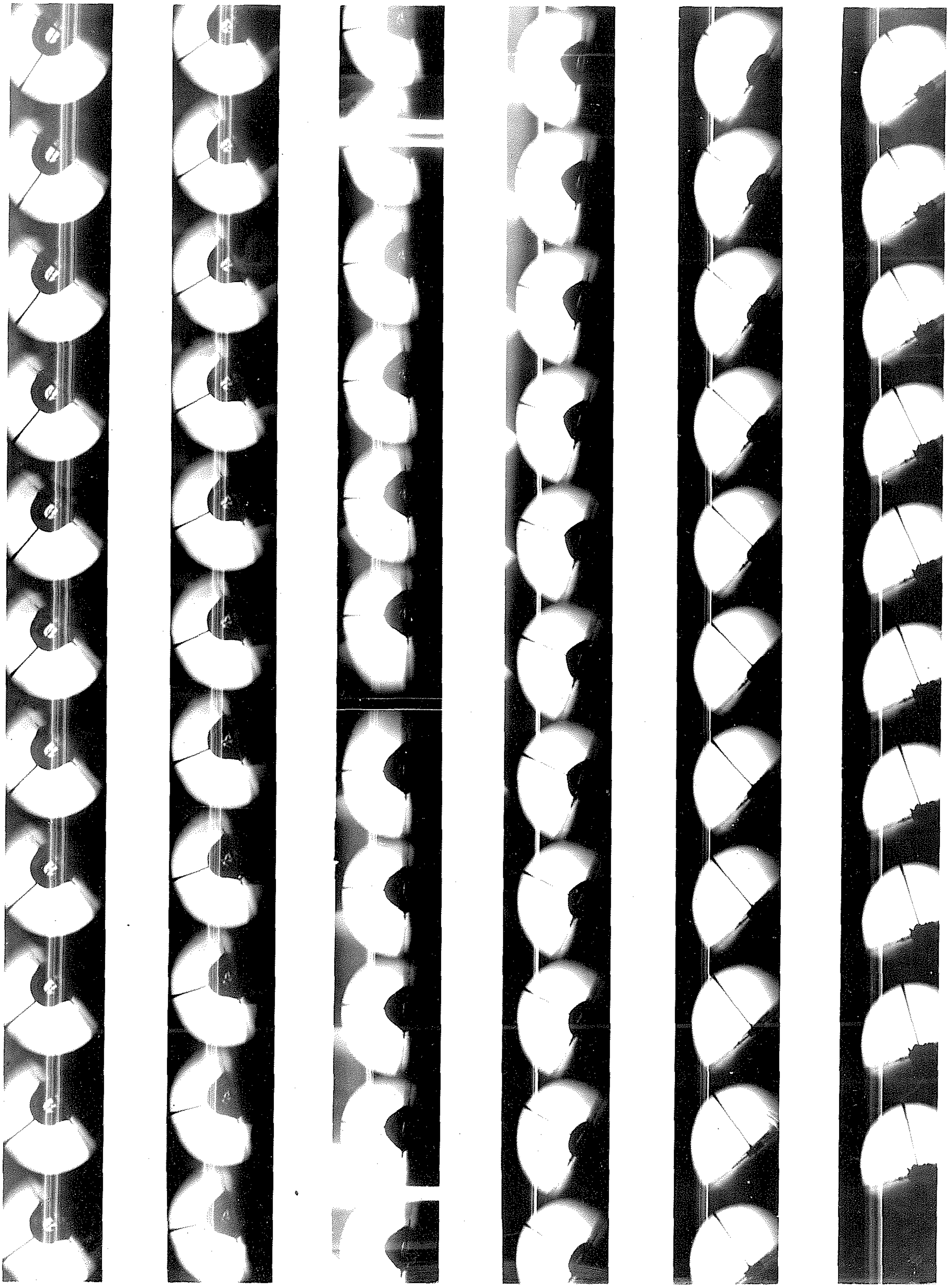

Fig. 5.4. A cavity collapsing on the quartz crystal pickup. The accompanying oscilloscope record is shown in figure 5.8. Time between frames is 10 microseconds.

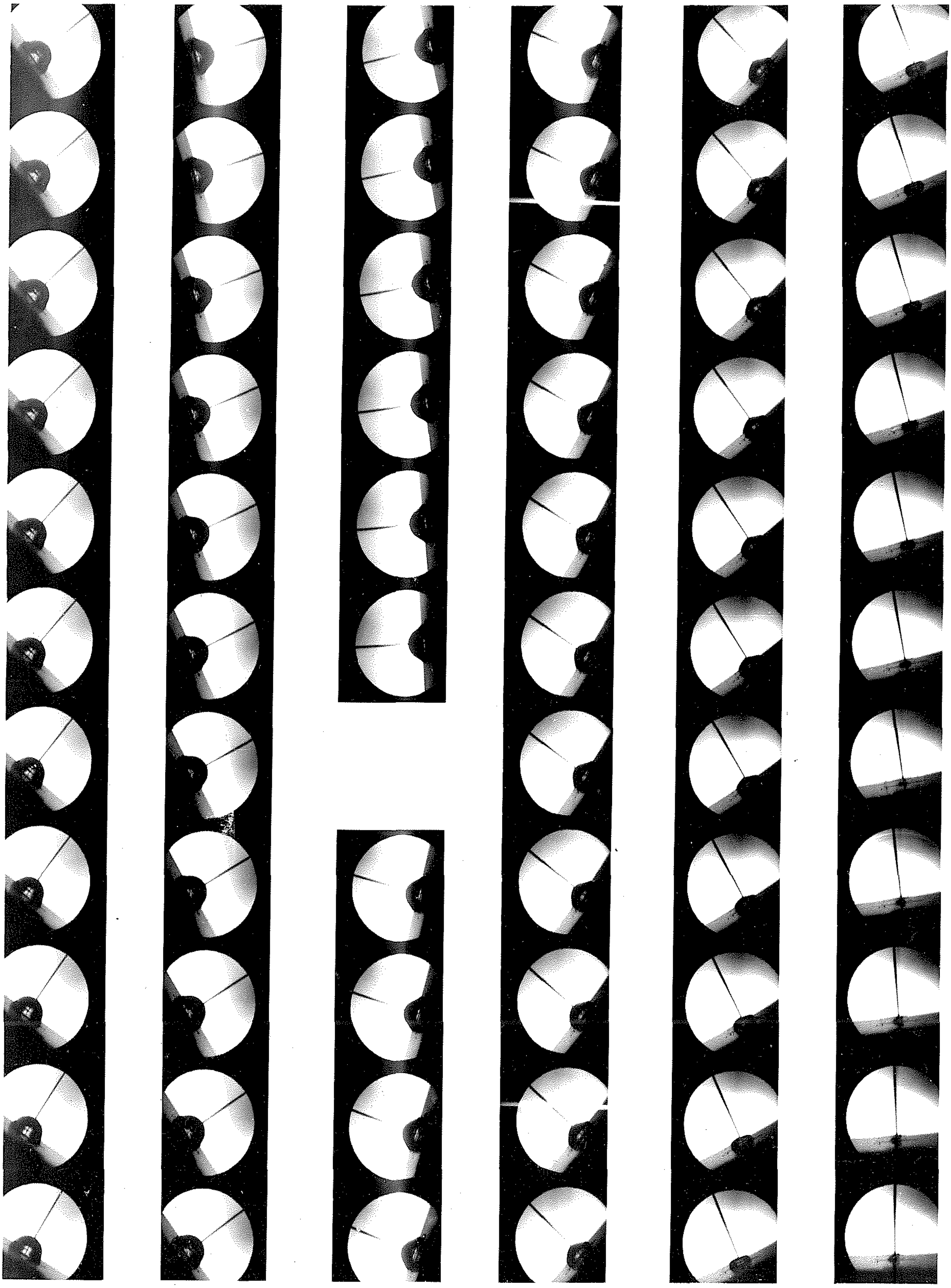

Fig. 5.5. A cavity collapsing on a soft aluminum sample. Time between frames is 10 microseconds. Frames 3,6 and 3,7 are 90 microseconds apart.

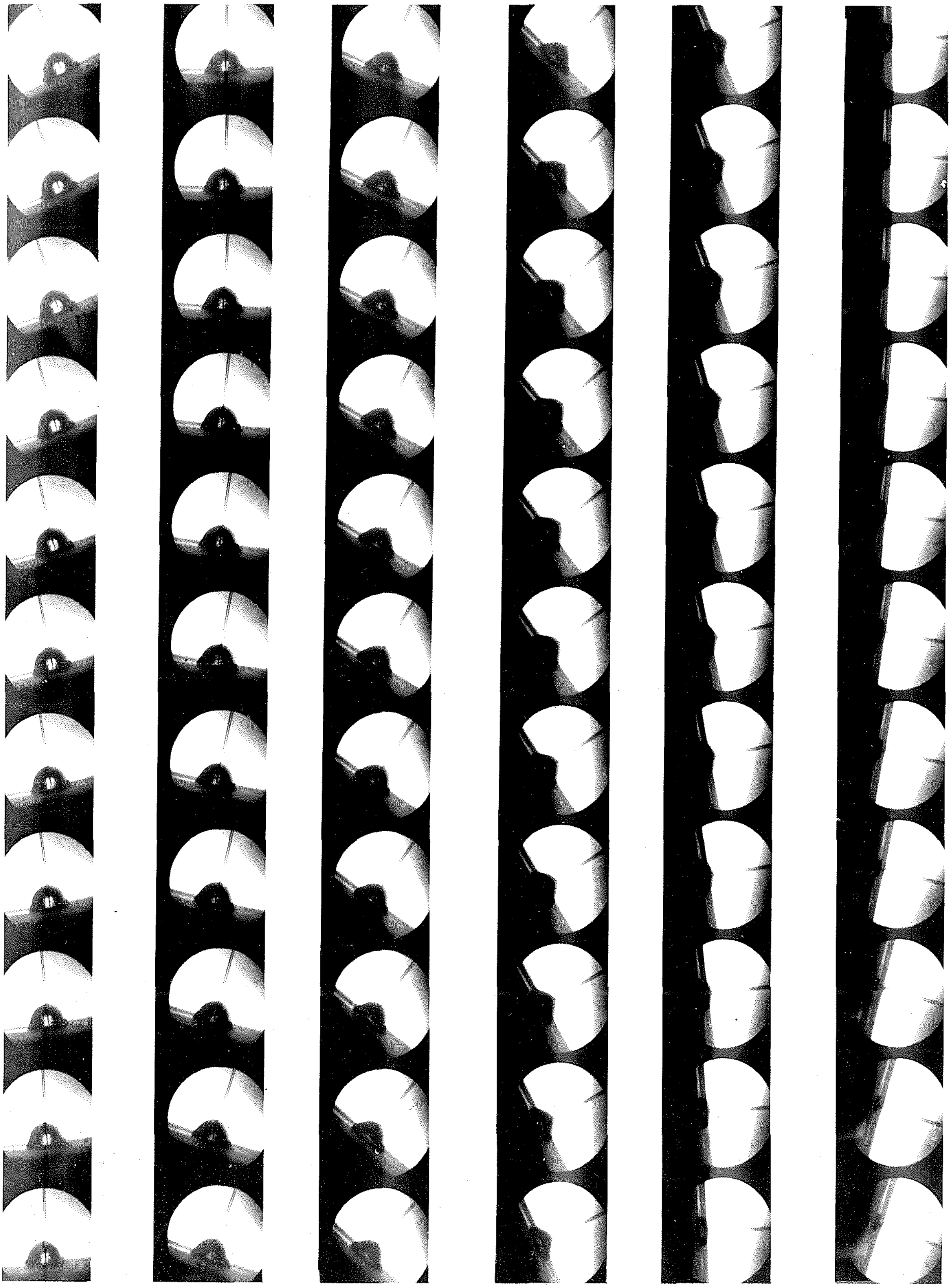

Fig. 5.6. A second cavity collapsing on a soft aluminum sample. Time between frames is 10 microseconds.

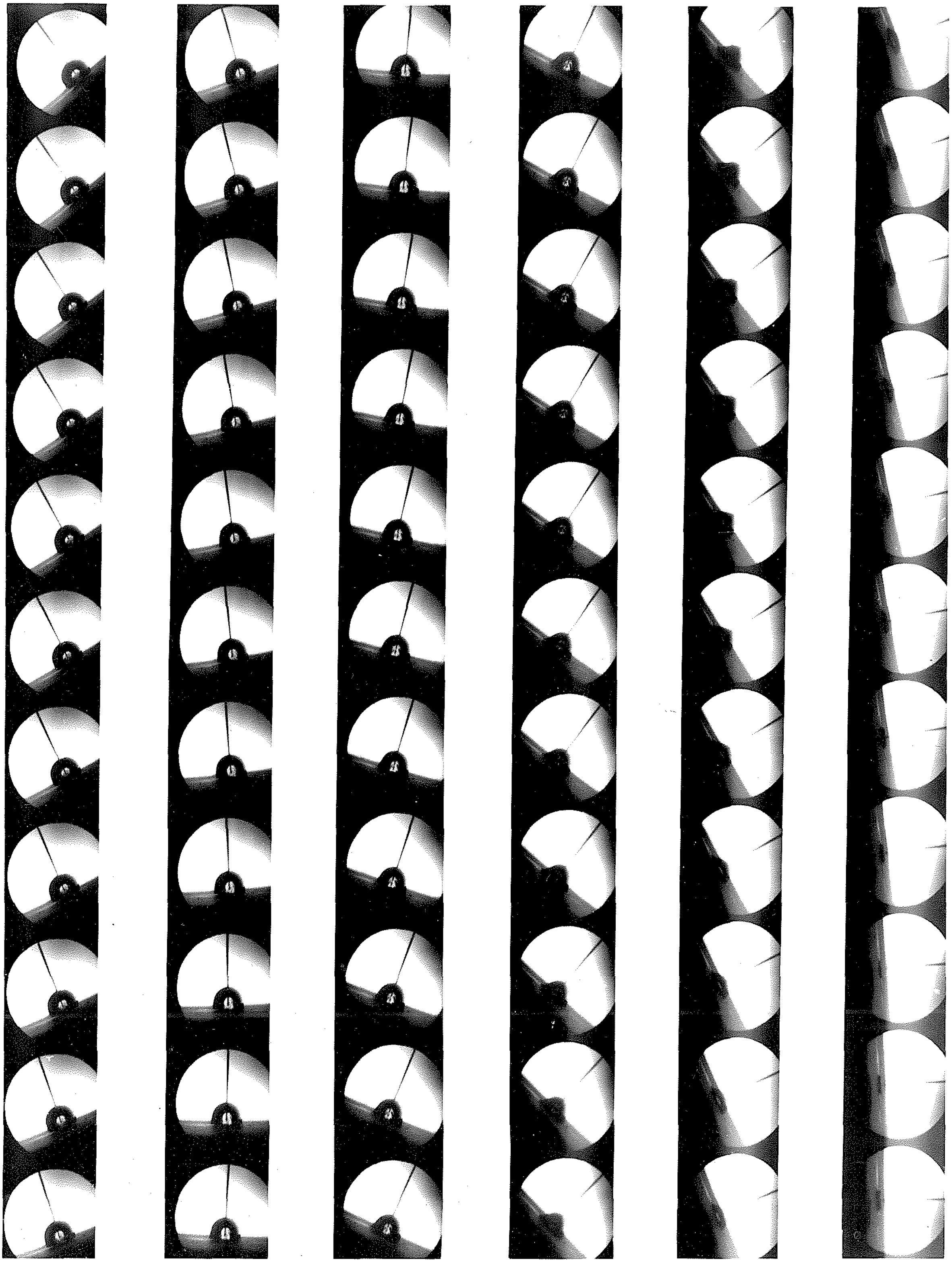

Fig. 5.7. A third cavity collapsing on a soft aluminum sample. Time between frames is 10 microseconds.

Fig. 5.8. The oscilloscope record accompanying the cavity of figure 5.4.

Horizontal scale 1 division = 20 μs.
Vertical scale 1 division = 0.2 V.

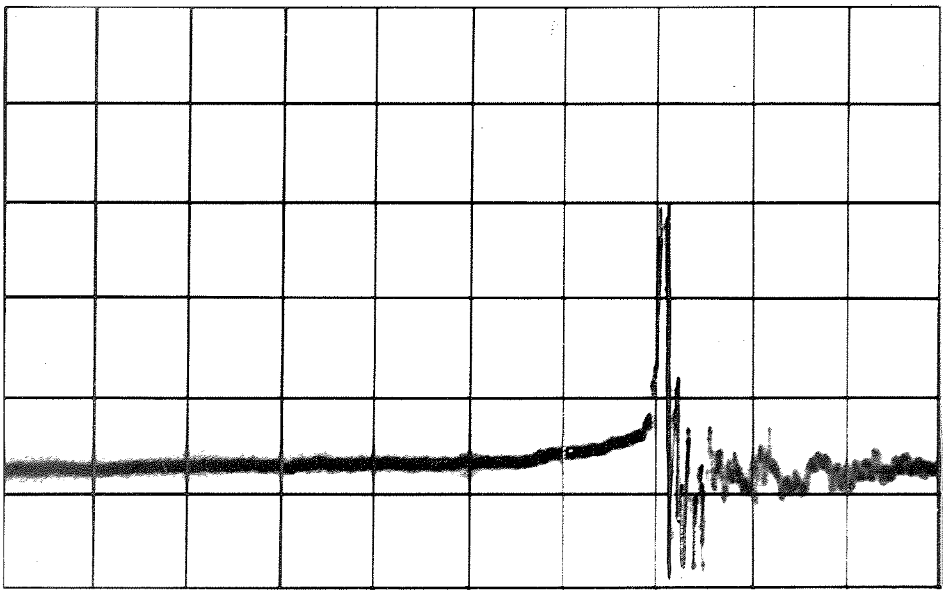

Fig. 5.9. An oscilloscope record obtained with a cavity very similar to the one of figure 5.7.

Horizontal scale 1 division = 50 μs.
Vertical scale 1 division = 0.02 V.

system which was used for the theoretical work. (Refer to figure 2.1.) These pressure pulses will be called water hammer pulses for the purpose of the discussion which follows. The observation of this effect indicates that the type of collapse which is shown in figure 2.5 indeed occurs in practice.

The photoelastic materials indicate that the force, which is initiated by the wall of the cavity striking the boundary, is sustained over a relatively long period. This effect is explained by regarding the folded-in portion of the cavity boundary as a jet which enters the cavity, strikes the solid surface and impinges upon the surface after its initial contact. The pressure necessary to deflect the liquid so that it eventually flows in a direction parallel to the solid boundary causes the water hammer pulse to appear sustained.

The water hammer pulse is followed by a second, and much larger, disturbance which coincides in time with the period during which the cavity reaches its minimum volume. During this period shock waves are usually visible in the liquid, even though no experimental provisions were made for their observation. It is believed that this second disturbance results from compression of gases in the cavity. It is accordingly referred to as the gas compression pulse for the remainder of this discussion.

The results which were obtained with the quartz crystal pickup were somewhat discouraging. The oscilloscope record of figure 5.8 which was obtained from connections C_4 and C_2 with C_1, C_3 and P grounded, shows no signs of a pulse from the C_4 connection (upper trace) before the pulse on the C_2 connection (lower trace) is observed.

At this stage a pulse appears on both traces which can be seen to correspond to the compression pulse because of the shock waves which are visible in frame 5, 10 of figure 5.4. It will be noted that the Kerr cell pulse which immediately follows the compression pulse in figure 5.8 corresponds in time to frame 5, 10 of figure 5.4.

The situation was explained when the amplification of the oscilloscope was increased. In figure 5.9 an oscilloscope record, which was obtained for a cavity almost exactly the same as the one of figure 5.7 is shown. In this case C_2, C_3 and C_4 were connected together while C_1 and P were still grounded. The small disturbance which is seen to start about 65 μs before the compression pulse is believed to correspond to the cavity wall striking the boundary. These disturbances were in general so small that it was difficult to separate them from noise in the system. For this reason the quartz crystal pickup was considered useless for purposes of detecting this effect.

One has no indication of the relative time at which the walls of the cavities of figures 5.5, 5.6 and 5.7 struck the boundary, because these bubbles were used to damage aluminum samples. These pictures were nonetheless included here because they are of extreme interest in the damage studies which are discussed in chapter VI.

The method of analyzing motion picture records will now be discussed.

Suppose the cavity of figure 5.10 can be described sufficiently accurately by the equation

$$R(\theta, t) = R_o P_o(\cos\theta) + R_2 P_2(\cos\theta) + R_4 P_4(\cos\theta) + R_6 P_6(\cos\theta). \quad (5.1)$$

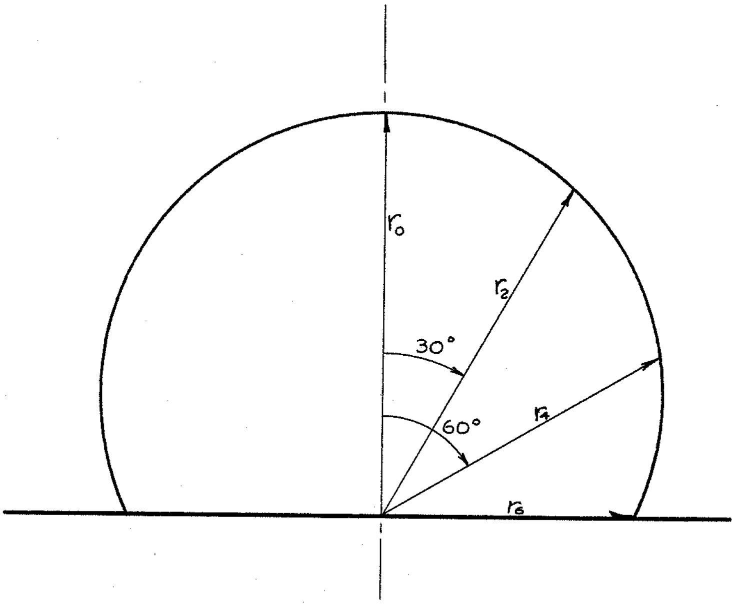

Figure 5.10

Then one may write

$$\begin{pmatrix} r_o \\ r_2 \\ r_4 \\ r_6 \end{pmatrix} = \begin{pmatrix} P_o(1) & P_2(1) & P_4(1) & P_6(1) \\ P_o(\sqrt{3}/2) & P_2(\sqrt{3}/2) & P_4(\sqrt{3}/2) & P_6(\sqrt{3}/2) \\ P_o(1/2) & P_2(1/2) & P_4(1/2) & P_6(1/2) \\ P_o(0) & P_2(0) & P_4(0) & P_6(0) \end{pmatrix} \begin{pmatrix} R_o \\ R_2 \\ R_4 \\ R_6 \end{pmatrix} \qquad (5.2)$$

where r_o, r_2, r_4 and r_6 are the values of R at 0^o, 30^o, 60^o and 90^o respectively.

Inverting the matrix of equation 5.2 and substituting the values of P_{2n}, one obtains

$$\begin{pmatrix} R_o \\ R_2 \\ R_4 \\ R_6 \end{pmatrix} = \begin{pmatrix} .0287 & .2540 & .4569 & .2604 \\ .1590 & .7616 & -.2540 & -.6666 \\ .4430 & -.2772 & -.9420 & .7762 \\ .3696 & -.7392 & .7392 & -.3696 \end{pmatrix} \begin{pmatrix} r_o \\ r_2 \\ r_4 \\ r_6 \end{pmatrix} . \qquad (5.3)$$

R_o, R_2, R_4 and R_6 may thus be obtained as functions of time if r_o, r_2, r_4 and r_6 are measured from the motion picture records, provided the time between frames of the motion picture is known.

In order to compare the $R_{2n}(t')$ which are measured in this way with the theory, it is necessary to find $R_o(0)$, T, $R_{2n}(0)$ and $\frac{dR_{2n}}{dt}(0)$ from the experimental results. It should be noted that t' above differs from the t used in the theoretical treatment by an additive constant.

The point $t = 0$ was found by a graphical determination of the maximum of R_o plotted against t'. $R_o(0)$ was then of course this maximum value of R_o.

Two procedures were used for determining T. The first was to fit the best Rayleigh curve (cf. figure 2.2) through the experimental points and then to find the value of t at which R_o becomes 0. These values of T will be called T_e. The other procedure was to calculate T from equation 2.39. The value of p_c was considered to be the vapor pressure of water at room temperature. For p_∞ atmospheric pressure plus the pressure due to 6 inches of water was used, since the depth of submergence of the cavities was approximately 6 inches. It was found that T_e and T never differed by more than a few percent.

$R_{2n}(0)$, with $n = 1$, 2 and 3, was determined by plotting R_{2n} against time, and determining its value at $t = 0$. The slope of R_{2n} at $t = 0$ gave $\frac{dR_{2n}}{dt}(0)$.

The most important parameters for the cavities of figures 5.1 through 5.7 are listed in table 5.1.

Number of fig. in which cavity is shown	Time between frames μs.	Position of t = 0	$R_o(0)$ in.	T_e μs.	T μs.	$R_2(0)$ in.	$\frac{T_e}{R_2(0)} \frac{dR_2}{dt}(0)$	$R_4(0)$ in.	$\frac{T_e}{R_4(0)} \frac{dR_4}{dt}(0)$	Observed position of water hammer pulse	Estimated position of water hammer pulse	Approx. position of compression pulse
Fig. 5.1	10	Fr.** 1,9	.244*	570	- -	.113	- .640	-.0334	-2.70	Fr. 5,12	- -	Fr. 6,9
Fig. 5.2	5	Fr. 1,6	.218*	508	- -	.070	- .949	-.0127	-6.18	Fr. 6,9	- -	Fr. 7,11
Fig. 5.3	10	Fr. 1,11	.287*	670	- -	.122	- .598	-.0313	-3.06	Fr. 6,2	- -	Fr. 6,10
Fig. 5.4	10	Fr. 1,5	.197	464	459	.027	-1.93	.0092	5.30	- -	Fr. 5,4	Fr. 5,9
Fig. 5.5	10	Fr. 2,2	.232	545	542	.012	-3.64	.0114	2.24	- -	Fr. 6,2	Fr. 6,7
Fig. 5.6	10	Fr. 1,8	.241	560	562	.021	-2.80	.0127	2.80	- -	Fr. 6,4	Fr. 6,9
Fig. 5.7	10	Fr. 1,11	.225	517	524	.065	- .930	-.0127	-6.10	- -	Fr. 6,3	Fr. 6,9

* Values of $R_o(0)$ were calculated from T_e.

** Frame has been abbreviated by Fr.

Table 5.1

The most important parameters for the cavities displayed in figures 5.1 through 5.7

In figure 5.11 experimental values of $R_o/R_o(0)$ are plotted against t/T for the cavities of figures 5.4 and 5.7. The dotted vertical line at $t/T = 0.82$ indicates where the cavity of figure 5.7 became indented. The other cavity became dented somewhat later. Points after the dotted line depend on estimating the shape of the folded-in portions of the cavities. The solid curve of figure 5.12 is the theoretical curve for $R_o/R_o(0)$ as a function of t/T calculated from equation 2.38.

In figures 5.12 through 5.18, the experimental points of $R_2/R_2(0)$ and $R_4/R_4(0)$ are plotted against $R_o/R_o(0)$ for the cavities of figures 5.1 through 5.7 respectively. The dotted vertical lines in these figures indicate where the cavities became indented. Points to the right of the vertical line are again based on an estimate of the shape of the folded-in portions of the walls of the cavities. The accuracy of these estimates depended a great deal on a knowledge of when the water hammer pulse occurred. The results should thus be more trustworthy in cases where a cavity collapsing on a photoelastic boundary was analysed.

The solid lines in figures 5.12 through 5.18 are the theoretical curves. $R_2/R_2(0)$ was calculated from the equation

$$\frac{R_2}{R_2(0)} = y_{21} + \left(0.892\,\frac{T_e}{R_2(0)}\,\frac{dR_2}{dt}(0)\right) y_{22}. \qquad (5.4)$$

$R_4/R_4(0)$ followed from

$$\frac{R_4}{R_4(0)} = y_{41} + \left(0.892\,\frac{T_e}{R_4(0)}\,\frac{dR_4}{dt}(0)\right) y_{42} + y_{4P} \qquad (5.5)$$

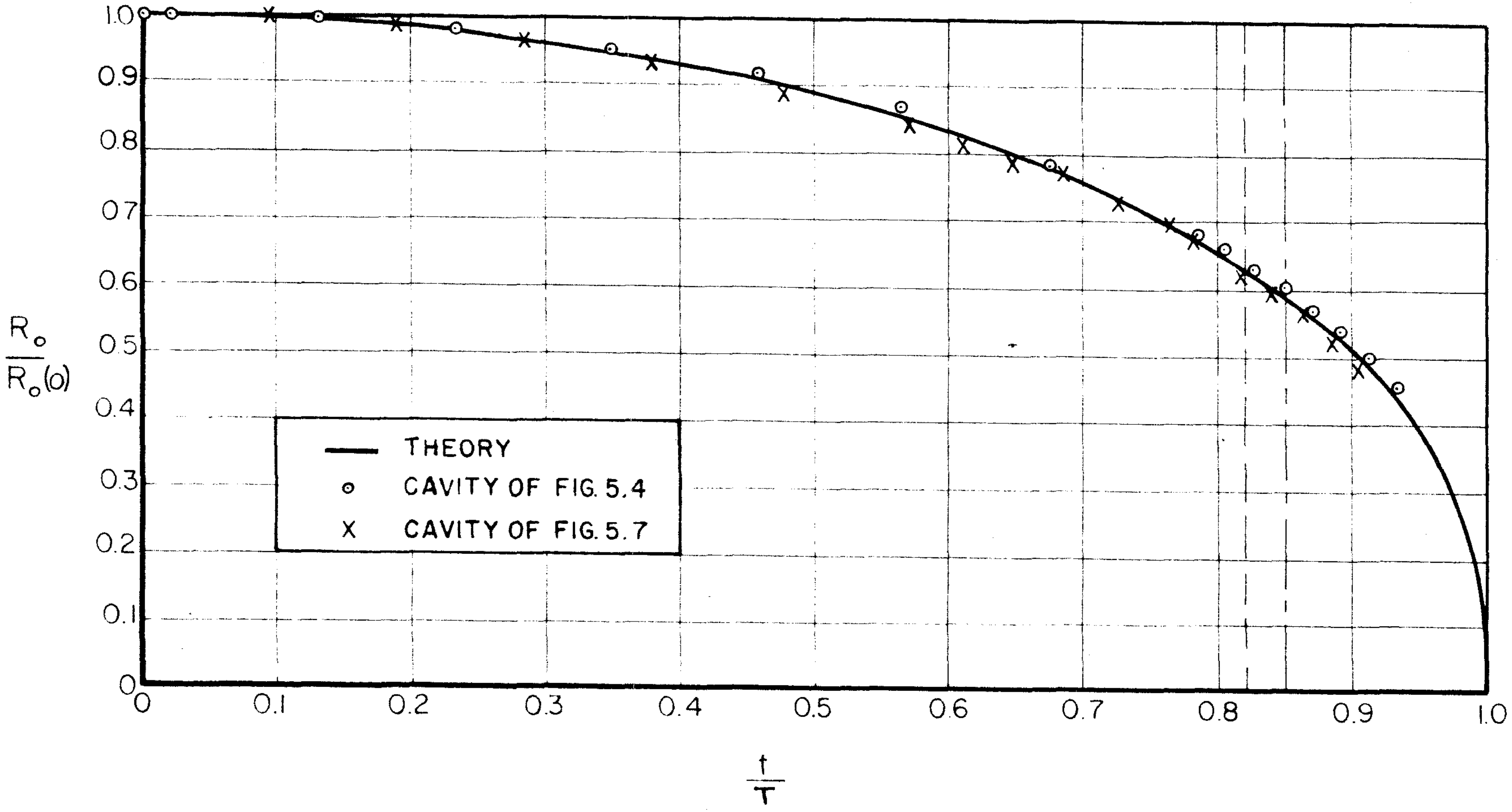

Fig. 5.11. $R_o/R_o(0)$ as a function of t/T.

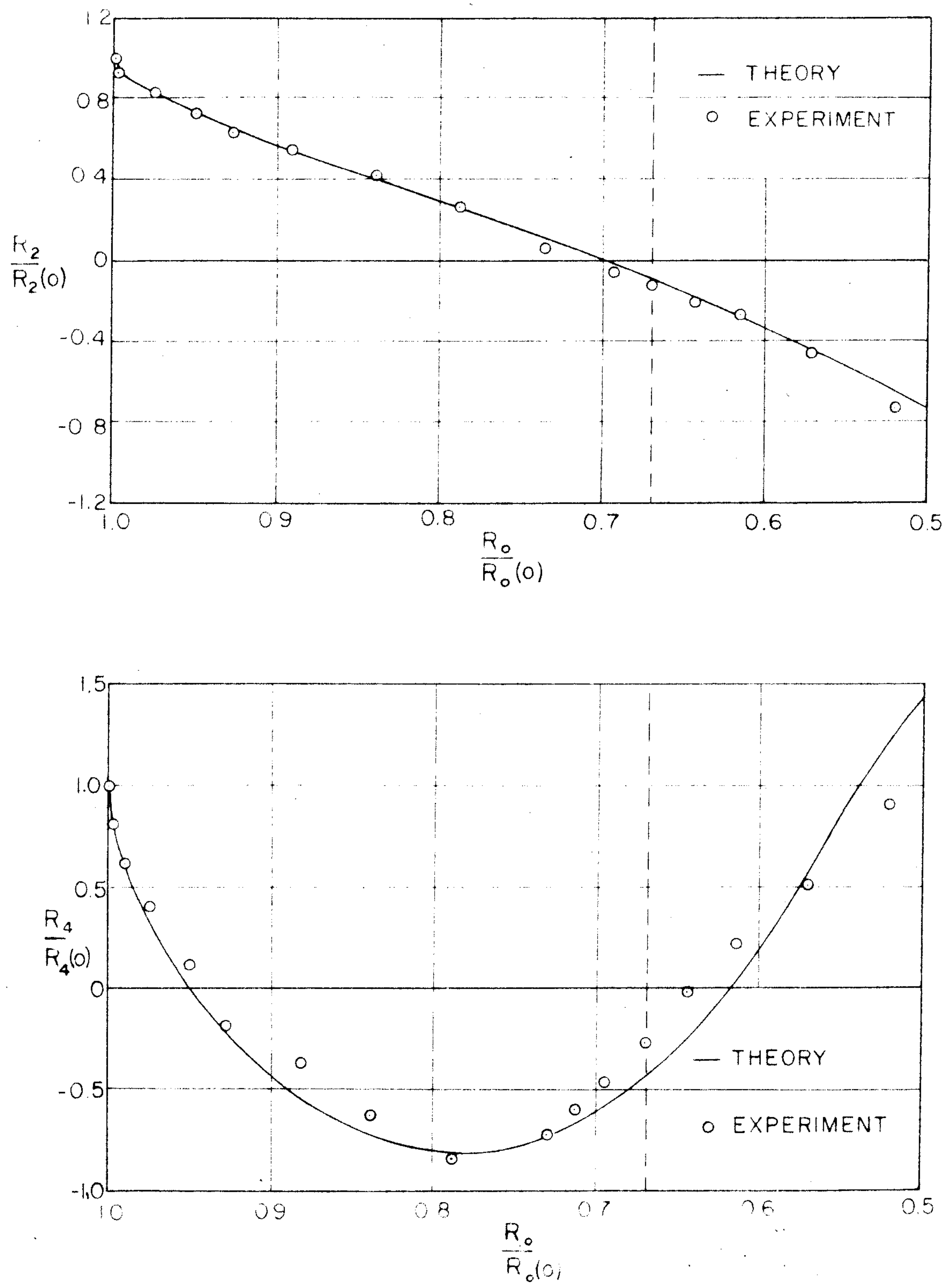

Fig. 5.12. R_2/R_2 (0) and R_4/R_4 (0) as functions of R_o/R_o (0) for the cavity of fig. 5.1.

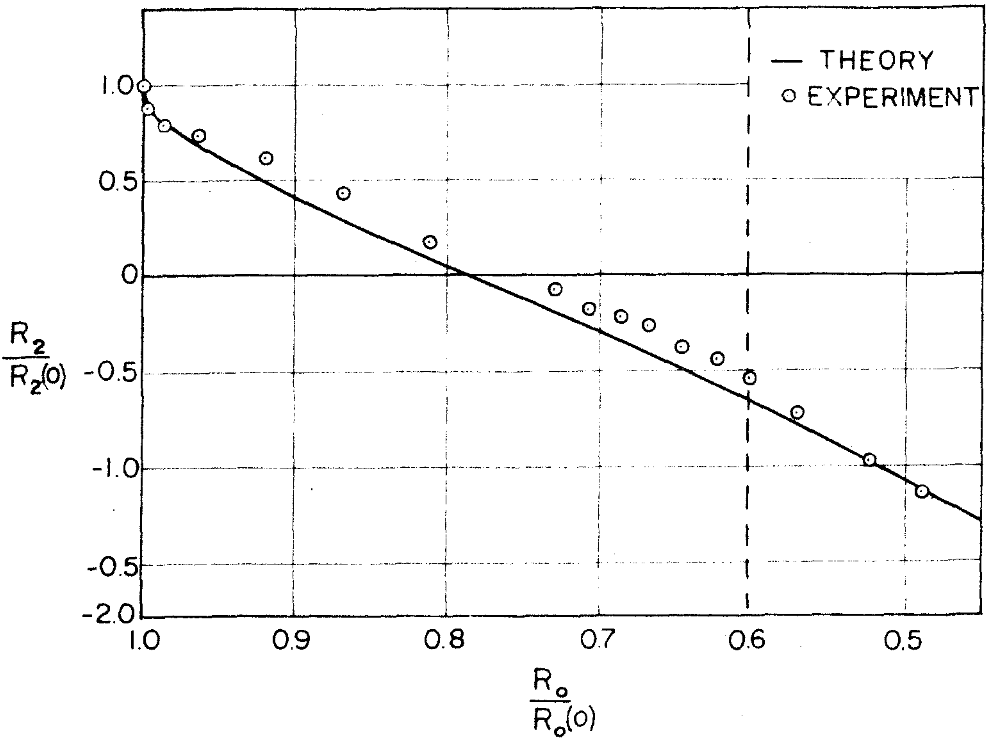

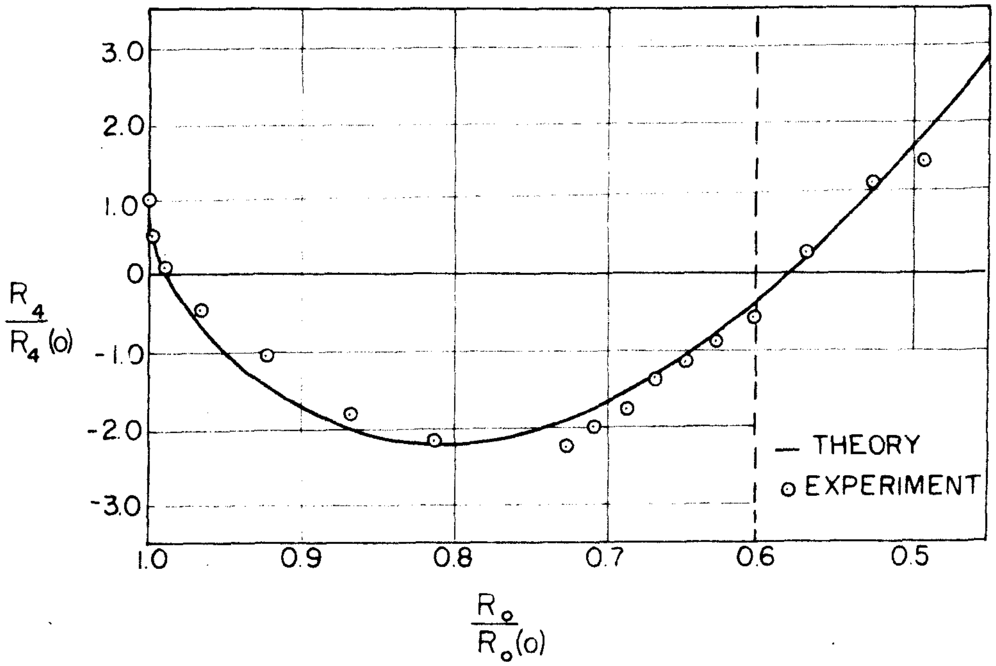

Fig. 5.13. R_2/R_2 (0) and R_4/R_4 (0) as functions of R_o/R_o (0) for the cavity of fig. 5.2.

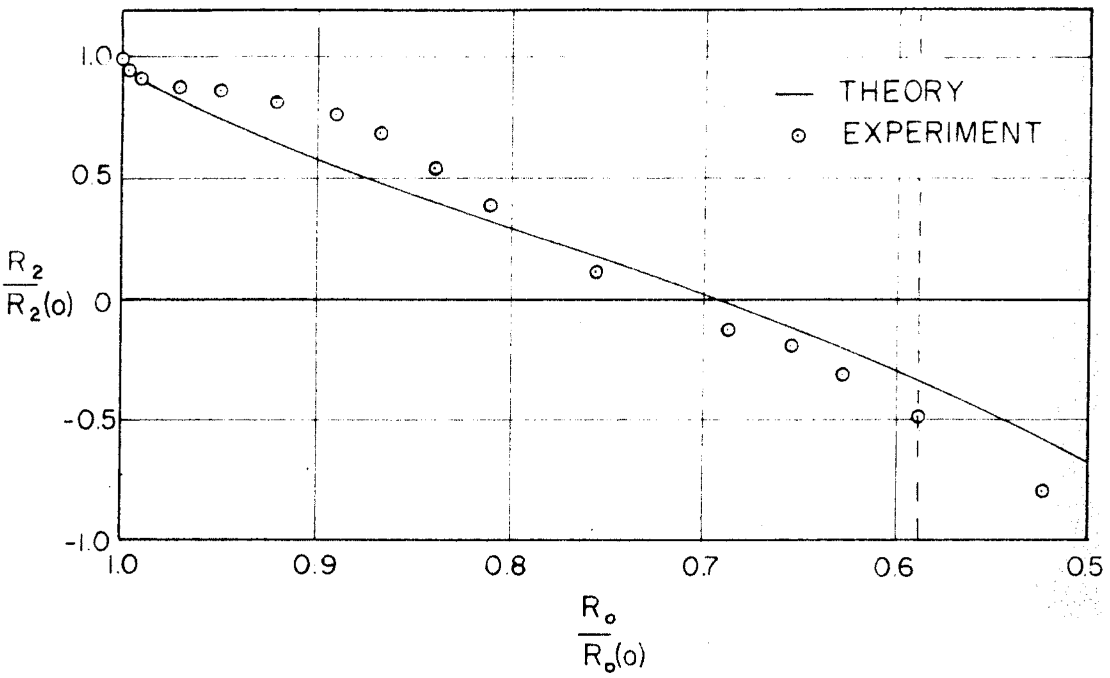

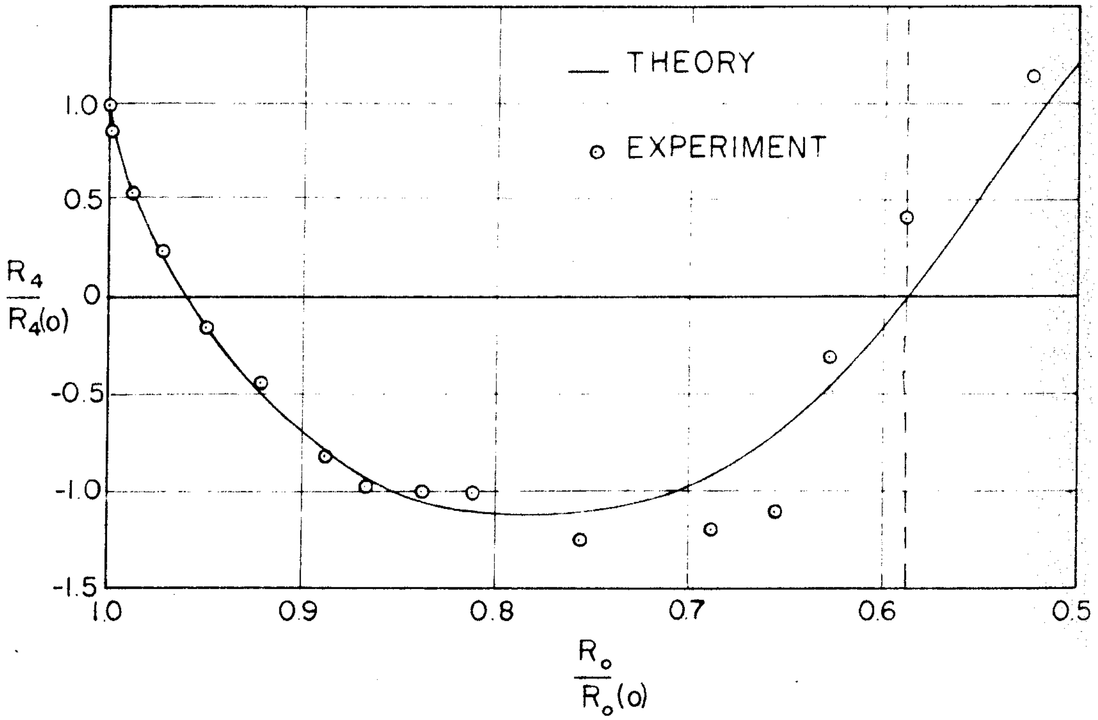

Fig. 5.14. $R_2/R_2(0)$ and $R_4/R_4(0)$ as functions of $R_o/R_o(0)$ for the cavity of fig. 5.3.

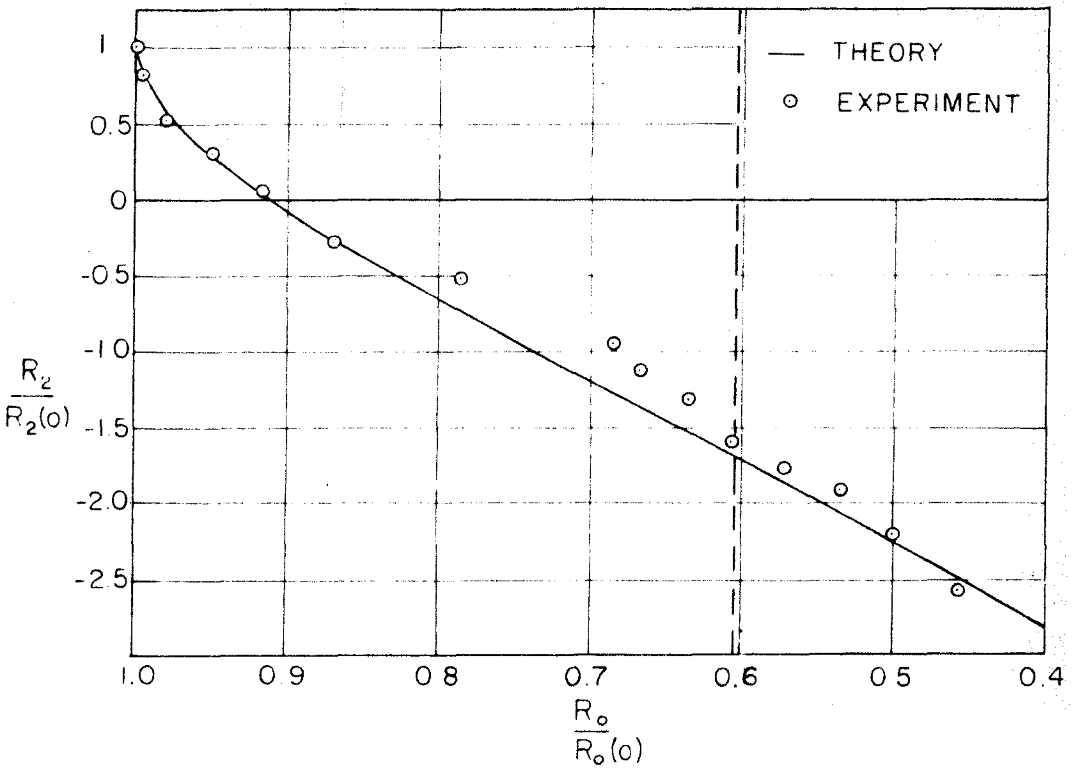

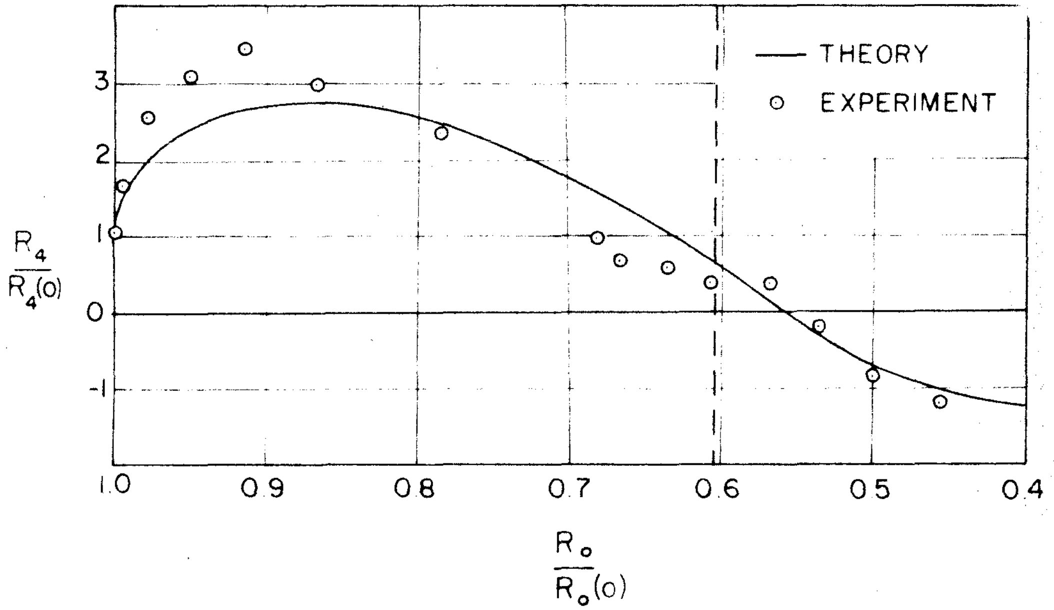

Fig. 5.15. R_2/R_2 (0) and R_4/R_4 (0) as functions of R_o/R_o (0) for the cavity of fig. 5.4.

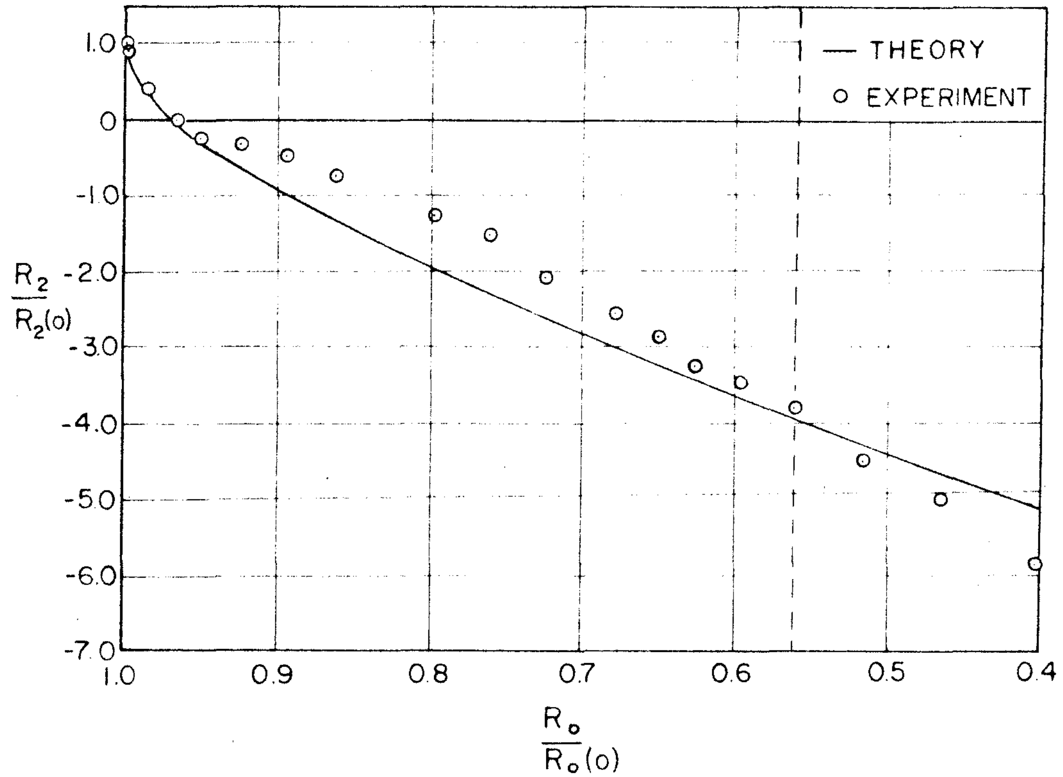

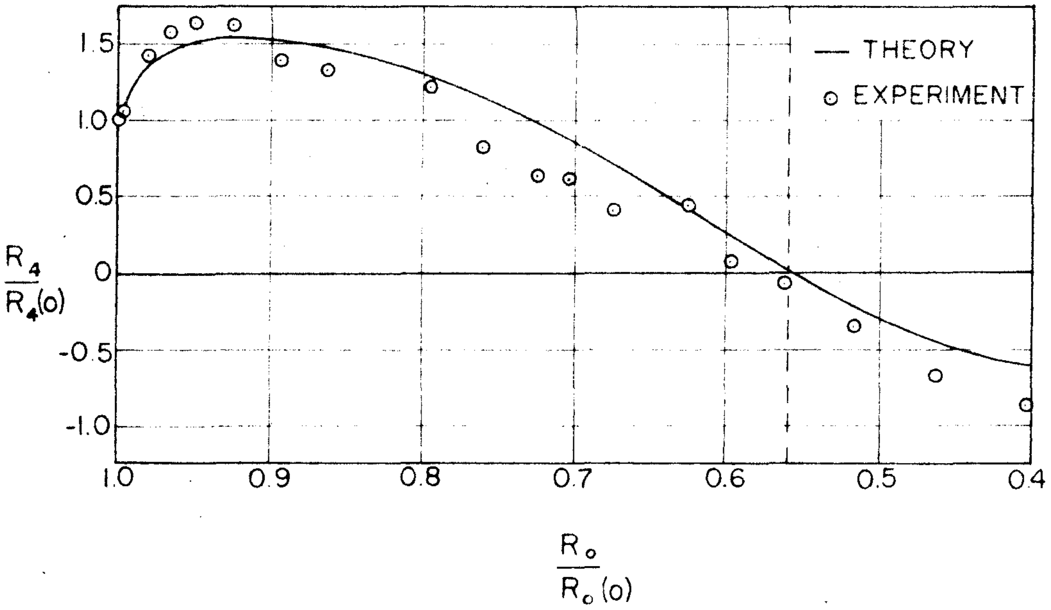

Fig. 5.16. R_2/R_2 (0) and R_4/R_4 (0) as functions of R_o/R_o (0) for the cavity of fig. 5.5.

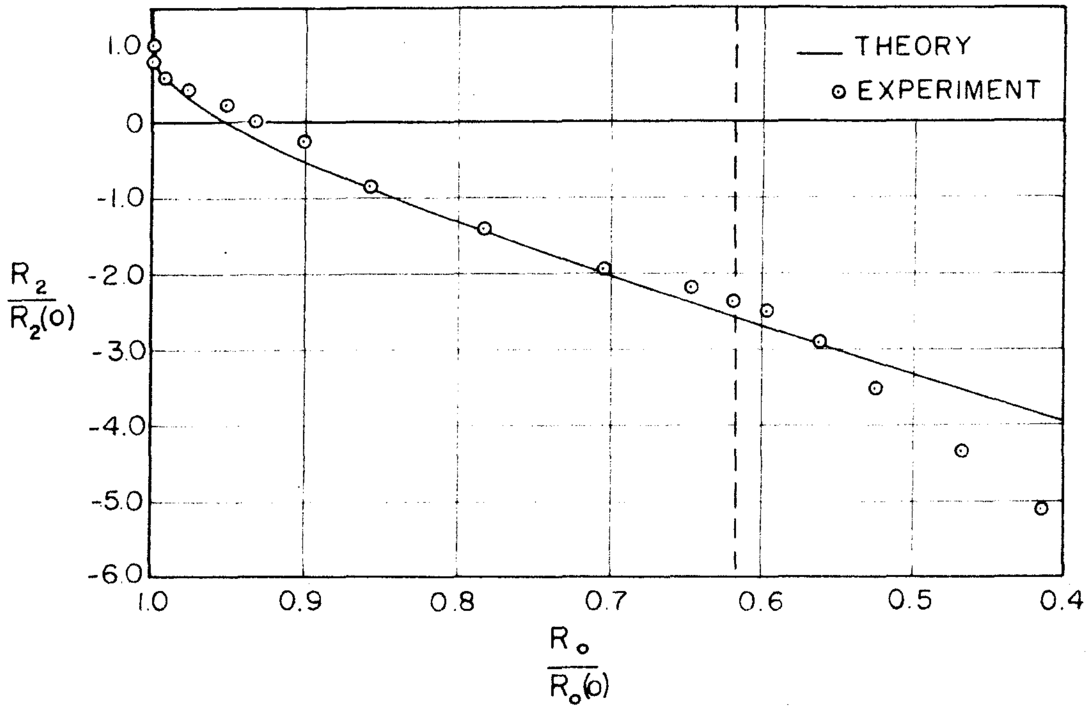

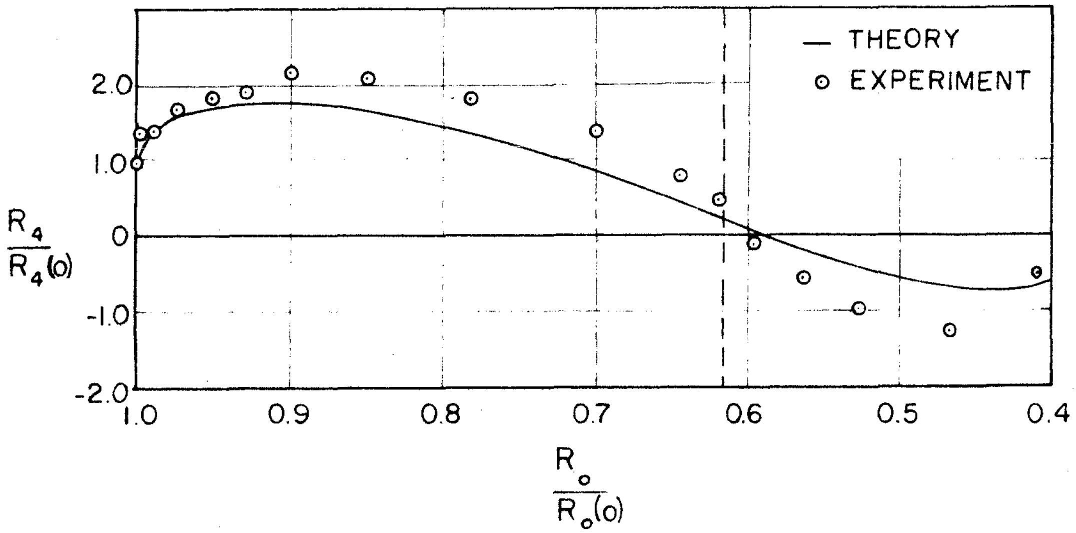

Fig. 5.17. R_2/R_2 (0) and R_4/R_4 (0) as functions of R_o/R_o (0) for the cavity of fig. 5.6.

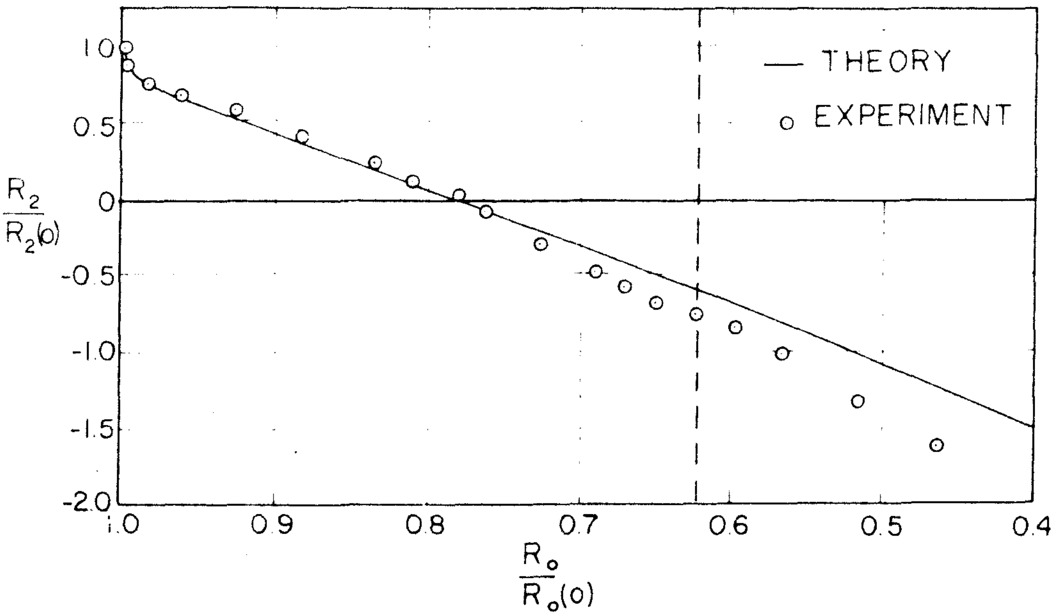

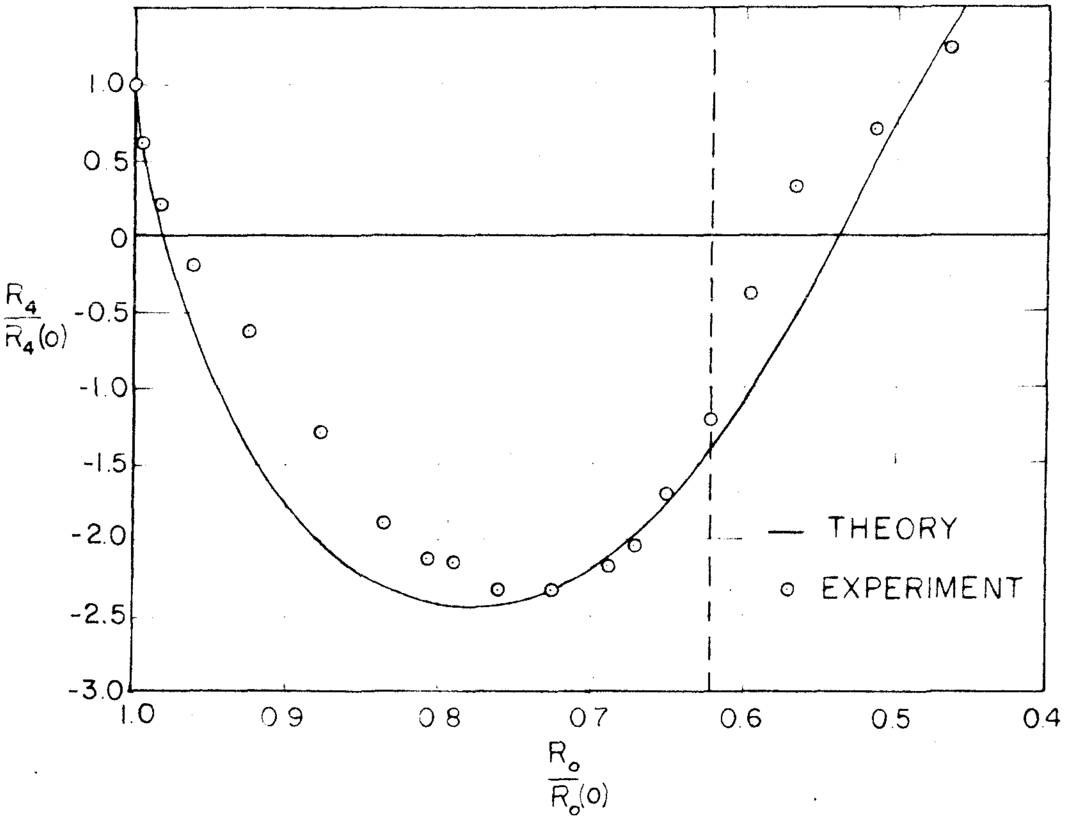

Fig. 5.18. $R_2/R_2(0)$ and $R_4/R_4(0)$ as functions of $R_o/R_o(0)$ for the cavity of fig. 5.7.

where y_{4P} is given by equation 3.48.

Calculating the theoretical curves in this fashion is consistent with the theoretical work of chapter III.

Discussion of the Results

The Hysol 8705 photoelastic material which was used in figure 5.3 is so sensitive that the pressure gradient under which the cavity collapsed is clearly visible. It is seen that no severe changes of the pressure in the cavity occur until after the water hammer pulse which appears in frame 6, 2. The pressure only changes drastically close to the compression pulse. This effect is seen in frame 6, 11. One might thus expect that the assumption of constant pressure in the cavity would be good for the cavities which were considered experimentally.

The comparisons with the theoretical curve in figure 5.12 demonstrate that $P_o(\cos\theta)$ components of the spark bubbles actually obey the simple Rayleigh theory very well in the range of the experiments which were done here. The spark method for producing cavities is thus proved satisfactory for purposes of the present study.

In figures 5.12 through 5.18 the theoretical curves are seen to describe the behavior of the $P_2(\cos\theta)$ and $P_4(\cos\theta)$ components of the collapsing cavities fairly well, especially if it is remembered that the experimental points were obtained from Legendre analyses of pictures which were at best somewhat blurred. One should also take into account that small deviations of R_o from its theoretical values close to $t = 0$ will introduce greatly amplified deviations in the curves for R_2 and R_4 close to $R_o/R_o(0) = 1$, because of the zero slope of the R_o curve at $t = 0$. The large differences between theory and experiment for small values of $R_o/R_o(0)$ in figures 5.15 through 5.18 could be the result of erroneous estimates of the times at which the water hammer pulses occurred for the cavities of figures 5.4 through 5.7.

In order to obtain an estimate of the significance of the differences between theory and experiment for the individual cavities which are presented here, an attempt was made to achieve a simultaneous comparison of the $P_2(\cos\theta)$ component of $R(\theta, t)$ with the theory for a fair number of cavities. Such a comparison is necessarily based on an apportioning of the difference between theory and experiment to the y_{2_1} and y_{2_2} parts of $R_2/R_2(0)$. The method of apportioning that was used is as follows:

Suppose that at $R_o/R_o(0) = \omega$, an experimental value of $R_2/R_2(0)$ was found to be y_{2e}. The difference, δ, between theory and experiment at this point is then

$$\delta = y_2(\omega) - y_{2e}(\omega) = y_{2_1}(\omega) + B_2 y_{2_2}(\omega) - y_{2e}(\omega)$$

One may then write

$$y_{2e}(\omega) = \left[y_{2_1}(\omega) - \delta \frac{|y_{2_1}(\omega)|}{|y_{2_1}(\omega)| + |B_2 y_{2_2}(\omega)|} \right]$$

$$+ B_2 \left[y_{2_2}(\omega) - \delta \frac{|B_2|}{B_2} \frac{|y_{2_2}(\omega)|}{|y_{2_1}(\omega)| + |B_2 y_{2_2}(\omega)|} \right]$$

$$= y_{2e_1}(\omega) + B_2 y_{2e_2}(\omega) \qquad (5.6)$$

The "experimental" points of y_{2e_1} and y_{2e_2} are compared with the theoretical curves for y_{2_1} and y_{2_2} in figures 5.19 and 5.20

respectively. These points were obtained from motion picture records of ten cavities different from the ones shown in figures 5.1 through 5.7. All the cavities collapsed on photoelastic boundaries, so that the experimental results for small $R_o/R_o(0)$ should be relatively trustworthy.

Even though the weakness of the method of apportioning differences between theory and experiment is quite apparent, figures 5.19 and 5.20 give an excellent indication of the scatter involved in the experimental data. The experimental points appear to be well grouped around the theoretical curves.

A similar representation of experimental data for $R_4/R_4(0)$ was not attempted because y_4 is a linear combination of five different functions of $R_o/R_o(0)$. Results based on assumptions about apportioning of differences between theory and experiment to each of these five curves would become quite meaningless. However, it may be expected that the scatter of the experimental data for $R_4/R_4(0)$ would be much more severe than the scatter of the $R_2/R_2(0)$ points.

Experimental data for $R_6/R_6(0)$ were extremely erratic because R_6 was usually comparable in magnitude to inaccuracy in the measurements. These experimental results are not presented here.

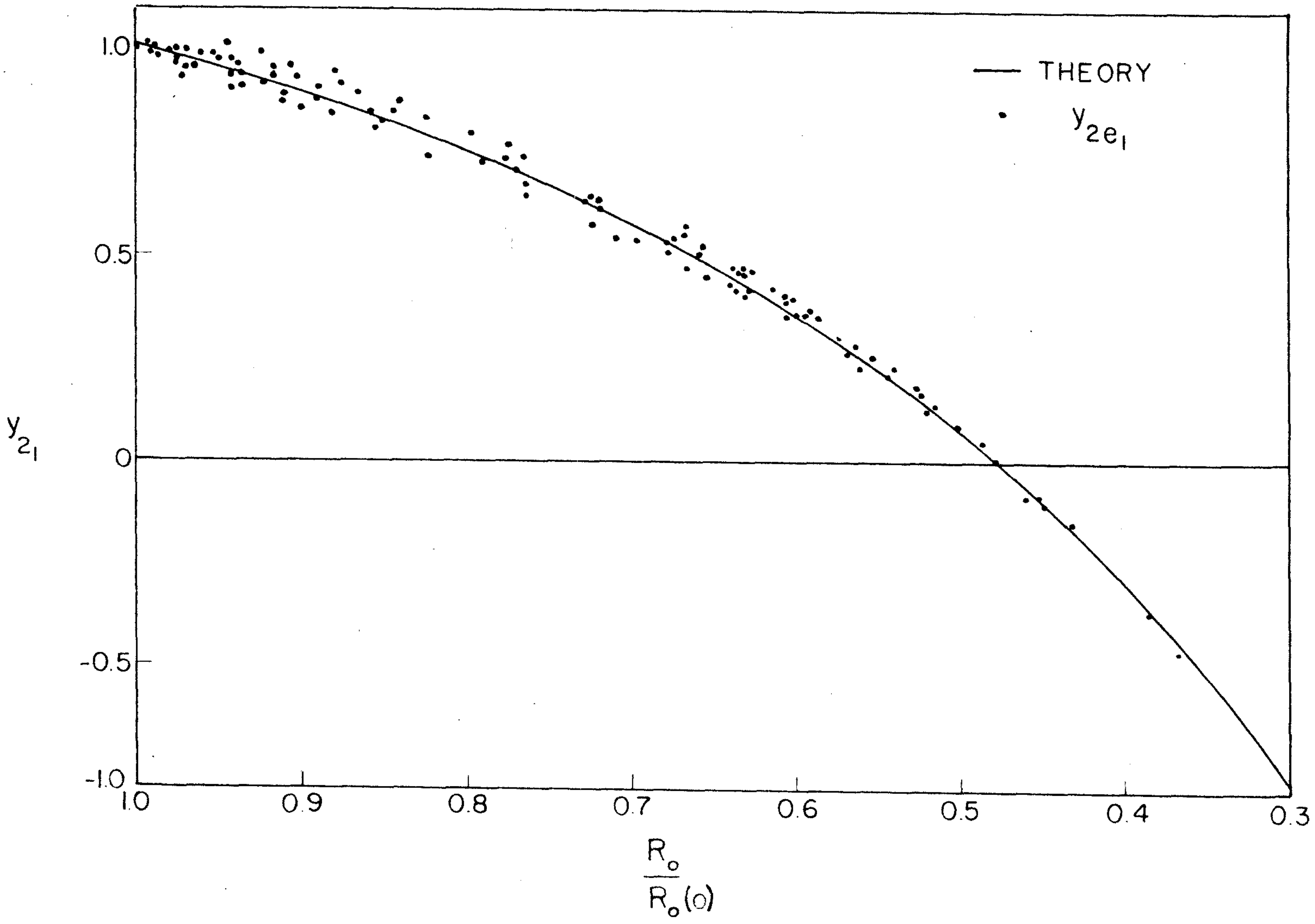

Fig. 5.19. y_{2_1} as a function of $R_o/R_o(0)$.

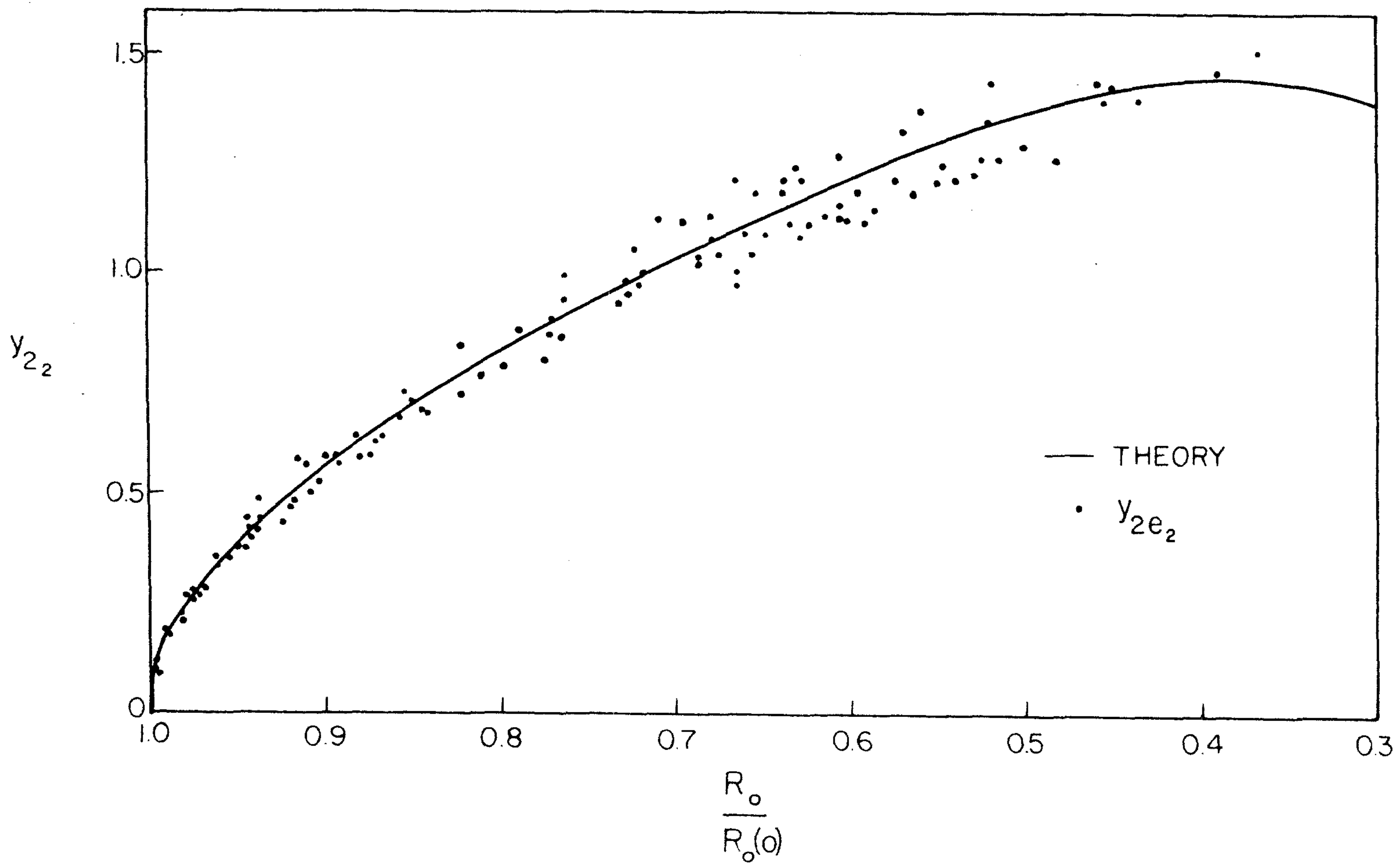

Fig. 5.20. y_{2_2} as a function of $R_o/R_o(0)$.

Chapter VI

The Pressures on the Solid Boundary

In chapter V one became acquainted with two types of pressure disturbances which act on the solid boundary during the collapse of a non-hemispherical cavity. The first is a result of the cavity boundary striking the solid surface, and the second is due to compression of the gases in the cavity. At this stage the relative importance of the two pressure pulses is undetermined. No conclusions can be drawn from the fringe patterns in the photoelastic materials, because the area over which the water hammer pulse acts is unknown.

The problem of determining the relative importance of the two disturbances was finally resolved by studying the damaging effects of cavities on metal samples. Figures 6.1, 6.2 and 6.3 show microscope pictures of pits which were produced by the cavities of figures 5.5, 5.6 and 5.7 respectively. The pits were made in samples of high purity aluminum which were annealed and chemically polished. The rather strange appearance of these pictures is due to the method of illuminating the sample surfaces. The small holes are a result of the chemical polishing and only the large dents were caused by the cavities. The scale in the photographs is .004" per division. Figure 6.4 shows a photograph of a pit in 2-S Aluminum which was made by a cavity very much the same as the one of figure 5.5. In this case the surface was smoothened with number 600 metallurgical emery paper, and no further polishing was employed.

Several facts are demonstrated by these pictures in conjunction with figures 5.5, 5.6 and 5.7. The most important is that the diameters

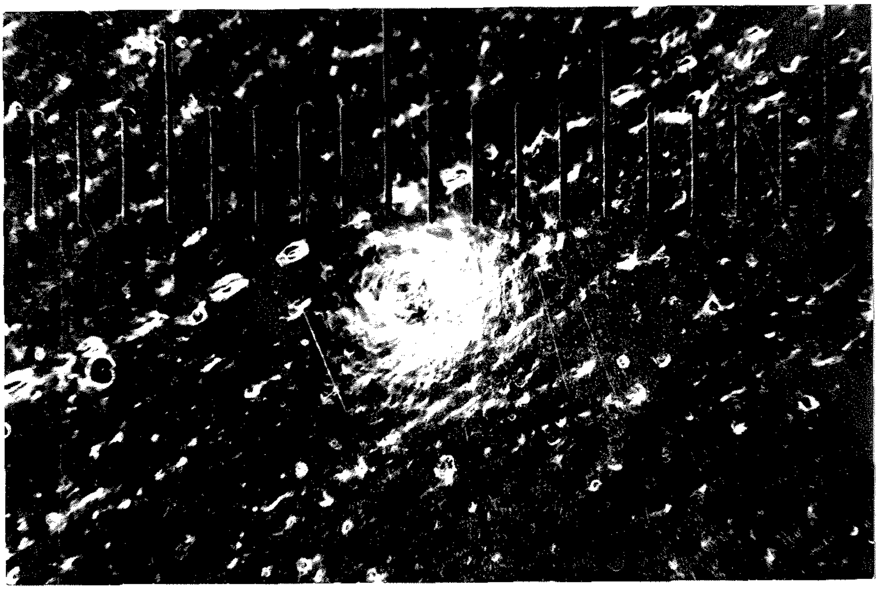

Fig. 6.1 The pit produced in high purity Aluminum by the cavity of figure 5.5.

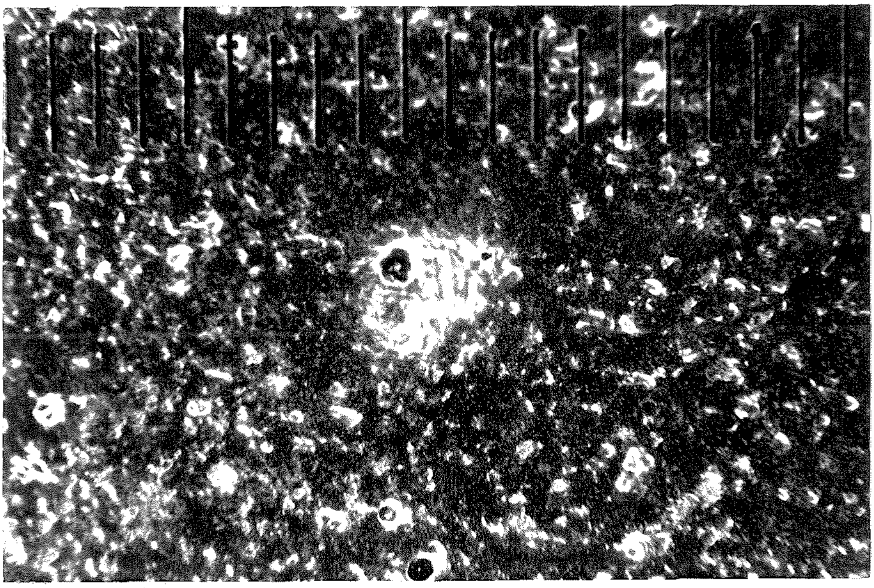

Fig. 6.2 The pit produced in high purity Aluminum by the cavity of figure 5.6.

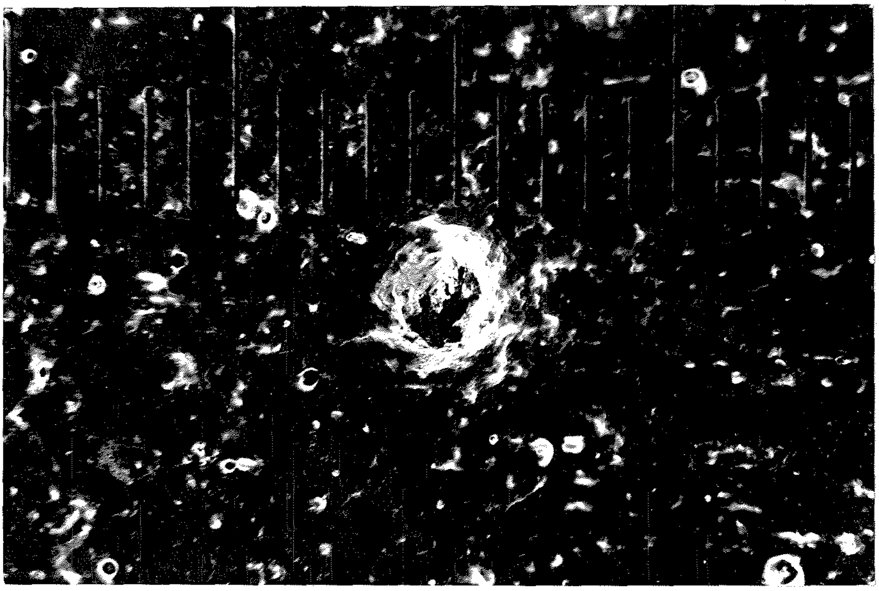

Fig. 6.3 The pit produced in high purity Aluminum by the cavity of figure 5.7.

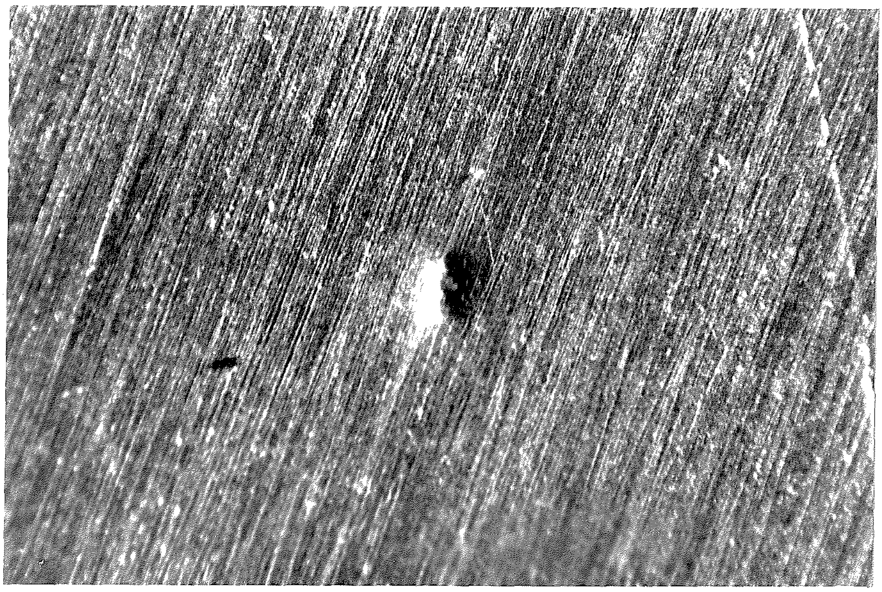

Fig. 6.4 The pit produced in 2-S Aluminum by a cavity similar to the one of figure 5.5. Average pit diameter is approx. 0.014".

of the pits are much smaller than the minimum base diameters of the cavities that caused them. It is further noted that the pit diameter decreases as the minimum base diameter of the cavity increases, or correspondingly, as the magnitude of the initial perturbation of the hemispherical shape is increased. Table 6.1 illustrates these facts numerically.

Figure number in which cavity is shown	Diameter of pit caused by cavity inches	Minimum base diameter of cavity inches
5.5	0.0150	0.111
5.6	0.0125	0.157
5.7	0.0120	0.179

Table 6.1 Results of the damage experiments

It becomes clear that the pits could not have been produced by the gas compression pulses, and that the water hammer pulses must have been responsible for the damage.

The fact that the pit diameter decreases as the minimum base diameter is increased cannot easily be explained on the basis of the experimental results. This effect is more pronounced than table 6.1 indicates, because cavities with slightly larger initial perturbations of the hemispherical shape than the one in figure 5.7 were found to cause no visible damage of the soft aluminum samples. Impact velocities that were estimated from the motion picture records were not significantly different for the three cavities of figures 5.5 through 5.7, and these velocities seemed to be of the order of 200 feet per second. Higher impact velocities than this were estimated for cavities with larger initial perturbations than the one of figure 5.7.

An explanation of this effect could possibly be found if the radius of curvature of the portion of the cavity wall which strikes the boundary could be estimated. The theory is of no help at this stage because it predicts that the radius of curvature will be zero at the point of impact. This is of course a physical impossibility which would not occur if surface tension had been included as a property of the liquid. Because the pictures do not show the indented portion of the cavity walls, one cannot determine the radius of curvature experimentally.

Another factor which should be taken into account is that the estimates of the impact velocities could be very inaccurate, because the details of the shapes of the cavities are not known in the period during which the cavities remain indented.

Now that it has been shown that the water hammer pulse is responsible for the damage, one expects that the pressure on the boundary will be given by

$$p = \rho c v \qquad (6.1)$$

where

p is the pressure

ρ is the density of the liquid

c is the velocity of sound in the liquid

v is the impact velocity of the cavity wall.

The equation 6.1 is the well known water hammer equation (17).

Pressures calculated from this equation using the estimated impact velocities for the cavities of figures 5.5, 5.6 and 5.7 are of the order of 18,500 p.s.i. These pressures could certainly cause damage of the high purity aluminum samples, which had a yield strength of approximately 2500 p.s.i., and also of the 2-S aluminum with a yield strength of approximately 5,000 p.s.i.

In order to afford an additional check on the results, the quartz crystal pickup was calibrated in a shock tube. Such a calibration enables one to form an idea of the pressures involved in the compression pulses which were recorded with the quartz crystal pickup. This pressure was only 2000 p.s.i. for the cavity of figure 5.4, so that it could not even damage the high purity aluminum.

The pressures due to the compression of gas in the cavity decreased as the initial perturbation of the hemispherical shape was increased. As the spark gap was moved further away from the wall, these pressures reached a very pronounced minimum, and then started increasing again. In figure 6.7 a curve of the magnitudes of the compression pulse on the boundary is shown as a function of the distance of the spark gap from the boundary. The spark energy was kept constant during these pressure recordings. Figure 6.5 shows a picture of the cavity corresponding to point A of figure 6.7 at maximum radius and a few frames at the time of the compression pulse. Figure 6.6 shows the same frames for the cavity corresponding to point B of figure 6.7.

It is seen that the minimum in pressure of the compression pulse results from a cavity which is barely touching the solid boundary initially, and which still collapses on the boundary. The pressure starts rising again when the cavities collapse away from the wall, and are more nearly spherically symmetric close to the collapse point. It reaches a maximum value when the inverse square dropoff due to the increase in distance cancels the gain of pressure due to the more nearly

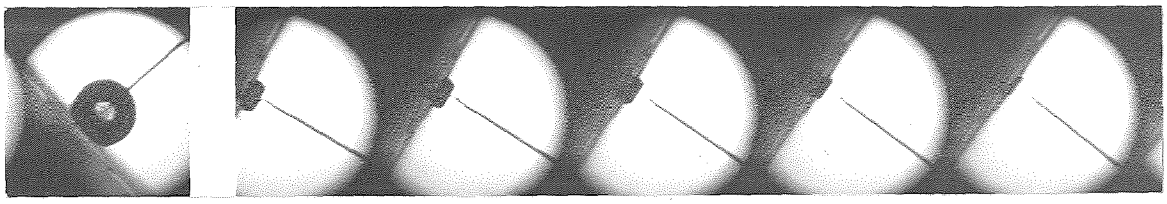

Fig. 6.5 The cavity corresponding to point A of figure 6.7 at maximum volume and close to minimum volume.

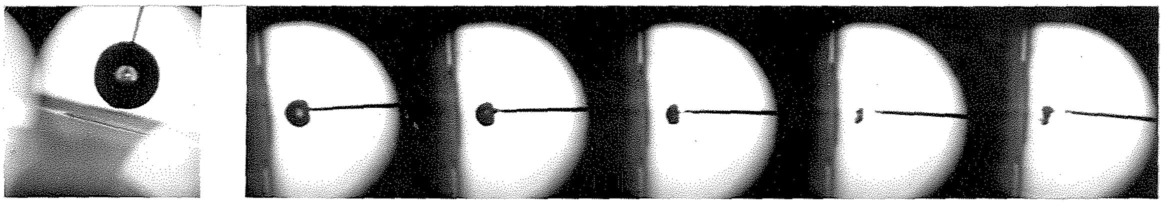

Fig. 6.6 The cavity corresponding to point B of figure 6.7 at maximum volume and close to minimum volume.

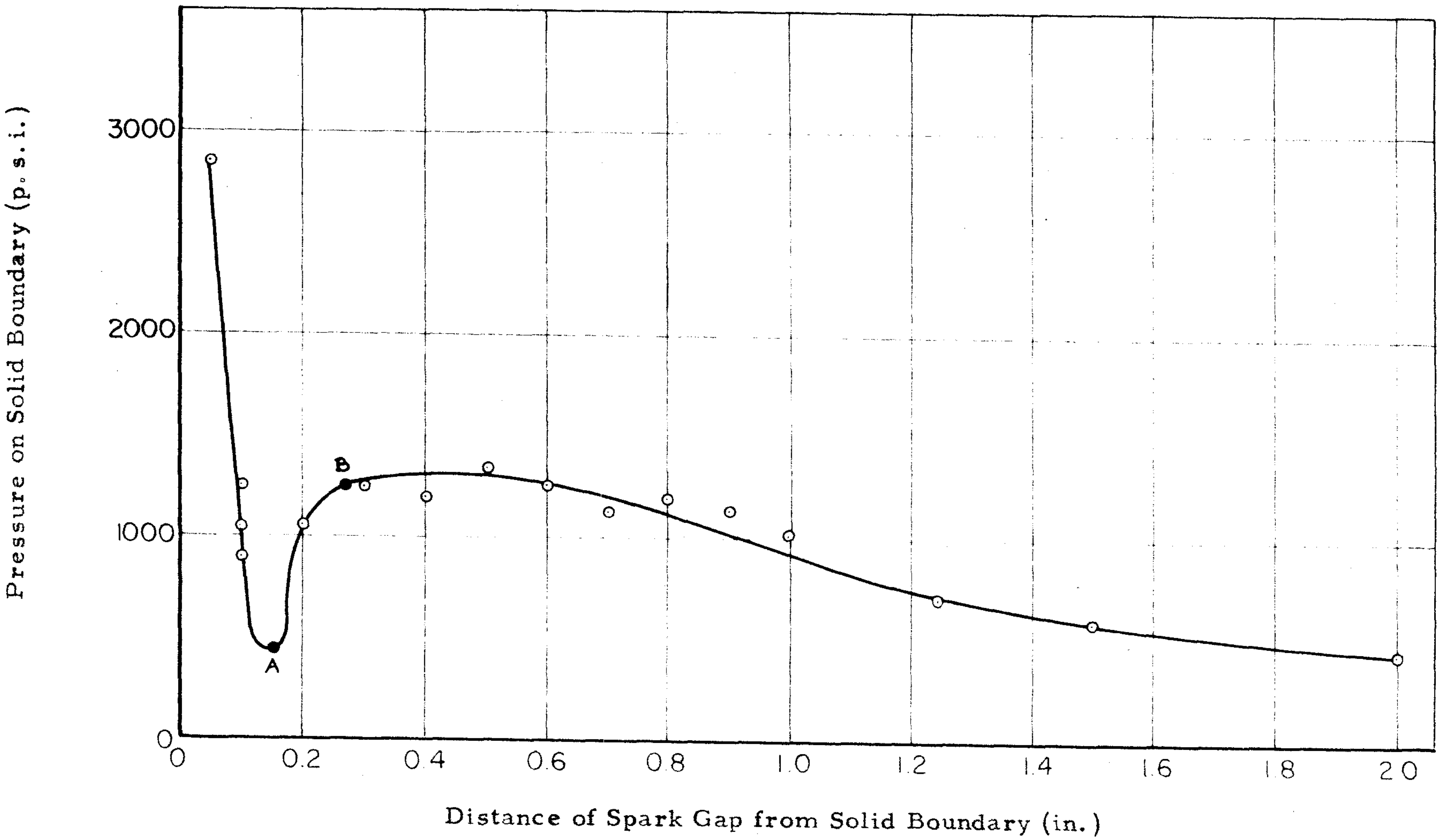

Fig. 6.7. Pressures on the Solid Boundary Resulting from the Gas Compression pulse.

spherical collapse, and then decreases gradually as the distance is increased further.

The mechanism of damage which was observed in the present work is not an entirely new concept. As early as 1950 Eisenberg (18) speculated that jets formed during the unsymmetrical collapse of cavitation bubbles could be responsible for damage. It is believed that the present results are the first in which this effect was actually observed.

It should be pointed out that this effect was observed for a very limited range of cavity types. When initial perturbations of the hemispherical shape were too large, cavities failed to cause damage of soft aluminum samples even though the jet could be shown to occur. Cavities with rather small initial perturbations of the hemispherical shape could not be studied in detail because of limitations imposed by the resolution of the high speed camera.

A further limitation of the present experimental data is that it was not shown that the initial conditions obtained with cavities generated by spark methods can be duplicated with cavities formed by strictly hydrodynamic processes.

Chapter VII

Summary and Conclusions

In order to collect the ideas which are distributed throughout the preceding chapters a brief summary is presented here.

The collapse process of non-hemispherical cavities in contact with a solid boundary was examined theoretically. In the theoretical treatment real fluid effects such as those of compressibility, viscosity, surface tension and adhesion were neglected. The effect of gravity was assumed to be small, and the pressure inside the cavity was assumed to remain constant.

Only cavities which remain axially symmetric with respect to a line normal to the solid boundary were considered. The radii of such cavities were expressed by the equation

$$R(\theta, t) = R_o(t) P_o(\cos\theta) + \sum_{n=1}^{\infty} R_{2n}(t) P_{2n}(\cos\theta). \qquad (7.1)$$

Two perturbation solutions for the collapse problem were obtained. For purposes of the first solution it was assumed that the sum $\sum_{n=1}^{\infty} R_{2n}(t) P_{2n}(\cos\theta)$ was much smaller than $R_o(t)$, and all the interactions between terms in the sum were neglected. It was found that the R_{2n} in this case all satisfied the equation

$$D(R_o, n) \left[R_{2n}(R_o) \right] = 0 \qquad (7.2)$$

where $D(R_o, n)$ is a linear second order differential operator in R_o which depends only on n. R_o was found to satisfy the Rayleigh theory to this approximation. It was realized that a small term in the sum of equation 7.1 can be seriously affected by interactions among other terms in the sum and that the coefficient of such a term may not satisfy the equation 7.2 at all. However, this effect is negligible as far as R (θ, t) is concerned provided $\sum_{n=1}^{\infty} R_{2n}(t)\, P_{2n}(\cos\theta)$ is small compared to R_o.

In the second solution the most important interactions between the terms of the sums in equation 7.1 were taken into account for the case where the following conditions were satisfied

$$R(\theta, t) = R_o(t)\, P_o(\cos\theta) + R_2(t)\, P_2(\cos\theta) + R_4(t)\, P_4(\cos\theta) + R_6(t)\, P_6(\cos\theta) + \ldots$$

where $R_{2n+2} < R_{2n}$

and R_{2n} was negligible compared to R_o for $n > 3$. (7.3)

The most important influence on R_o arose from interactions of R_2 with itself. These terms were still considered negligible. R_2 was also affected most seriously by nonlinear terms in itself, but this effect was considered small enough to neglect. The quadratic nonlinear terms in R_2 could however have an appreciable effect on R_4 and these terms were retained for purposes of calculating R_4. Similarly, cubic nonlinear terms in R_2, and interaction terms between R_2 and R_4 were retained in calculating R_6.

Inclusion of terms of this type caused no nonlinearity in the equations, and it was found that $R_{2n}(R_o)$, with $n = 1$, 2 and 3 now satisfied the equation

$$D(R_o, n)\left[R_{2n}(R_o)\right] = F_{2n}(R_o) \qquad (7.4)$$

where D is still the same operator as in equation 7.2, and $F_{2n}(R_o)$

is a forcing function. In the special case of $n = 1$, $F_2 = 0$. R_o still satisfied the Rayleigh theory to this approximation.

The behavior of the theoretical solutions for the $R_{2n}(R_o)$ suggest the possibility that the cavity wall may strike the solid boundary before the cavity reaches its minimum volume. This effect has as a consequence the possibility of damage by a water hammer mechanism, and is therefore of great interest. Unfortunately, large perturbation quantities are involved at the time that this type of impact occurs, so that one is not justified in drawing any definite conclusions. The theory also shows that the radius of curvature of the part of the cavity wall which strikes the boundary is zero at impact. This is a physical impossibility which results from the perfect fluid assumption.

Because of these questionable results, which could conceivably be an attempt of the mathematics to describe some important physical effects, experiments were performed with spark bubbles in water which collapsed in contact with a solid boundary. The shapes of these cavities were analyzed and compared with the theory and the detailed mechanism of damage was examined experimentally.

The main conclusions that can be drawn from the study are listed below.

1). Experimental cavities were all found to satisfy the conditions of equation 7.3. The theoretical work which was based on these assumptions described the behavior of the $P_2(\cos\theta)$ and $P_4(\cos\theta)$ terms of the experimental cavities fairly well. When the scatter of the experimental data was taken into account, it was apparent that no definite conclusions about the difference between the theoretical curves and experimental points could be drawn.

2). The fact that the experimental points for the $P_2(\cos\theta)$ and $P_4(\cos\theta)$ components of the cavity radius fell so close to the theoretical curves indicates that gravity, viscosity, surface tension, compressibility and adhesion were indeed negligible for the type of cavities considered in the experiments.

3). The effect of a cavity deforming to the extent that its wall strikes the solid boundary before the cavity reaches minimum volume was observed to occur by means of photoelastic boundaries.

4). The pressure pulse caused by the cavity wall striking the solid boundary was followed by a second pressure disturbance, which appeared to be the result of a compression of gases in the cavity. No evidence was found that the gas compression pulse gave rise to higher pressures than the water hammer effect, and in cases where the cavities damaged the solid boundary, it was proved conclusively that the water hammer pulse caused the damage.

5). It was found that pressures calculated from the equation

$$p = \rho c v$$

p = pressure

ρ = liquid density

c = velocity of sound in the liquid

v = estimated impact velocity

were large enough to explain the observed damage.

Another parameter, however, appeared to play an important role in the damaging process, because nearly equal estimated impact velocities could produce vastly different pit sizes. It appeared that the radius of curvature of the portion of the cavity wall which struck the solid boundary could be the other parameter. No evidence could, however, be found to prove this hypothesis. It is also conceivable that errors in the estimated collapse velocities could be responsible for the observed effects.

6). Measurements of the pressure arising from compression of gases in the cavity showed that these pressured dropped sharply as the initial perturbation of the hemispherical shape was increased. Pressures obtained from cavities with very large initial perturbations which still collapsed on the solid surface were in some cases lower than shock wave pressures on the surface due to cavities of the same energy that collapsed away from the boundary. This result can be explained by the fact that cavities which collapse away from the solid surface remain much more closely spherically symmetric than largely perturbed hemispherical cavities which collapse on the boundary, and that the included gases are compressed much more.

7). Experimental evidence showed that the spark method for making cavities was very satisfactory. The P_o (cos θ) components of such cavities obeyed the Rayleigh theory extremely well in the range of the experiments. Sensitive photoelastic materials showed that no pressure rise occurred inside the cavities for a range of R_o well exceeding the requirements of the experiments.

8). The cavities that were studied experimentally all deformed to strike the solid surface for $R_o/R_o(0) > 0.3$. This is the result of using fairly large initial perturbations of the hemispherical shape.

Even at these large values for R_o/R_o (0) optical resolution of the high speed photography limited the accuracy of the experiments. The results obtained here cannot be extended to cavities which collapse much more nearly hemispherically without further experimental verification, because of the high collapse velocities, and the pressure rise in the cavity which would occur. It is believed, however, that the water hammer mechanism of damage may be important even in these cases. Further investigation of this question will require high speed motion picture cameras with optical resolution beyond that of the one used in the present study.

Appendix 1

A Property of Integrals Arising from the Variation of Parameters Method

Consider a general second order linear differential equation

$$L(y) = p_2(x) \frac{d^2y}{dx^2} + p_1(x) \frac{dy}{dx} + p_o(x) = w(x) \qquad (A.1)$$

and suppose that u (x) satisfies the equation

$$L(u) = 0. \qquad (A.2)$$

It is desired to find a particular solution of eq. A.1 by the method of variation of parameters.

The particular solution is then expressed as follows

$$y_p = u(x)\, U(x) \qquad (A.3)$$

Substituting eq. A.3 in eq. A.1 one obtains

$$p_2(x)\, u \frac{d^2U}{dx^2} + \left[2p_2(x) \frac{du}{dx} + p_1 u\right] \frac{dU}{dx} = w \qquad (A.4)$$

Multiplying through with the integrating factor

$\dfrac{uq}{p_2}$ where $q = e^{\int \frac{p_1}{p_2} dx}$ one obtains

$$\frac{d}{dx}\left[u^2 q \frac{dU}{dx}\right] = \frac{w\,u\,q}{p_2} \qquad (A.5)$$

The case of present interest arises when u vanishes for some value of x. Without loss of generality one may choose this value of x to be the point x = 0. Thus

$$u(0) = 0 \qquad (A.6)$$

In the case where

$$\frac{du}{dx}(0) \neq 0 \qquad (A.7)$$

$$p_2\,(0) \neq 0 \qquad (A.8)$$

$$\text{w and q are well behaved at } x = 0 \qquad (A.9)$$

one may then write

$$\frac{dU}{dx} = \frac{H(x)}{u^2 q} \qquad (A.10)$$

where $$H(x) = \int \frac{w\,u\,q}{p_2}$$

Expanding H (x) and $u^2 q$ in the neighborhood of $x = 0$ one obtains

$$H(x) = H(0) + \frac{d^2 H}{dx^2}(0)\,x^2 + \ldots \qquad (A.11)$$

because of eqs. A.5 and A.6 and

$$u^2 q = \left[\frac{du}{dx}(0)\,x + 1/2\,\frac{d^2 u}{dx^2}(0)\,x^2 + ..\right]^2 \left[q(0) + \frac{dq}{dx}(0)\,x..\right] \qquad (A.12)$$

because of eq. 6.5.

From eq. A.2 it follows that

$$\frac{d^2 u}{dx^2}(0) = -\frac{p_1}{p_2}\,\frac{du}{dx}(0). \qquad (A.13)$$

Furthermore $$\frac{dq}{dx}(0) = \frac{p_1}{p_2}\,q(0). \qquad (A.14)$$

Eq. A.12 thus takes the form

$$u^2 q = \left(\frac{du}{dx}(0)\right)^2 q(0)\,x^2 + O(x^4)$$

so that

$$\frac{dU}{dx} = \frac{1}{x^2}\left[\frac{H(0)}{\left(\frac{du}{dx}(0)\right)^2 q(0)} + O(x^2)\right]$$

Thus $\frac{dU}{dx}$ contains no terms of order $\frac{1}{x}$ in its expansion around the origin, and

$$y_p = \left[\frac{du}{dx}(0)\,x + O(x^2)\right]\left[\int \frac{H(0)}{(\frac{du}{dx}(0))^2\ q(0)\,x^2}\right] dx + O(x)$$

$$= -\frac{H(0)}{\frac{du}{dx}(0)\ q(0)} + O(x) \qquad \text{(A. 15)}$$

The integral in the expression for y_p thus gives rise to no log x term. This is of importance because otherwise the resulting particular solution y_p would not be analytic around the origin.

References

(1) Plesset, M. S., The Dynamics of Cavitation Bubbles. Journal of Applied Mechanics (1949), Vol. 16, pp. 277-282.

(2) Parsons, C. A. and Cook, S. S., Investigations into the causes of Corrosion or Erosion of Propellors. Engineering (1919), Vol. 107, pp. 501 and 515-519.

(3) Rayleigh, Lord, On the Pressure Developed in a Liquid during the Collapse of a Spherical Cavity. Philosophical Magazine (1917), Vol. 34, pp. 94-98.

(4) Besant, W., Hydrostatics and Hydrodynamics (1859), 158. Referred to in reference (3)).

(5) Schneider, A. J. R., Some Compressible Effects in Cavitation Bubble Dynamics. California Institute of Technology Ph. D. Thesis (1949), pp. 11-61.

(6) Gilmore, F. R., The Growth or Collapse of a Spherical Bubble in a Viscous Compressible Liquid. California Institute of Technology Hydrodynamics Laboratory Report No. 26-4 (1952).

(7) Kirkwood, J. G. and Bethe, H. A., The Pressure Wave Produced by an Underwater Explosion. OSRD Report No. 588 (1942).

(8) Plesset, M. S. and Mitchell, T. P., On the Stability of the Spherical Shape of a Vapor Cavity in a Liquid. Quarterly of Applied Mathematics (1956), Vol. 13, pp. 419-430.

(9) Milne-Thomson, L. M., Theoretical Hydrodynamics Macmillan (1955). pp. 68 and 74.

(10) Stoker, J. J., Water Waves Interscience (1957), pp. 7 and 11.

(11) Lamb, Sir H., Hydrodynamics Dover (1945), pp. 122.

(12) Erdélyi et al. Higher Transcendental Functions Vol. 1 McGraw-Hill (1958), pp. 56, 105-106, 58.

(13) Wayland, H., Differential Equations in Science and Engineering Van Nostrand (1957), pp. 120.

(14) Ellis, A. T., Observations on Cavitation Bubble Collapse. California Institute of Technology Hydrodynamics Laboratory Report No. 21-12 (1952).

(15) Beams, J. W., A Review of the Use of Kerr Cells for the Measurement of Time Intervals and the Production of Flashes of Light. Review of Scientific Instruments (1930), Vol. 1, pp. 780-793.

(16) Kingsbury, E. F., The Kerr Electrostatic Effect. Review of Scientific Instruments (1930), pp. 780-793.

(17) Gibson, A. H., Hydraulics and its Applications Constable (1952), pp. 232-235.

(18) Eisenberg, P., On the Mechanism and Prevention of Cavitation. David Taylor Model Basin Report 712, pp. 51-52.